COLLISIONAL BROADENING OF SPECTRAL LINES
IN THE X $\rightarrow$ b SYSTEM OF O_2 AND THE FIRST
VIBRATIONAL BAND OF NO BY THE NOBLE GASES

THESIS

John Joseph Cornicelli, Captain, USAF

AFIT/ENP/GAP/97D-01

DEPARTMENT OF THE AIR FORCE
AIR UNIVERSITY
AIR FORCE INSTITUTE OF TECHNOLOGY

DTIC QUALITY INSPECTED 3

Wright-Patterson Air Force Base, Ohio

19980120 123

COLLISIONAL BROADENING OF SPECTRAL LINES
IN THE X $\rightarrow$ b SYSTEM OF O_2 AND THE FIRST
VIBRATIONAL BAND OF NO BY THE NOBLE GASES

THESIS

John Joseph Cornicelli, Captain, USAF

AFIT/ENP/GAP/97D-01

AFIT/ENP/GAP/97D-01

AFIT/GAP/ENP/97D-01

COLLISIONAL BROADENING OF SPECTRAL LINES IN THE X → b SYSTEM OF

O_2 AND THE FIRST VIBRATIONAL BAND OF NO BY THE NOBLE GASES

THESIS

Presented to the Faculty of the School of Engineering

of the Air Force Institute of Technology

Air University

In Partial Fulfillment of the

Requirements for the Degree of

Master of Science in Applied Physics

John Joseph Cornicelli, B.S.

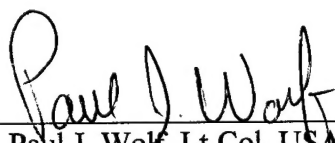Captain, United States Air Force

December 1997

Approved for public release; distribution unlimited

i

AFIT/GAP/ENP/97D-01

COLLISIONAL BROADENING OF SPECTRAL LINES IN THE X → b SYSTEM OF

O$_2$ AND THE FIRST VIBRATIONAL BAND OF NO BY THE NOBLE GASES
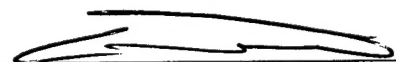
John Joseph Cornicelli, B.S.

Captain, United States Air Force

Approved:
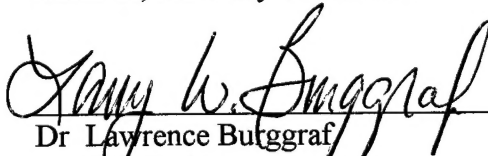
_____   24 Nov-97
Paul J. Wolf, Lt Col, USAF   Date
Chairman, Advisory Committee

_____   24 Nov 97
Glen A. Perram, Lt Col, USAF   Date
Member, Advisory Committee

_____   24 Nov 97
Dr Lawrence Burggraf   Date
Member, Advisory Committee

ii

Acknowledgments

I would like to express my sincere appreciation to Lt Col Paul Wolf, my thesis advisor for all his patience and expertise as well as his willingness to do wrench turning with us. I would also like to thank Dr Lawrence Burggraf for all of his help in matters theoretical as well as patience in explaining quantum mechanics to me and Lt Col Glen Perram for his assistance, be it in experimental or theoretical spectroscopic matters. I would also like to thank the laboratory technician crew, Jim Reynolds, Belinda Johnson and Greg Smith for their patience and assistance. I would especially like to thank my laboratory partner Rob Pope for all of his help with things experimental, theoretical and for letting me share space with him and break his equipment. He took time out from his own studies to help me out. I would also like to express my appreciation to Tom Niday for his assistance in data analysis. Without his help, we would have a lot of data in a pile and no results (or thesis). Without all of these folks' help, we would not have even gotten started.

I would definitely not even have gotten this far without the loving support given me by my wife Nathalie, my daughter Marianne and our families. Nathalie, instead of the laboratory, now has possession of her husband, and Marianne has her daddy back.

Table of Contents

List of Figures

List of Tables

Abstract

Collisional broadening of the rotational spectral lines of the $X \rightarrow b$ system of O_2 and the first vibrational band of NO by the noble gases is examined by Fourier transform spectroscopy. Peaks of the individual rotational lines are modeled with a Voigt function, from which Lorentzian half widths are extracted. Lorentzian widths are plotted vs. pressure of foreign gas, from which the pressure broadening coefficients and pressure broadening cross sections are calculated. The pressure broadening coefficients are compared to theoretical values determined by past research for O_2. NO coefficients are compared to similar research using N_2 as collision partner. O_2 broadening coefficients/cross sections were found to increase with decreasing rotational quantum number. Also, a linear dependence is found between cross section and both polarizability of the collision partner and reduced mass of the collision pair.

Collisional Broadening of Spectral Lines in the X → b System of O$_2$ and the First Vibrational Band of NO by the noble gases.

I. Introduction

Purpose

Absorption spectral line broadening has been discussed in literature for quite a while. We study radiative heat balance of planetary atmospheres, as well as remotely measure the temperature, pressure and density of atmospheric constituents. We also need to measure the working cavity temperature of military lasers to optimize output and efficiency. The Chemical Oxygen Ion Laser (COIL), under development for the Airborne Laser Antiballistic Missile Defense System, is one example where optical diagnoses are necessary.

The O$_2$ transition we are studying (often called the A-band), lies in the atmospheric transmission region of the solar spectrum. Additionally, oxygen is a relatively poor absorber. This makes it ideal for remote sensing of atmospheric conditions (Ritter, 1987). To do so, we need to accurately measure spectral line strengths, widths and changes with temperature and pressure. We can measure the broadening of the spectral lines and relate it to the temperature using the Doppler width of the line (Rees, 1989):

$$\Delta v_D = v_0 \sqrt{\frac{8 k_B T \ln 2}{mc^2}} \tag{1-1}$$

where Δv_D is the Doppler line width, v_0 is the line center frequency, and T is the environmental kinetic temperature. We will discuss more about line broadening in Chapter 1.3.

Knowledge of NO chemistry in the upper atmosphere is limited. NO is a minor, albeit important, constituent of the upper atmosphere and is important in reactions concerning stratospheric ozone. NO reactions adjust the concentration of this ozone and infrared absorption is used for remote sensing of NO concentrations (Ballard, 1988) The chemiluminescent reaction (Rees, 1989):

$$O_2^+ + N_2 \rightarrow NO^+ + NO + 0.933eV \tag{1-2}$$
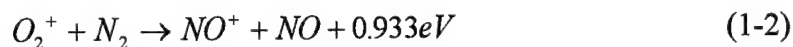
produces NO ions as well as neutral NO in vibrationally excited states (Billingsley, 1976). This reaction produces infrared radiation observable from the ground, and can be converted to absolute concentration of NO if we understand the emission rates and know the Einstein coefficients. To study emission rates, we must understand the spectral properties of NO, which requires knowledge of spectral line center positions, line strengths and line broadening methods (Ballard, 1988), and line shapes (Pine, 1985). To understand the line shapes, we must understand how the lines broaden.

For remote sensing of temperature in lasers, as well as for measuring flow fields (Vyrodov, 1995), NO has been considered as a "seed" gas due to its inherent stability (DiRosa, 1994). A seed gas is one that we add to our working medium, measure its spectral properties, and relate them to the environmental conditions. We can measure the broadening of the NO lines and relate it to the temperature using the Doppler width of the line (Rees, 1989).

Problem

Our goal in this study is to experimentally determine the pressure broadening coefficients (PBCs) for molecular oxygen (O_2) and nitric oxide (NO) using Fourier transform spectroscopy, both using the individual noble gases as collision partners. We then intend to plot the pressure broadening coefficients and pressure broadening cross sections as a function of rotational quantum number (J") and observe the pattern. The pressure broadening coefficient is expected to increase with decreasing J" (Ritter, 1987). We will also compare the pattern in the PBC vs. J" plots to other researchers' data in the case of O_2. There will be no comparison for NO since there has been no other research in this area, although we still expect the same type of pattern as with O_2 (Ritter, 1989). We will also compare the effects of the different collision partners and attempt to explain them.

Theory and Background

Line Broadening

We often imagine spectral lines to be perfect delta functions, that is, a certain energy transition emitting (or absorbing) *one* frequency of radiation. However, spectral lines exhibit natural broadening, Doppler broadening and collisional broadening. In this study, we are concerned with collisional broadening, but we must understand natural broadening and take Doppler broadening into account in our collisional broadening calculations.

Spectral lines would be delta functions if the emitted wave were an infinite wave train. In fact, the wave pulse has a start and an end. The Heisenberg uncertainty principle states that we cannot simultaneously know the energy levels' exact values and the start and end time of a transition:

$$\Delta E \Delta t = h \tag{1-3}$$

If we relate this to frequency instead of energy,

$$\Delta v = \frac{1}{2\pi t} \tag{1-4}$$

we can determine the natural line width by converting frequency to wave number. Here, t is the state lifetime (Rees, 1989). The spectral *intensity* distribution of the natural line width is Lorentzian (Rees, 1989):

$$\phi_N(v) = \frac{\Delta v_N / 2\pi}{(v - v_0)^2 + (\Delta v_N / 2)^2} \tag{1-5}$$

4

where v_0 is the line center frequency, and Δv_0 is the line width at half maximum as shown in Figure 1-1.

Doppler broadening is due to the fact that the molecules in a gas move randomly in direction and exhibit a Boltzmann distribution of velocities. Molecules moving in different directions will absorb slightly different frequencies off line center. At our operating temperatures (and in the thermosphere, where temperatures range from 300K down to 180K) Doppler broadening becomes significant (Rees, 1989). The distribution of frequencies is Gaussian centered on the line center frequency. The full width at half maximum (FWHM) is related to the temperature by this relation: (Rees, 1989)

$$\Delta v_D = v_0 \sqrt{\frac{8 k_B T \ln 2}{m c^2}} \tag{1-6}$$

where k is Boltzmann's constant, m is the mass of the absorbing or emitting species, and v_0 is the line center in wave number (Rees, 1989). Doppler broadening exhibits a Gaussian distribution of spectral intensity, where M is the mass of O_2, v is the energy in wave number units and v_D is the doppler width in wave number units. (Rees, 1989):

$$\phi_D(v) = \frac{c}{v_0} \sqrt{\frac{M}{2 \pi k_B T}} \exp \left[\frac{-(v - v_0)^2}{\frac{2 k_B T v_0^2}{M c}} \right] \tag{1-7}$$

Collisional (pressure) broadening happens in high density situations where the time between collisions is less than the time between the start and end of an emission due to a transition between energy levels. The collision interrupts the emission event. This

introduces a broadening of the line around the line center in a Lorentzian profile, with the same form as with natural broadening (Rees, 1989):

$$\phi_P(v) = \frac{\Delta v_P / 2\pi}{(v - v_0)^2 + (\Delta v_P / 2)^2} \tag{1-8}$$

where Δv_P is the line width due to collisions. In collisional broadening, the line width is proportional to the mean collision frequency (Rees, 1989):

$$\Delta v_P = f_P / 2\pi \tag{1-9}$$

Now, when we measure the width of a spectral line, we must take into account all of these broadening methods when we determine the line shape. The two Lorentzian functions add to give us another Lorentzian. Then when we superimpose the resulting Lorentzian and the Gaussian distributions, we are in effect broadening each element of the Lorentzian curve by a Gaussian function. A convolution of the two gives us our Voigt profile (Jansson, 1984):

$$\phi_V = \frac{1}{\Delta v_D} \sqrt{\frac{\ln 2}{\pi}} \frac{\mu}{\pi} \int_{-\infty}^{\infty} \frac{\exp(-t^2)}{\mu^2 + (\zeta - t)^2} \tag{1-10a}$$

$$t = \frac{x - v_0}{\sqrt{2}\Delta v_P} \tag{1-10b}$$

$$\mu = \sqrt{\ln 2}\frac{\Delta v_P}{\Delta v_D} \tag{1-10c}$$

$$\zeta = \sqrt{\ln 2}\frac{v - v_0}{\Delta v_D} \tag{1-10d}$$

6

As an example, Figure 1-2 depicts Voigt curves with different ratios of Lorentzian and Gaussian half widths using (Rees, 1989):

$$ratio = \sqrt{\ln 2} * \frac{\Delta v_L}{\Delta v_D} \qquad (1-11)$$

where Δv_L is the addition of natural and collisional broadening half widths and Δv_D is the Doppler half width. In Chapter 2.2 we will cover the use of this equation in data analysis.
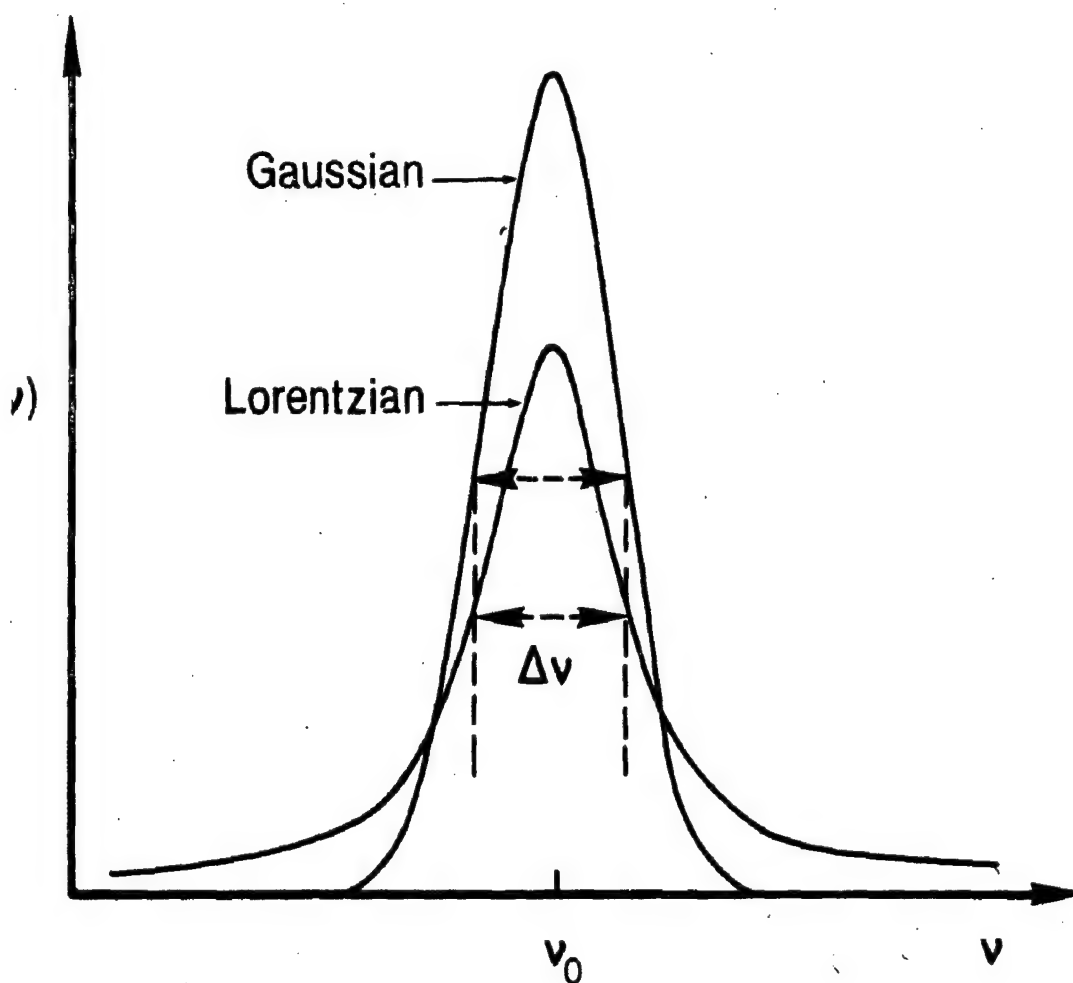
Figure 1-1: Comparison of Lorentzian and Gaussian line profiles. The two curves have the same equivalent width, the same area, and the same half width value (Rees, 1989).
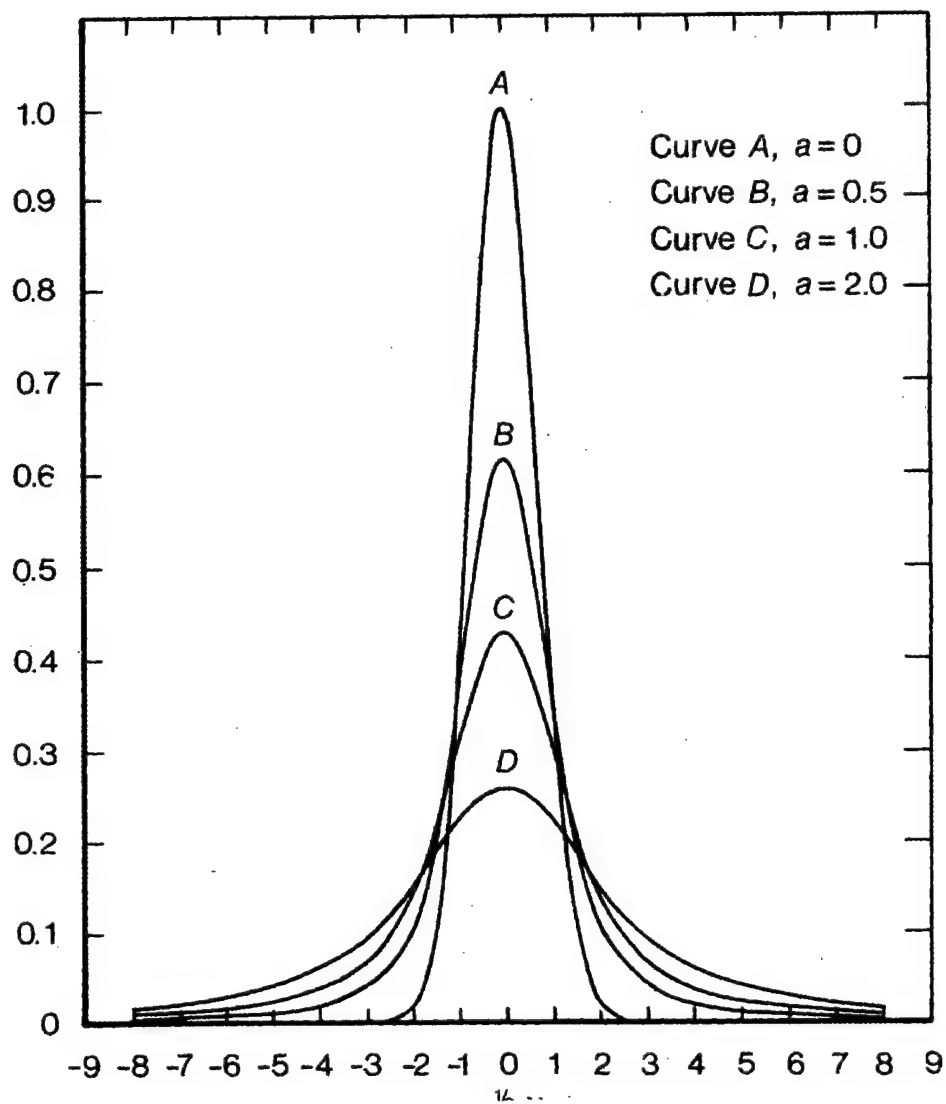
Figure 1-2: Normalized Voigt profiles for a range of ratios of the Lorentzian to Doppler half widths. Here, the x-axis is frequency (wave number) and the y-axis is amplitude. (Rees, 1989).

Spectroscopy

The O_2 absorption transition we are studying is the $X\,^3\Sigma_g^- \rightarrow b\,^1\Sigma_g^+$ electronic transition from the ground state to the second electronically excited state (see Figure 1-3) and is centered at 13123 cm^{-1} or 762 nm (Rees, 1989). One notices from a rough measurement of the potentials' energy differences that the $X \rightarrow b$ transition requires ~1.6 eV which upon conversion gives us ~13,000 cm^{-1} which is about where our transition lies (Rees, 1989).

The b state has a radiative lifetime of 7-12 s. (Kearns, 1971). This transition is the $(v''= 0) \rightarrow (v'= 0)$ vibrational change. We see this transition in the upper atmosphere, and it is often called the oxygen A-band. (Kearns, 1971). Molecular oxygen has no electric dipole moment and a very small quadrupole moment, but the transition is not a quadrupole-quadrupole interaction (de Angelis et. al., 1996). The $X \rightarrow b$ is a magnetic-dipole transition (de Angelis et. al., 1996).

The ground state of O_2 has a total spin, S, of 1. This gives us an electron spin angular momentum (Σ) of 1, 0, -1, which describes a spin multiplicity $(2\Sigma + 1)$ of 3. The molecule has electron orbital angular momentum component parallel to the internuclear axis (Λ) of 0 giving us the "Σ" state. (Herzberg, 1950). Repeating this procedure for the b state (no unpaired electrons), we get $S = 0$, $\Sigma = 0$, spin multiplicity of 1, and $\Lambda = 0$. Like the ground state, the b state is a Σ state.

Since O_2 is a homonuclear diatomic molecule, any plane that cuts through the internuclear axis is a plane of symmetry (Herzberg, 1966). The eigenfunctions of the S states depend on the relative azimuths of the electrons. (Herzberg, 1966). The ground

state has two unpaired electrons, and since Σ states are non-degenerate, the electronic eigenfunction changes sign on reflection across these planes, giving us the Σ^- designation. Since the b state has no unpaired electrons, the eigenfunction will not change sign on reflection, giving us the Σ^+ designation. The fact that O_2 is homonuclear tells us that the molecule has a center of symmetry along the internuclear axis, and hence, even symmetry. This gives us the Σ_g designation on both states, which, in German, is "gerade" or even.

Since $\Lambda = 0$ and $S \neq 0$, the spin vector S is not coupled to the internuclear axis (Herzberg, 1966). Therefore, since O_2 is a homonuclear molecule, it follows Hund's case (b) coupling (See Table 1-1 and Figure 1-4). Now, we calculate K, the total angular momentum including molecule rotation but excluding spin (Herzberg, 1966), using:

$$K = \Lambda, \Lambda + 1, \Lambda + 2, \Lambda + 3 \ldots \ldots \qquad (1\text{-}12)$$

Here, $\Lambda = 0$ which, according to Figure 1-4, makes K perpendicular to the internuclear axis and identical to N (Herzberg, 1966). K becomes 0,1,2,3,..... Now we can calculate J, the total angular momentum including spin by adding K and S vectorially like this (Herzberg, 1966):

$$J = (K + S), (K + S - 1), (K + S - 2) \ldots \ldots |K - S| \qquad (1\text{-}13)$$

which gives us integer values 0,1,2,3,4,...

For an absorption, the lower (start) level is J" and the higher (end) level is J'. So, for example, the line at 13098 cm^{-1}, which we label as J" = 7 is the rotational energy change from quantum number 7 in the X state to quantum number 6 in the b state. Since $\Delta J = -1$, this is a P-branch line. The line at 13140 cm^{-1} is an R-branch line with quantum number change from 7 to 8 ($\Delta J = +1$ for the R-branch). This is due to the Hund's case (b)

selection rules that govern the transition. Using the rules $\Delta J = -1$ for the P-branch and $\Delta J = +1$ for the R-branch, we can predict that the first P-branch line will be the $J'' = 2 \rightarrow J' = 1$ line and the first R-Branch line will be the $J'' = 1 \rightarrow J' = 2$ line. Note that the quantum number $0 \rightarrow 0$ rotational transition is not in the spectrum. There will be no Q-Branch since $\Delta J = 0$ is not allowed. (Burch et. al., 1969 and Hertzberg, 1966)
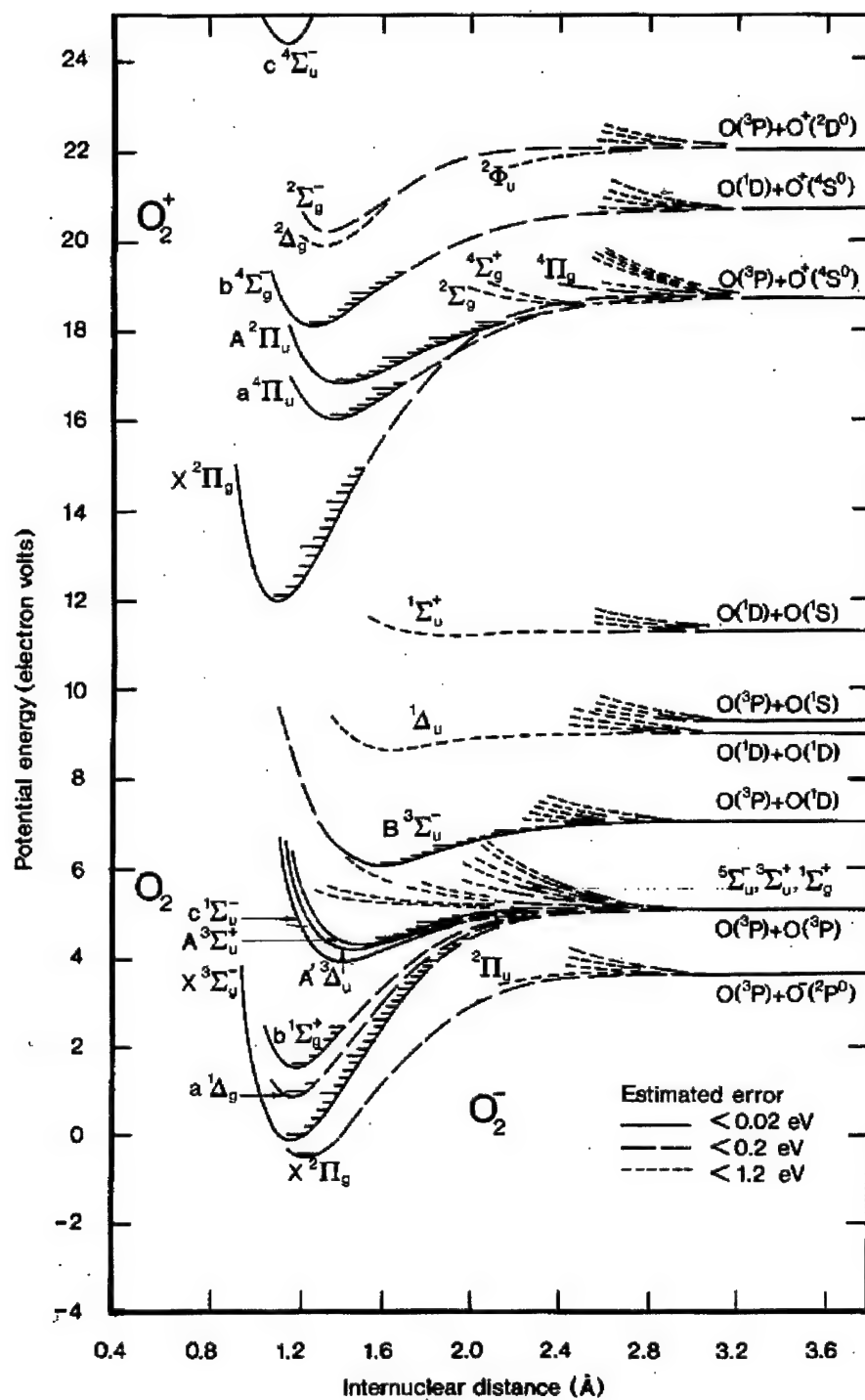
Figure 1-3: O₂ energy diagram (Rees, 1989).

Table 1-1: **Magnetic dipole selection rules for a homonuclear diatomic molecule obeying Hund's case (b) coupling. (Hertzberg, 1966)**

Total angular momentum.	$\Delta J = \pm 1$ but $\Delta J = 0$ forbidden
Total angular momentum excluding spin	$\Delta K = 0, \pm 1$ but $\Delta K = 0$ forbidden for Σ to Σ transitions
Electronic orbital angular momentum	$\Delta\Lambda = 0, \pm 1$ but $\Delta\Lambda = 0$ only for singlet/triplet transitions
Electronic wave function symmetry	$(+ \rightarrow +)$, $(- \rightarrow -)$, no $(+ \rightarrow -)$, no $(- \rightarrow +)$
Like nuclear charge symmetry	$(g \rightarrow g)$, $(u \rightarrow u)$, no $(g \rightarrow u)$, no $(u \rightarrow g)$
Identical nuclei symmetry	$(s \rightarrow s)$, $(a \rightarrow a)$, no $(s \rightarrow a)$, no $(a \rightarrow s)$
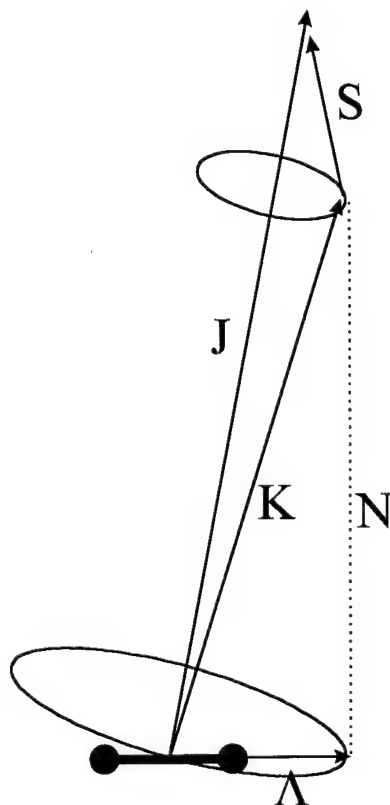
Figure 1-4: Hund's case (b) coupling
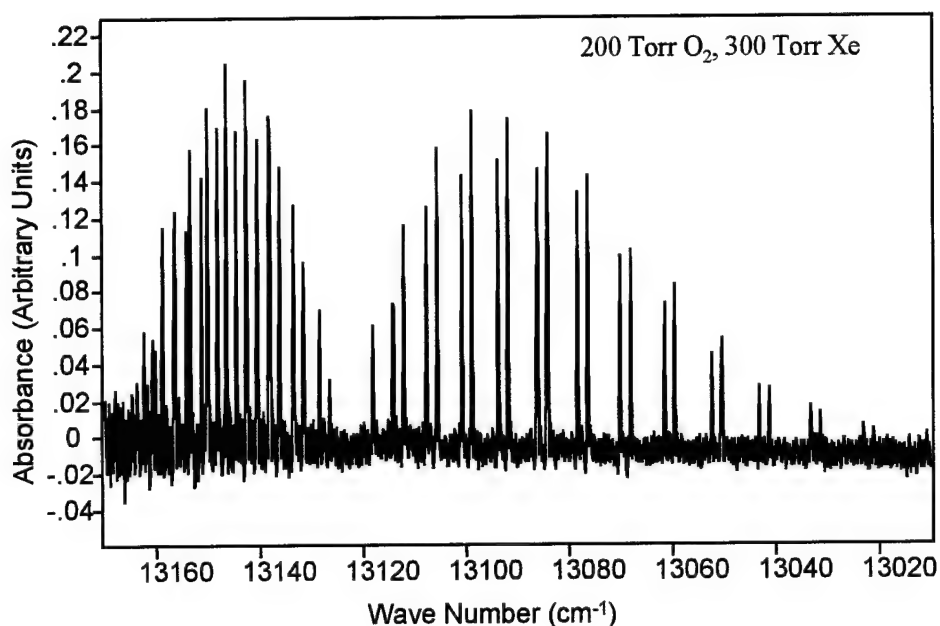
Figure 1-5: **Spectrum of X to b v"= 0 → v'= 0 transition in O₂.**

Table 1-2: **Line positions for X to b v"= 0 → v'= 0 transition in O₂ (Burch, 1969).**

P-Branch: $\Delta J = -1$			R-Branch: $\Delta J = +1$		
J"	J'	ν(cm^-1)	J"	J'	ν(cm^-1)
1	0	13118	1	2	13126
2	1	13114	2	3	13128
3	2	13112	3	4	13131
4	3	13107	4	5	13133
5	4	13105	5	6	13136
6	5	13100	6	7	13138
7	6	13098	7	8	13140
8	7	13093	8	9	13142
9	8	13091	9	10	13144
10	9	13086	10	11	13146
11	10	13084	11	12	13148
12	11	13078	12	13	13150
13	12	13076	13	14	13151
14	13	13069	14	15	13153
15	14	13068	15	16	13154
16	15	13061	16	17	13156.2
17	16	13059	17	19	13156.6
18	17	13052	19	18	13158.6
19	18	13050	18	21	13158.7
20	19	13042	21	20	13160.3
21	20	13041	20	21	13160.8

Figure 1-6 illustrates the transitions according to the selection rules. Note that, in reality, O_2 has four branches. What we call the P-branch in this study is made up of ^PP and ^PQ and what we call the R-branch is made up of ^RR and ^RQ. This is why the R-branch lines start overlapping. Note (- → -) transitions are not allowed due to nuclear spin. K" Is the total angular momentum quantum number. (Pope, 1997)
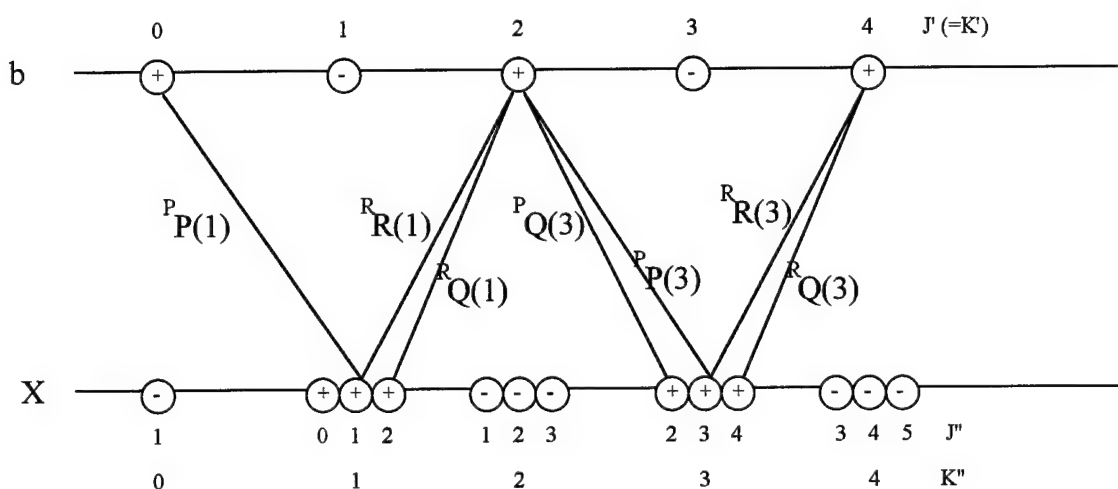
Figure 1-6: O_2 X → b electronic transition setup using selection rules (Herzberg, 1950)

With molecules that follow Hund's case (b), like O_2, we expect Λ-doubling of the spectral lines which is due to the interaction of the nuclear rotation and L, the orbital angular momentum. Remember, Λ is the orbital angular momentum component along the internuclear axis. However we expect no L-doubling of the lines with O_2 since L is perpendicular to the internuclear axis in Σ states (Herzberg, 1966).

The NO absorption spectrum we are studying is the first vibrational transition, designated "(v"=0) → (v'=1)," of the ground state (see Figure 1-7) This transition is centered at ~1880 cm^{-1}, which puts it in the infrared. Like with O_2, we can calculate the

energy requirement for the transition of .23 eV. As with O_2, we wish to categorize the states studied.

NO has a total spin (S) of 1/2. The electron spin angular momentum, Σ, is then 1/2 or -1/2. This gives it a spin multiplicity ($2\Sigma + 1$) of 2. The electron orbital angular momentum parallel to the internuclear axis, Λ, is 1 giving us a "Π" state (Herzberg, 1966). The electron orbital angular momentum and the spin angular momentum add to give us the total electron angular momentum, Ω, which can be parallel or antiparallel ($\Omega = \Lambda\pm\Sigma$) giving us 1/2 and 3/2. To calculate our J values which designate total angular momentum including electron spin, we use Ω, $\Omega + 1$, $\Omega + 2$, $\Omega + 3$.......So we have for the two states 1/2, 3/2, 5/2...for $^2\Pi_{1/2}$ and 3/2, 5/2, 7/2...for $^2\Pi_{3/2}$.

The NO rotational transition we are studying can be explained based on a Hund's case (a) description (Herzberg, 1966). Figure 1-8 and Table 1-3 show the coupling scheme. In transitions where $\Delta J = 0$ are allowed we expect a Q-branch, as well as P and R-branches using $\Delta J = -1$ and $\Delta J = 1$, respectively. From the J values we calculated we expect the first line of the P-branch to be J" = 2.5 for the 3/2 state and J" = 1.5 for the 1/2 state. The Q-branch should have its first lines at J" = 1.5 for the 3/2 state and J" = .5 for the 1/2 state. And, lastly, we expect the first line for the R-branch to be J" = 1.5 for the 3/2 state and J" = .5 for the 1/2 state. This pattern can be seen in Figure 1-9. This verifies the data found in Spencer, et. al, 1994. The spectrum and center frequencies of all the lines are listed in Figure 1-10 and Table 1-2.

With a closer look at Figure 1-10, one will notice that the spectral lines of the 1/2 and 3/2 states are split in two. This is the Λ-doubling discussed in the O_2 section and is

due to the interaction of the nuclear rotation and L, the orbital angular momentum. In this Π-state, L is not constrained to be perpendicular to the internuclear axis, so Λ is not 0. We expect the splitting to increase with increasing J. The two components are labeled e and f and have slightly different energies on the order of 0.01 cm^{-1} for the $\Omega = 1/2$ state and $.001$ cm^{-1} for the $\Omega = 3/2$ state (Herzberg, 1966). As we will see later, this means we can resolve the 1/2 state lines and not the 3/2 state lines. This gives us two lines to analyze for each J" for each state (1/2 and 3/2). This will be discussed in Chapter 2.
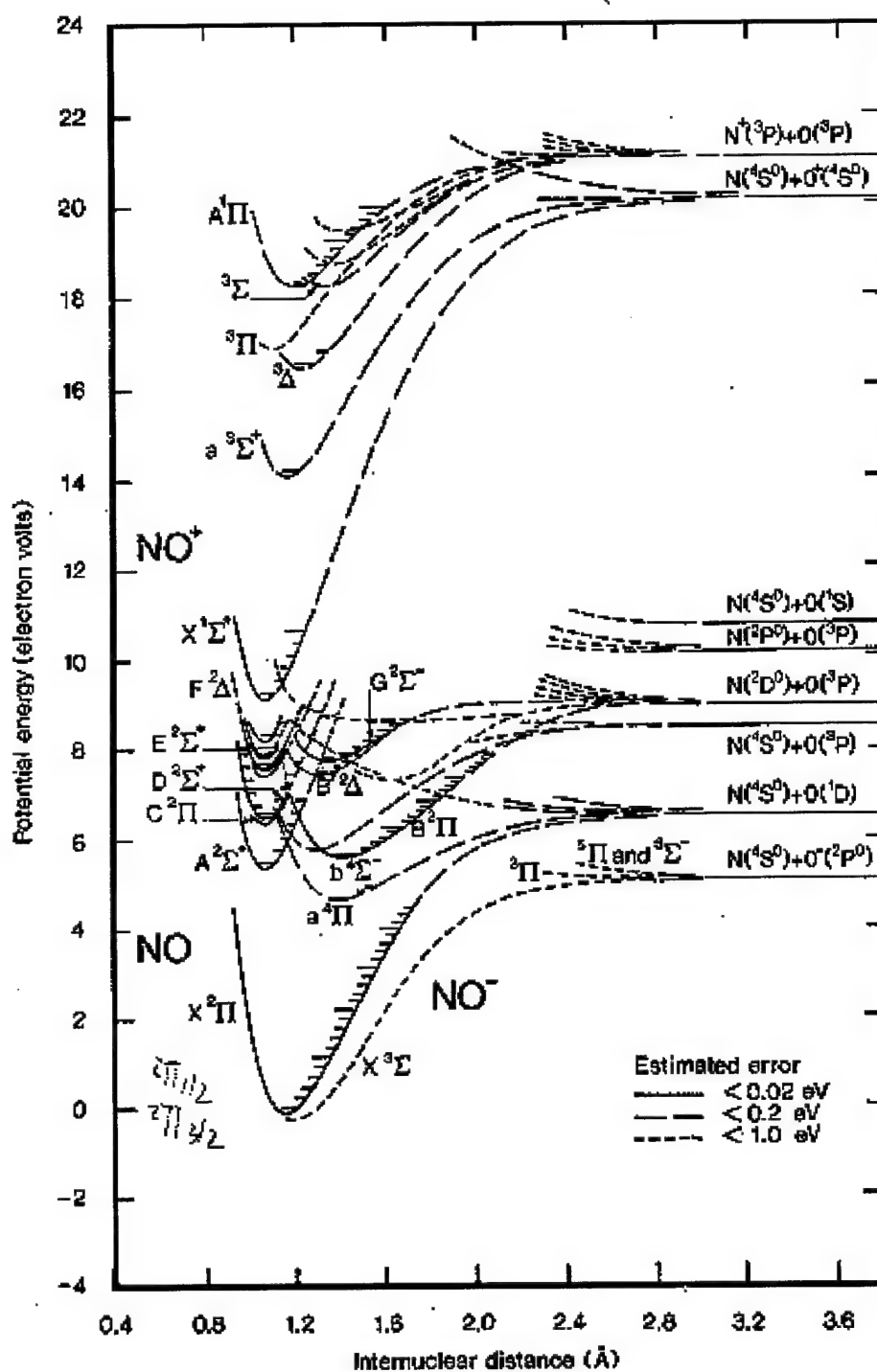
Figure 1-7: NO energy level diagram (Rees, 1989)

18

Table 1-3: Selection rules for a heteronuclear diatomic molecule obeying Hund's case (a) coupling. (Herzberg, 1966)

Total angular momentum.	$\Delta J = 0, \pm 1$ but no J" = 0 to J = 0
Total angular momentum excluding spin	$\Delta K = 0, \pm 1$ but $\Delta K = 0$ forbidden for $\Sigma \rightarrow \Sigma$ transitions
Electronic orbital angular momentum	$\Delta\Lambda = 0, \pm 1$ but $\Delta\Lambda = 0$ only singlet/triplet transitions
Electronic wave function symmetry	$(+ \rightarrow +)$, $(- \rightarrow -)$, no $(+ \rightarrow -)$, no $(- \rightarrow +)$
Like nuclear charge symmetry	$(g \rightarrow g)$, $(u \rightarrow u)$, no $(g \rightarrow u)$, no $(u \rightarrow g)$
Identical nuclei symmetry	$(s \rightarrow s)$, $(a \rightarrow a)$, no $(s \rightarrow a)$, no $(a \rightarrow s)$

Figure 1-8: Hund's case (a) coupling (Herzberg, 1966)

Figure 1-9: Spectral line comparison for the states of NO (Herzberg, 1966)

Figure 1-10: Spectrum of $v'' = 1 \rightarrow v' = 0$ transition in NO (500 mTorr NO, 40 Torr He).

21

Table 1-4:   Line center locations of v"= 0 → v'= 1 transition in NO. (Spencer, 1994).

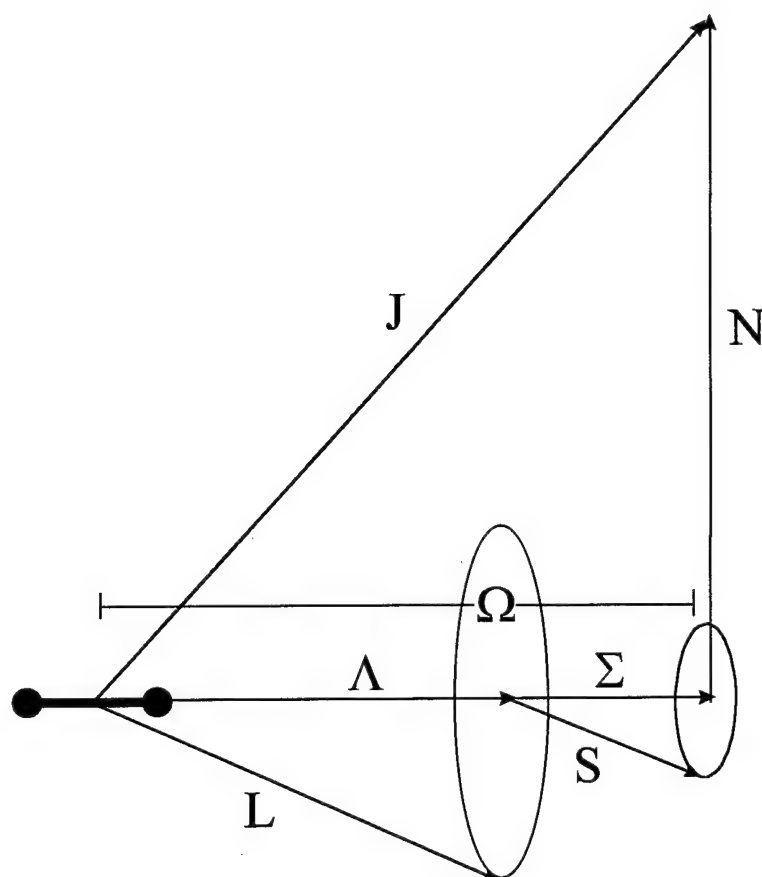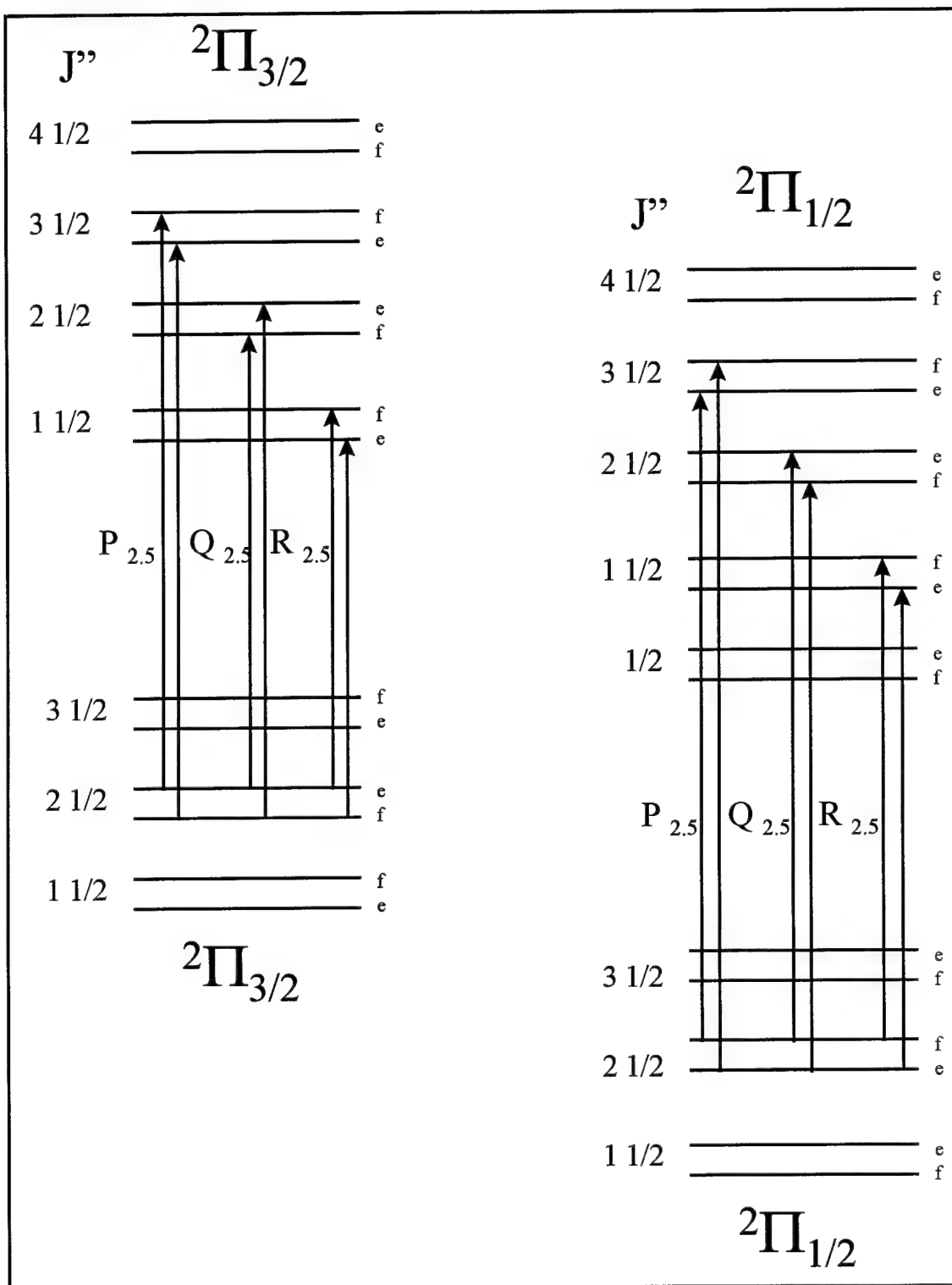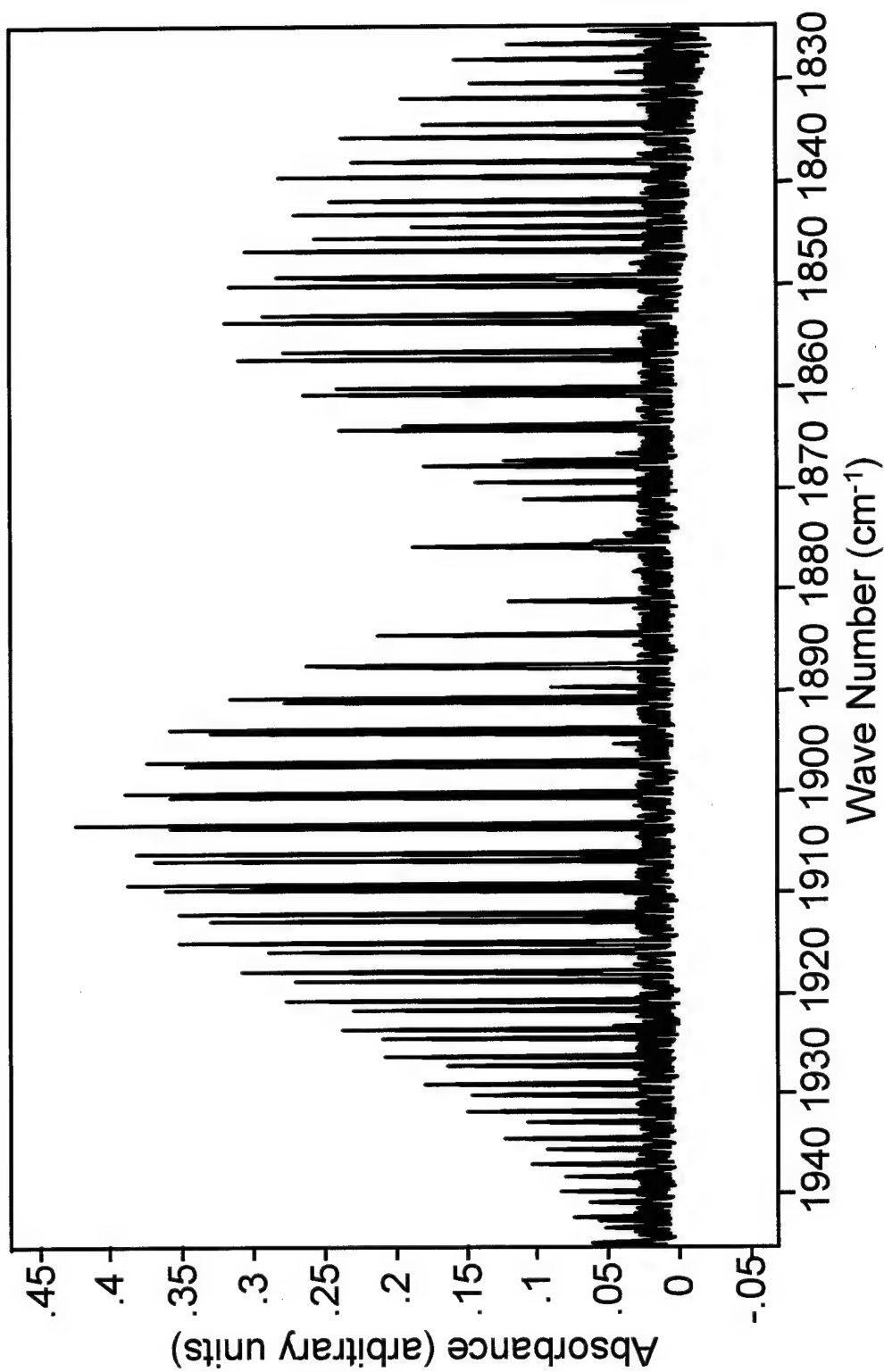| P-Branch state	J"	ν(cm^-1)	Q-branch state	J"	ν(cm^-1)	R-branch state	J"	ν(cm^-1)
3/2	18.5	1806.6539	3/2	5.5	1875.2351	3/2	0.5	no line
1/2	18.5	1808.6946	1/2	5.5		1/2	0.5	1881.0349
3/2	17.5	1810.6865	3/2	4.5	1875.4336	3/2	1.5	1884.2932
1/2	17.5	1812.6344	1/2	4.5		1/2	1.5	1884.3232
3/2	16.5	1814.6871	3/2	3.5	1875.5963	3/2	2.5	1887.5174
1/2	16.5	1816.5406	1/2	3.5	1875.772	1/2	2.5	1887.6363
3/2	15.5	1818.6553	3/2	2.5	1875.7226	3/2	3.5	1890.7072
1/2	15.5	1820.4129	1/2	2.5	1875.904	1/2	3.5	1890.9124
3/2	14.5	1822.5911	3/2	1.5	1875.8129	3/2	4.5	1893.8627
1/2	14.5	1824.2516	1/2	1.5	1876.001	1/2	4.5	1894.1515
3/2	13.5	1826.4941	3/2	0.5		3/2	5.5	1896.9839
1/2	13.5	1828.0563	1/2	0.5		1/2	5.5	1897.3531
3/2	12.5	1830.3644				3/2	6.5	1900.0706
1/2	12.5	1831.8271				1/2	6.5	1900.5171
3/2	11.5	1834.2016				3/2	7.5	1903.1228
1/2	11.5	1835.5639				1/2	7.5	1903.6434
3/2	10.5	1838.0055				3/2	8.5	1906.1405
1/2	10.5	1839.2666				1/2	8.5	1906.7318
3/2	9.5	1844.7759				3/2	9.5	1909.1234
1/2	9.5	1842.9352				1/2	9.5	1909.7821
3/2	8.5	1845.5127				3/2	10.5	1912.0716
1/2	8.5	1846.5697				1/2	10.5	1912.7939
3/2	7.5	1849.2155				3/2	11.5	1914.9848
1/2	7.5	1850.1701				1/2	11.5	1915.7674
3/2	6.5	1852.8842				3/2	12.5	1917.8631
1/2	6.5	1853.7363				1/2	12.5	1918.7021
3/2	5.5	1856.5185				3/2	13.5	1920.7061
1/2	5.5	1857.2682				1/2	13.5	1921.5983
3/2	4.5	1860.1181				3/2	14.5	1923.5139
1/2	4.5	1860.7661				1/2	14.5	1924.4554
3/2	3.5	1863.6827				3/2	15.5	1926.2862
1/2	3.5	1864.2296				1/2	15.5	1927.2735
3/2	2.5	1867.2122				3/2	16.5	1929.0229
1/2	2.5	1867.6592				1/2	16.5	1930.0526
3/2	1.5	no line				3/2	17.5	1931.7238
1/2	1.5	1871.0543				1/2	17.5	1932.7925
						3/2	18.5	1934.3888
						1/2	18.5	1935.4931

Historical Background

O$_2$ Study

No previous experimental work has been done on noble gas broadening of O$_2$ X $\rightarrow$ b spectral lines. However, work has been done on line strength measurement, width and shape measurement for O$_2$ self broadening and N$_2$ broadening of O$_2$. Theoretical work has been done on noble gas broadening, which gives us a basis for comparison with our experimental data.

Burch and Gryvnak (1969) carried out a series of experiments to measure the strengths, widths and shapes of the oxygen A-band lines using a grating spectrometer with an incandescent source and photomultiplier detector. They accurately mapped out the P- and R-branches out to J" = 30. Their half width measurements were done by calculating the integrated absorptance from the spectra and backing out the half width from that, although they noticed that problems arose using too high or too low pressure of O$_2$. Too low of a pressure over weighted the Doppler broadening by increasing the mean free path of the molecules to where a Lorentzian profile no longer was valid. Too high of a pressure introduced pressure broadening which we now know can broaden the lines so much that they become unresolvable. In the end they were able to compare O$_2$ and N$_2$ broadening and found that N$_2$ broadened lines were 1.06 $\pm$ .03 times wider then the self broadened lines. See Figure 1-11 for results of this study compared to other researchers discussed here.

An additional self broadening study was carried out by J. H. Miller, et. al. (1974) using a scanning grating spectrometer. Instead of using integrated absorptance to

determine the half widths of the lines, they used an iterative procedure whose initial value came from direct measurement of the widths of the digitized spectra. As we will see later, this is similar to our strategy. They used an alternate method of width determination for low pressures which took into account the Doppler width of the lines and used a Voigt profile. As we will see later, we incorporated Doppler widths into our data analysis and used a Voigt profile for all of our lines at all pressures. As with Burch et. al., they attempted N_2 broadening measurements, but found *no* difference in the broadening coefficients. See Figure 1-11 for results of this study compared to other researchers.

Other research on O_2 self broadening was done by Ritter and Wilkerson (1987). Their goal was to measure strengths, widths, and line shapes, and to calculate broadening coefficients. Improvements to spectroscopic analysis using a tunable dye laser allowed researchers to increase the resolution of spectra, where past researchers had to rely on white light sources and scanning grating spectrometers. Using the laser's narrow bandwidth ($<.0001$ cm^{-1}) the resolution increased to smaller than the Doppler width (.015) by an order of magnitude. Ritter and Wilkerson used a Voigt profile for their curve fitting algorithm. They found that use of the Doppler width was necessary, and took this requirement further by increasing the Doppler width share of the width by 4% to reduce the fit residuals. Their hypothesis is that the increase in Doppler width is the result of Dicke narrowing of the lines, which we will not explore in this study.

Ritter (1986) also completed a study of noble gas broadening which is directly related to this study in that his calculated values have never been experimentally verified. His Ph.D. dissertation covers his O_2 self broadening work and his theoretical noble gas

broadening work. The above paper he submitted covered only self broadening, and he has not published the noble gas work. He measured the broadening of a few lines and then used the mass of the foreign gas atom to modify the Galatry profile he used to fit the curves and calculate the widths and pressure broadening coefficients for the rest of the lines. We will compare our work to Ritter's since his is the only other data available. See Appendix A for diagrams of Ritter's noble gas broadening data compared with ours.

Pope (1997) completed an O_2 self broadening study using the same method of data collection and analysis used in our study. His values for the pressure broadening coefficients match the Miller group's self broadening data. Since we are using much of the procedure used by Miller et. al., this is a good sign. Pope's data is shown compared to other researchers in Figure 1-11.
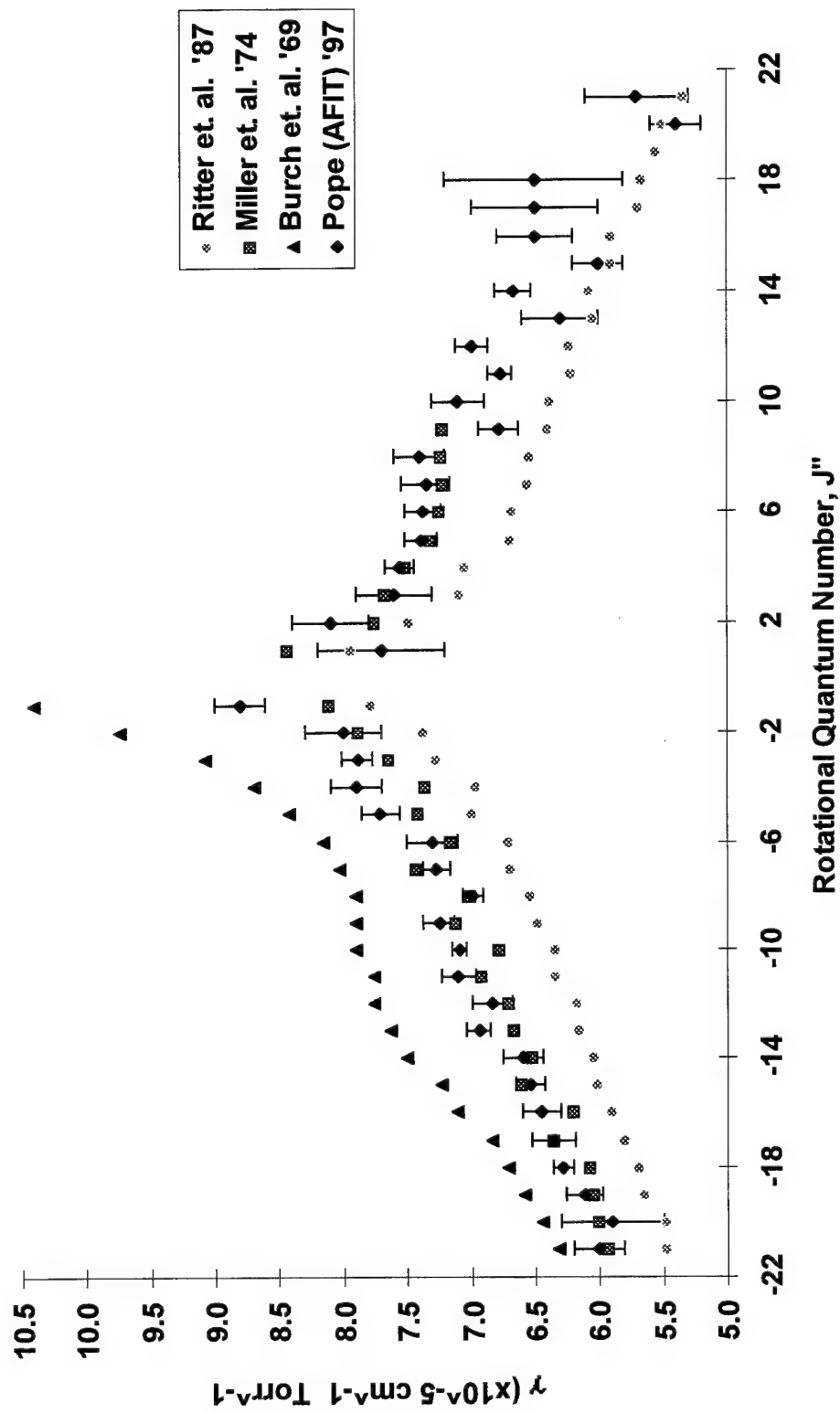
Figure 1-11: O_2 Self broadening by research group.

NO Study

Considerable amounts of work have been done on broadening in the A-X , fundamental vibrational (v"=1 $\rightarrow$ V'=0) and second vibrational (v"=2 $\rightarrow$ v'=1) bands of NO using many different collision partners. In particular we are interested in the fundamental band, but methods used in other studies are also of interest.

As far as the A $\rightarrow$ X band of NO, self broadening as well as foreign broadening using N_2, argon, and helium was studied in depth by A. O. Vyrodov et. al. (1994). He used a laser-induced fluorescence technique yielding broadening coefficients and line shape parameters. The second overtone was studied by Pine and Maki (1985) using tunable infrared laser system and they recorded line shape parameters for self and N_2 broadening.

For our study, we were interested in broadening of the fundamental band. Only self broadening and foreign broadening using N_2, O_2, and H_2O at room temperature has been previously examined. A studies of relevance to us is the self and N_2 broadening study by Ballard and Johnston (1988). This is significant in that the experimental method, as with ours, is Fourier transform spectroscopy. They measured broadening by N_2 and NO and compared line widths to J", but did not report broadening coefficients. The Ballard group is working on noble gas broadening with the goal of producing broadening coefficients. For coefficients for which to compare our work, the only study done so far is by Spencer et. al. (1994). They produced an expansive study of the NO fundamental band where they measured line shapes, widths and pressure broadening coefficients. They used Fourier transform spectroscopy with a similar setup to ours for gas handling and

pressure measurement. They chose to use long path lengths through the gas cell of 150 cm compared to our 11 cm cell, with NO pressures on the order of 10 mTorr compared to 500 mTorr in our study. What is significant is their data analysis scheme. They were not able to resolve the Λ-doubled 3/2 state lines but were able to resolve the 1/2 state lines. They assumed that the Λ-doubled lines must be equal and they locked the distance between the line centers for the fits. They used theoretical data provided by A. G. Maki and J. S. Wells for the line center distance data, but did not support the Λ-doublet intensity equality. As we will see later, this differs from our method.

Also of interest is a temperature dependent study of N_2 broadening of the fundamental band by M. N. Spencer et. al. in 1997. This study used the same setup a with their previously mentioned study, but they used cryogenically cooled cells to vary the temperature to atmospheric levels. We used this study as a reference for follow on work to ours.

II. Experimental

Apparatus

General Design

For our study, we used the Bomem DA8-002 Fourier transform spectrometer for both O_2 and NO. It is basically a Michelson interferometer with one beam path mirror on a movable track whose output beam is absorbed by the sample gas in the beam path. See Figure 2-1.
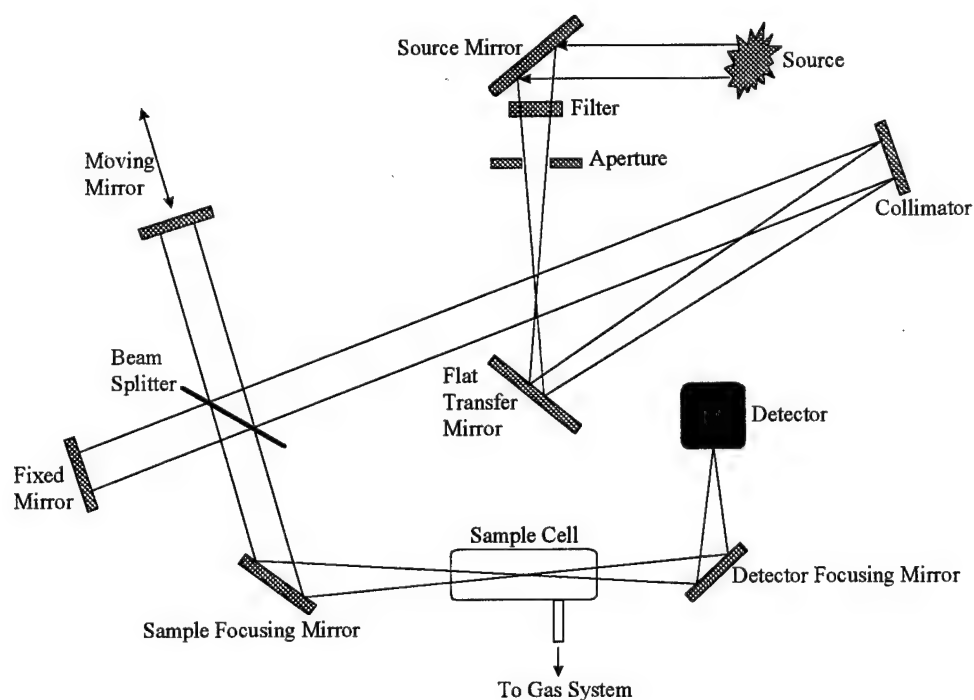
Figure 2-1: Spectrometer diagram (Bomem Spectrometer System Manual, Revision 3.2)

This section will cover how we used the spectrometer, not the theory of its operation, so see Appendix A for the theory behind Fourier transform spectroscopy. For the O_2 study we used a quartz halogen visible light source whose output is between 2500 and 25,000 cm^{-1}. We used a filter centered at 766.5 nm with a wavelength range of $\pm$ 10 nm which gave us a beam with wave number between 12850 and 13350 cm^{-1}. Our beam splitter was quartz visible with a range of 4000 to 25,000 cm^{-1}. Our detector was an amplified silicon avalanche type with range 9000 to 22000 cm^{-1}.

Next we had to choose our cell length and working pressure. We used Beer's Law:

$$I = I_0 \exp(-kx) \tag{2-1}$$

and rearranged it using the definition of absorption coefficient (Equation 2-2) and the ideal gas law (Equation 2-3):

$$k = n\sigma \tag{2-2}$$

$$n = P / k_B T \tag{2-3}$$

to get:

$$\frac{I}{I_0} = \exp\left[-\frac{P\sigma_{ABS}x}{k_B T} \right] \tag{2-4}$$

where x is the length of the cell, k is the absorption coefficient, and P is the pressure in Pascal. (Rees, 1989) σ_{ABS} is the absorption cross section which we had to find using the Einstein A-coefficient and the line shape partition function (g) (Verdeyen, 1982). The

Einstein A_{21} coefficient is the inverse of the state lifetime, τ. τ turns out to be 9 seconds (Kearns, 1971). To calculate σ:

$$\sigma(\nu_D) = \frac{A_{21}\lambda^2}{8\pi n^2} g(\nu) \qquad (2\text{-}5)$$

Here, n is the index of refraction (~1). We compute the line shape partition using (Verdeyen, 1982):

$$g(\nu_D) = \frac{1}{\nu_D}\sqrt{\frac{mc^2}{2\pi k_B T}} \qquad (2\text{-}6)$$

We calculated g to be 1 x 10^{-9}s. This gives us a cross section (σ_{ABS}) of 2.54 x 10^{-20} cm^2. This is the cross section for the entire band. Now we must factor in rotation of the molecule to calculate the cross secton for each line. This is done by multiplying the absorption cross section by the fraction of the population in each rotational level:

$$\sigma_\nu = \sigma_{ABS} f_J \qquad (2\text{-}7)$$

The *relative* populations of each rotational level is given by the multiplicity multiplied by the Boltzmann factor:

$$\frac{N(J'')}{N(0)} = (2J+1)Exp\left[\frac{-E_J}{k_B T}\right] \qquad (2\text{-}8)$$

where

$$E_J = B(J'')(J''+1) \qquad (2\text{-}9)$$

and B is the rotational constant which is known for each molecule (Herzberg, 1966). For O_2, B is 1.40041 cm^{-1} which gives us E_J of 154.05 cm^{-1} for the J'=10 line. To get the fraction of the population in each rotational level, we must divide the multiplicity and Boltzmann factor by the rotational partition function, Q_{ROT}:

$$Q_{ROT} = \frac{k_B T}{hcB} \qquad (2\text{-}10)$$

$$f_J = \frac{(2J+1)Exp\left[\dfrac{-E_J}{k_B T}\right]}{\dfrac{k_B T}{hcB}} \qquad (2\text{-}11)$$

where h is Planck's constant, c is the speed of light and B is the same rotational constant. For the J''=10 line, we find f_J to be 0.0775 (unitless). Now we adjust our cross section using equation 2-7. For the J''=10 line we get σ_v of 1.97×10^{-21} cm^2. See Figures 2-2 and 2-3. Notice how both the fractional populations and cross sections exhibit a Boltzmann distribution with J''. The peak absorption at this temperature is at the J''=10 line, but at higher temperatures, we expect this peak to shift to higher J''.

We would like a usable absorption, and one e-fold is a good number to start with. Going back to our Beer's Law equation, and using one e-fold,

$$P = \frac{k_B T}{\sigma x} \qquad (2\text{-}12)$$

we get a pressure of 155 Torr of O_2 for a 10 m cell at the J''=10 line. See Figure 2-4 for a plot of pressure needed for an e-fold absorption vs. J''. Notice how it exhibits an inverse Boltzmann distribution. We used these as a start and ran a few spectra at different pressures of O_2 with no broadening gas. We found that with this particular spectrometer and cell we needed 200 Torr to give us a 50% absorption for most lines. Figure 2-5 is a diagram of the 10m multipass cell. We set the mirror to move 0.5 cm/s and used the spectrometer's detector gain and software gain "4" feature to increase intensity on the

detector. To increase signal-to-noise ratio, we used 100 scans (coads) of the movable mirror for the lower pressures of broadening gas and 400 scans for the higher pressures. We used trial and error to determine the best procedure. We used a 1000 Torr Baratron head with an MKS digital display to monitor the pressure in the cell and gas manifold. The gases were stored in bottles connected to the manifold via high vacuum fittings, valves and lines.

For the NO study we used an infrared source whose output is between 200 and 10000 cm^{-1}. We used a filter centered at 5.2 μm with a transmission wave number range of 1750-2200 cm^{-1}. Our beam splitter this time was calcium fluoride (CaF_2) with a transmission range of 1200 to 8500 cm^{-1}. Our detector was a liquid nitrogen cooled MCT type with a sensitivity range of 800 to 5000 cm^{-1}. Again, these were chosen to be centered on our transition at 1880 cm^{-1}.

With NO we used the same type of calculations as with O_2, only we used the A_{10} Einstein A-coefficient as 10.78 (Verdeyen, 1982). We calculated 120.15 for the rotational partition function value (Q), and 7×10^{-9}s for the line shape partition function value (g). This gives us a cross section (σ_{ABS}) 9.062×10^{-16} cm^2, which is much larger than O_2, hence the shorter cell. Using the same formulas for rotational energy distribution and Beer's law we arrive at cross sections on the order of 7×10^{-17} cm^2, and working pressures of tenths of Torr of NO with an 11cm cell. Figures 2-6,2-7 and 2-8 show the distributions of fractional populations, cross sections and pressures for NO. Note the same Boltzmann distributions as with O_2. Figure 2-9 is a diagram of the NO cell.

Mirror speed was set at 0.5 cm/s and used the spectrometer's software gain "4" feature to increase intensity on the detector. To increase signal-to-noise ratio, we used 32 scans (coads) of the movable mirror for the low pressure broadening and 100 scans for the higher pressures. NO broadening increases fast with increasing pressure so we had to keep SNR down. We used a 1000 Torr Baratron head with an MKS digital display to monitor the pressure in the cell and gas manifold.

Now that we had working pressures of gas, we planned our study with representative points of broadening gas pressure and collected the data. For O_2 we chose broadening gas pressures from 100 to 400 Torr at 50 Torr increments with an O_2 pressure of 200 Torr. For NO we chose broadening gas pressures of 10, 25, 40, and 55 Torr with an NO pressure of 0.5 Torr. For the O_2 study we used all of the noble gases except helium and radon as collision partners (Rob Pope used helium as part of his self-broadening study), and we included nitrogen to make things interesting. For the NO study we used all of the noble gases except radon. These broadening gas pressures were chosen by trial and error by observing the spectra and determining if the broadening was too high or low for accurate measurement by our curve fitting program. For purity control we chose broadening gases of research quality 5.0 or greater (better than 99.997%) purity, used high purity regulators, and used high vacuum lines and fittings. Any losses or gains of pressure were noted and those spectra were discarded and repeated. After we collected the data we examined it for anomalies, such as abnormally low signal to noise ratio, uneven spectrum baseline, warped or asymmetrical peaks, etc. We fixed low signal to noise ratio spectra by running the measurement with 100 scans (coads) of the

spectrometer for the higher pressures. To ensure zero baselines, we ran 100 scan measurements with the cell at vacuum, at low resolution before each gas measurement. This allowed us to choose the best background spectrum to match the envelope of each measurement spectrum.

Figure 2-2: Boltzmann distribution of fractional populations in O_2 rotational levels.

36

Figure 2-3: Boltzmann distribution of cross sections for O_2.

37
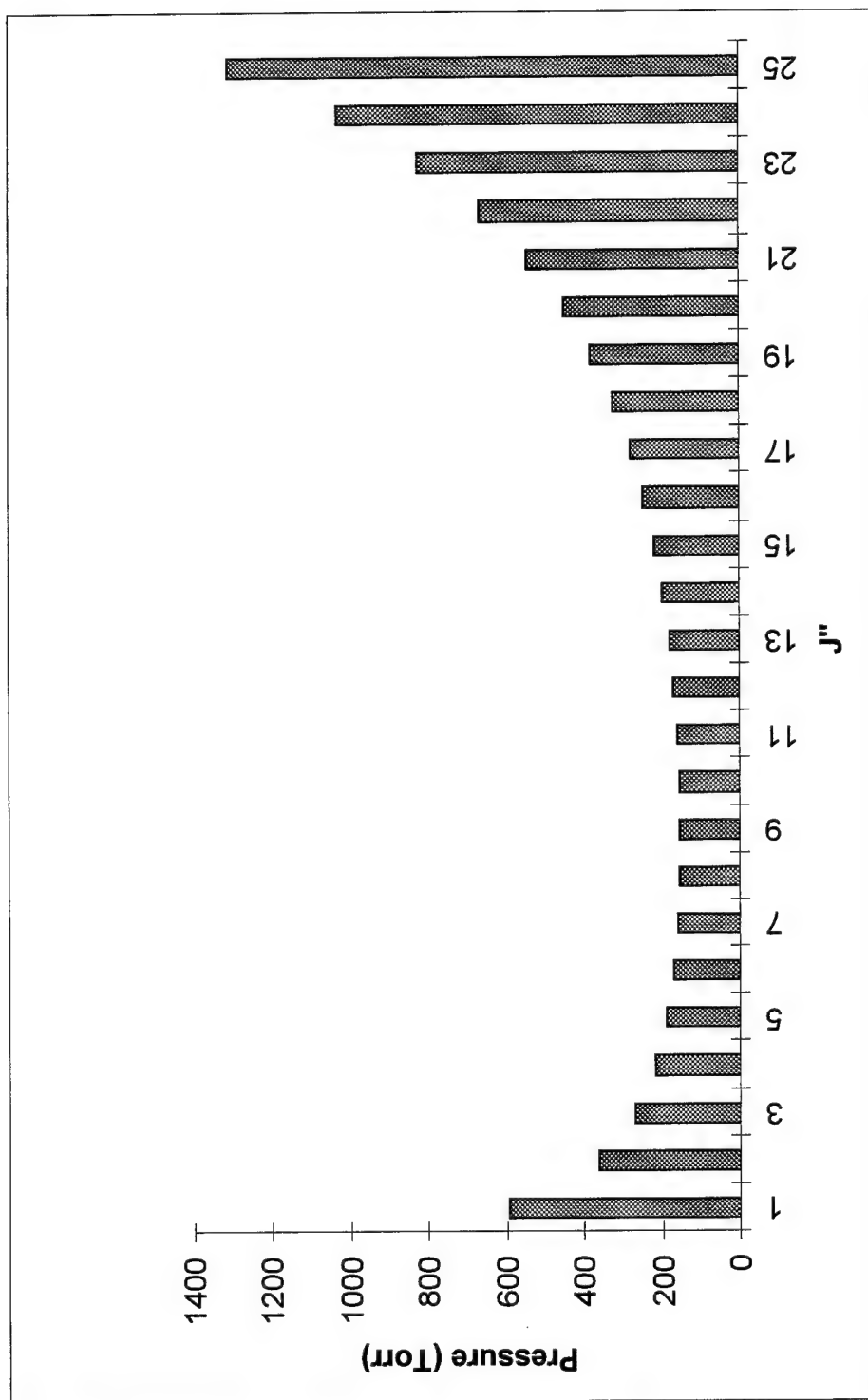
Figure 2-4: Pressures for one e-fold absorption for the spectral lines of O_2.

38

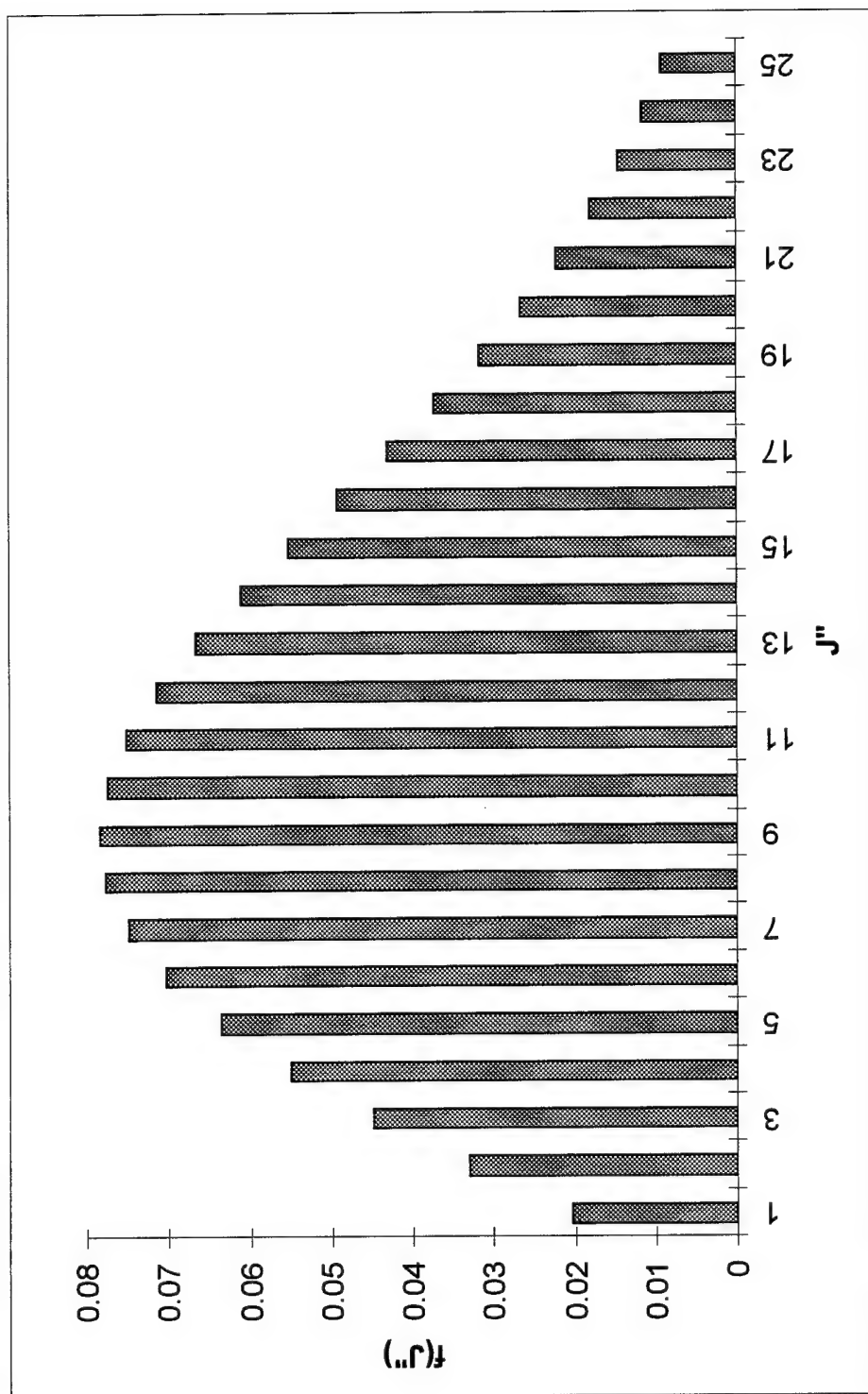**Figure 2-5: O₂ multipass cell and gas system.**

39
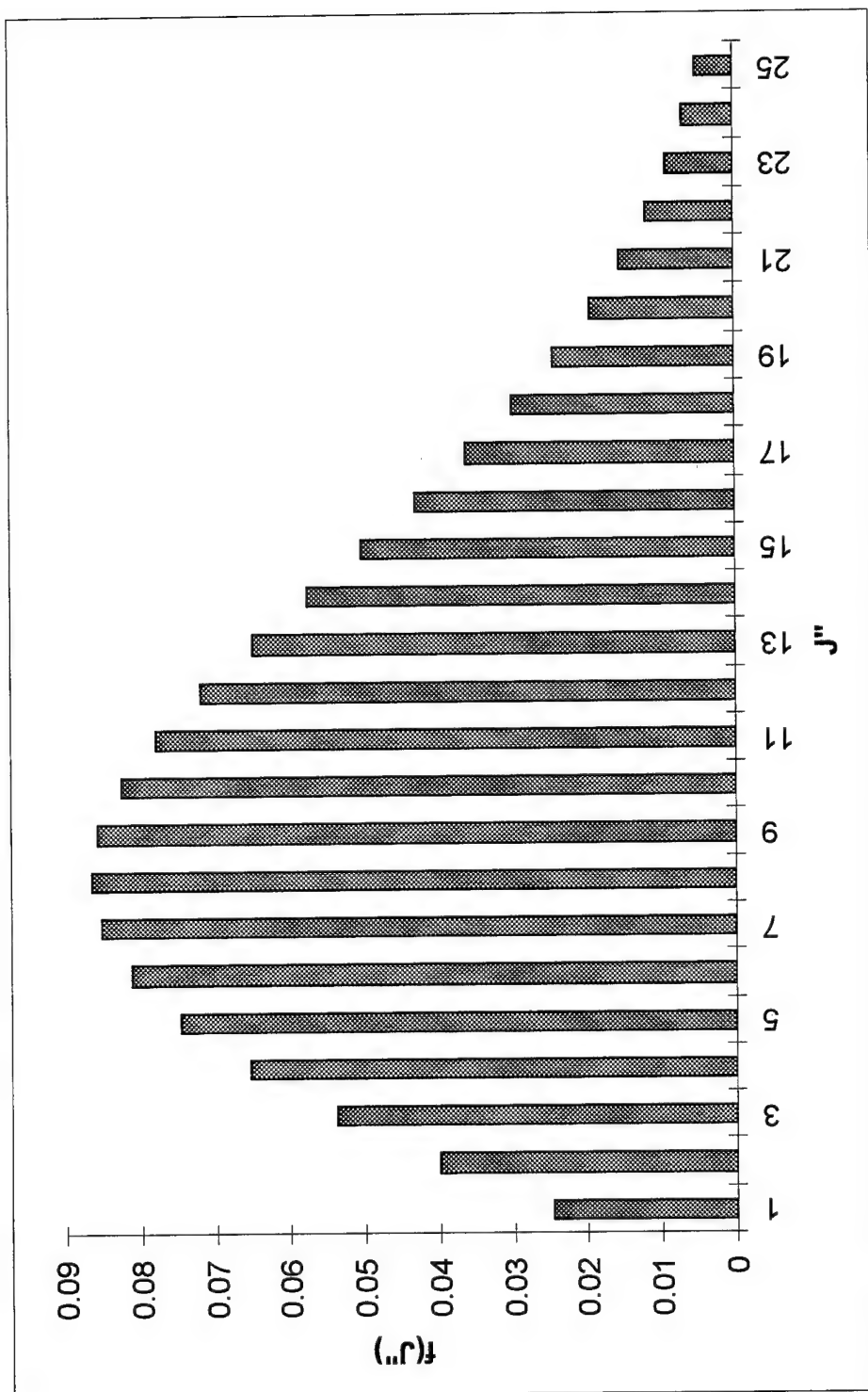
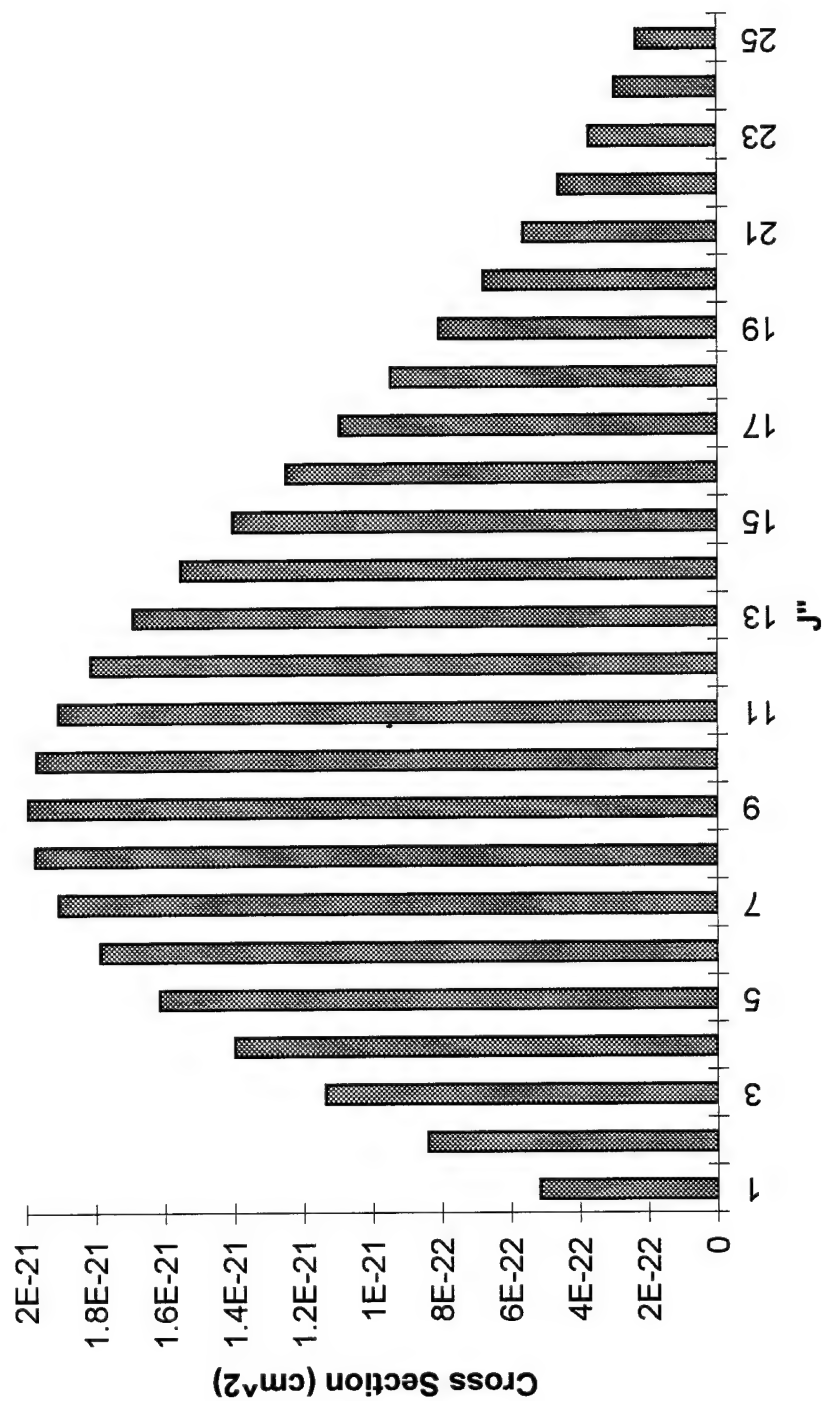Figure 2-6: Boltzmann distribution of fractional populations in NO rotational levels.

40

Figure 2-7: Boltzmann distribution of cross sections for NO.

41
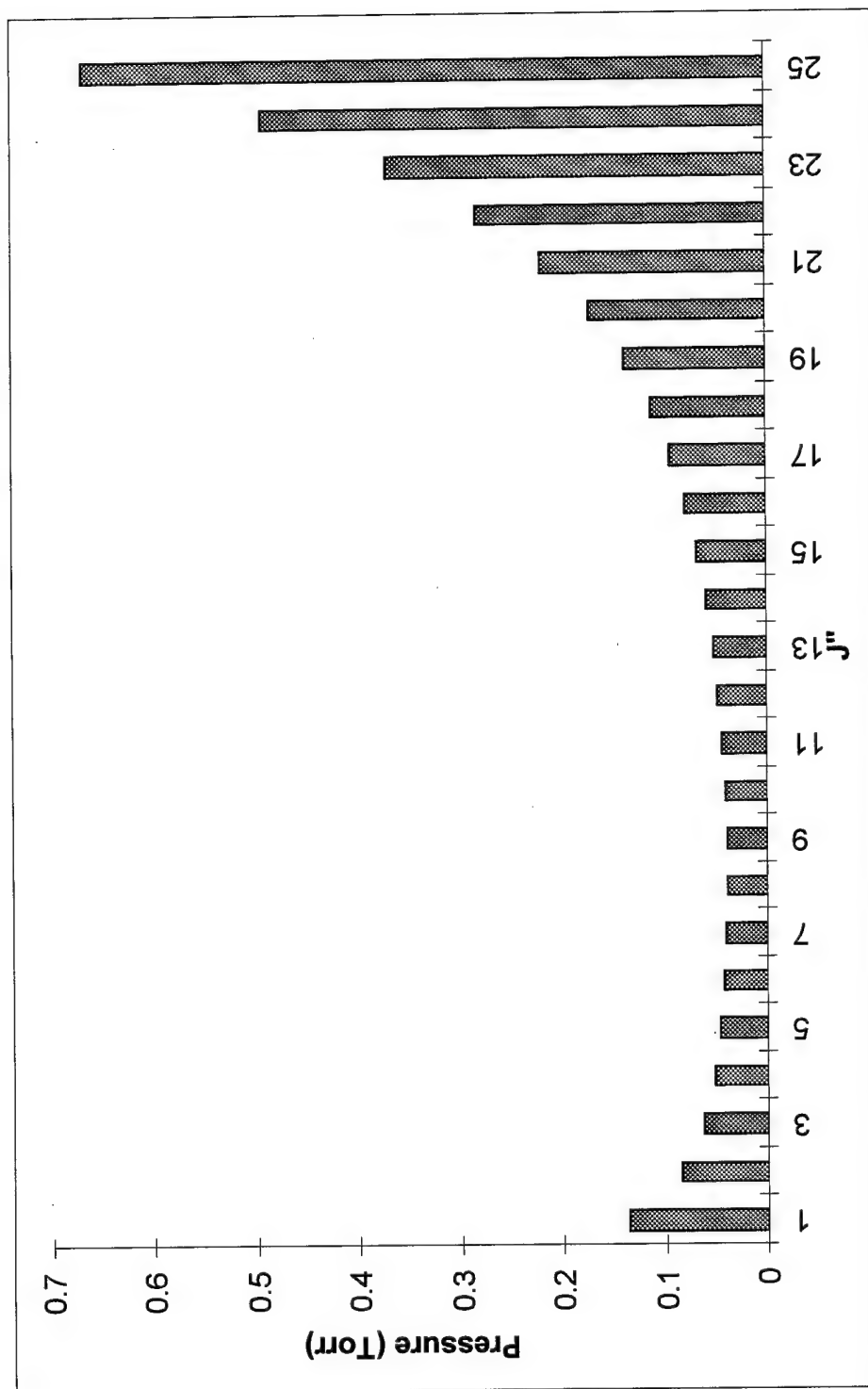
Figure 2-8: Pressures for one e-fold absorption for the spectral lines of NO.

42

Beam From Source
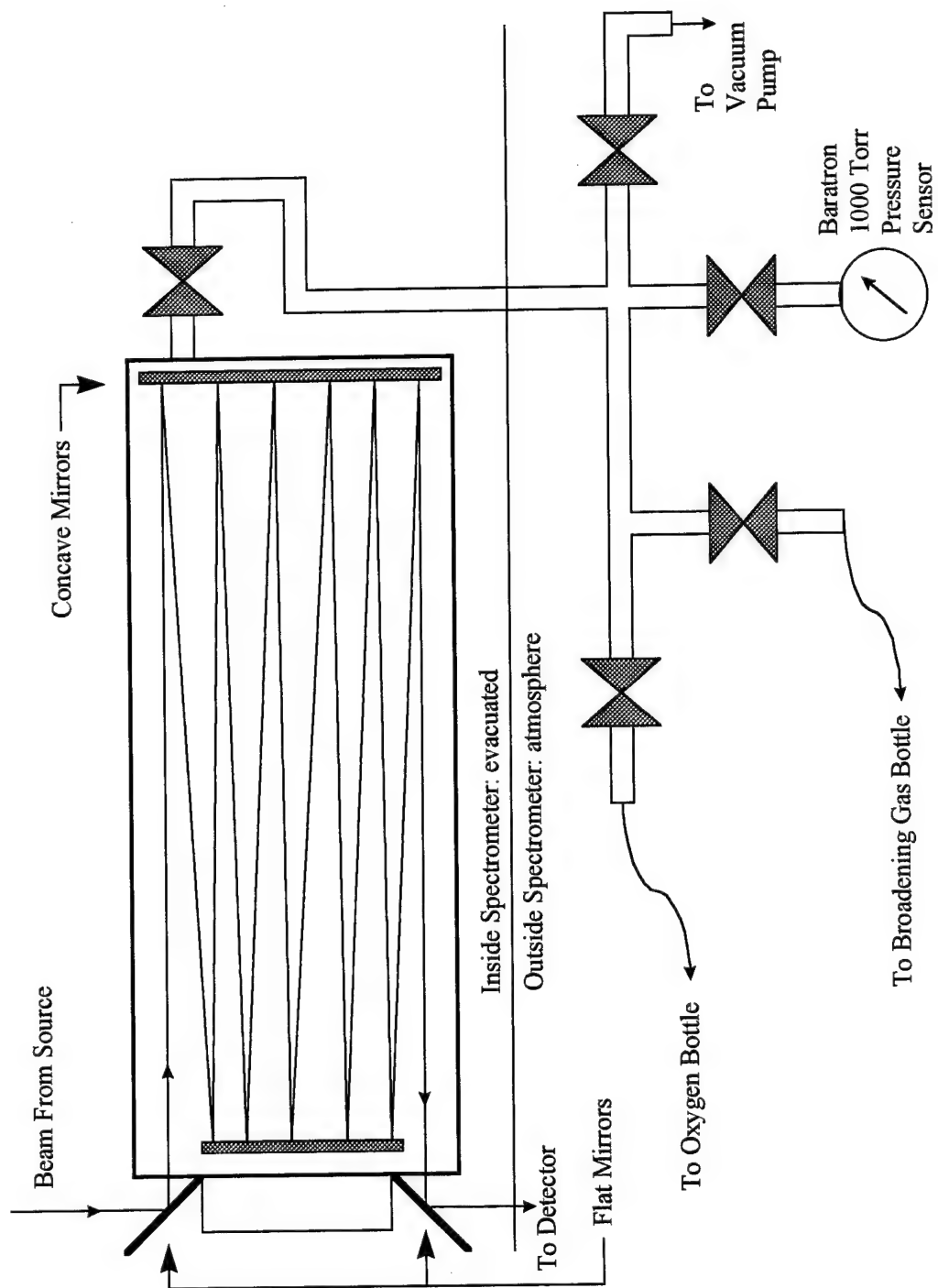
CaF$_2$ Windows

To Detector
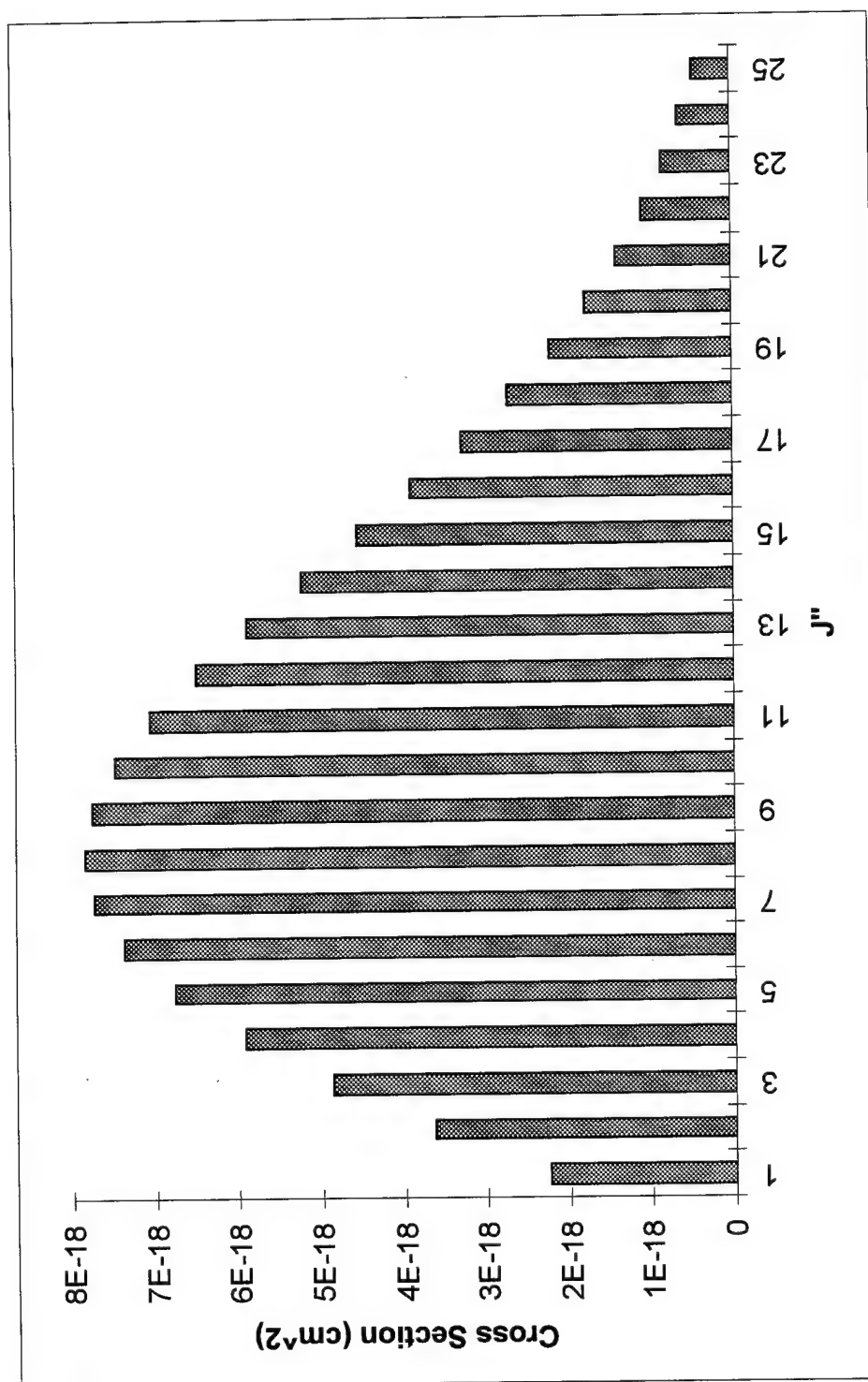
Inside Spectrometer : Evacuated

Outside Spectrometer : Atmosphere

To Vacuum Pump

Baratron 10, 1000 Torr Pressure Sensors
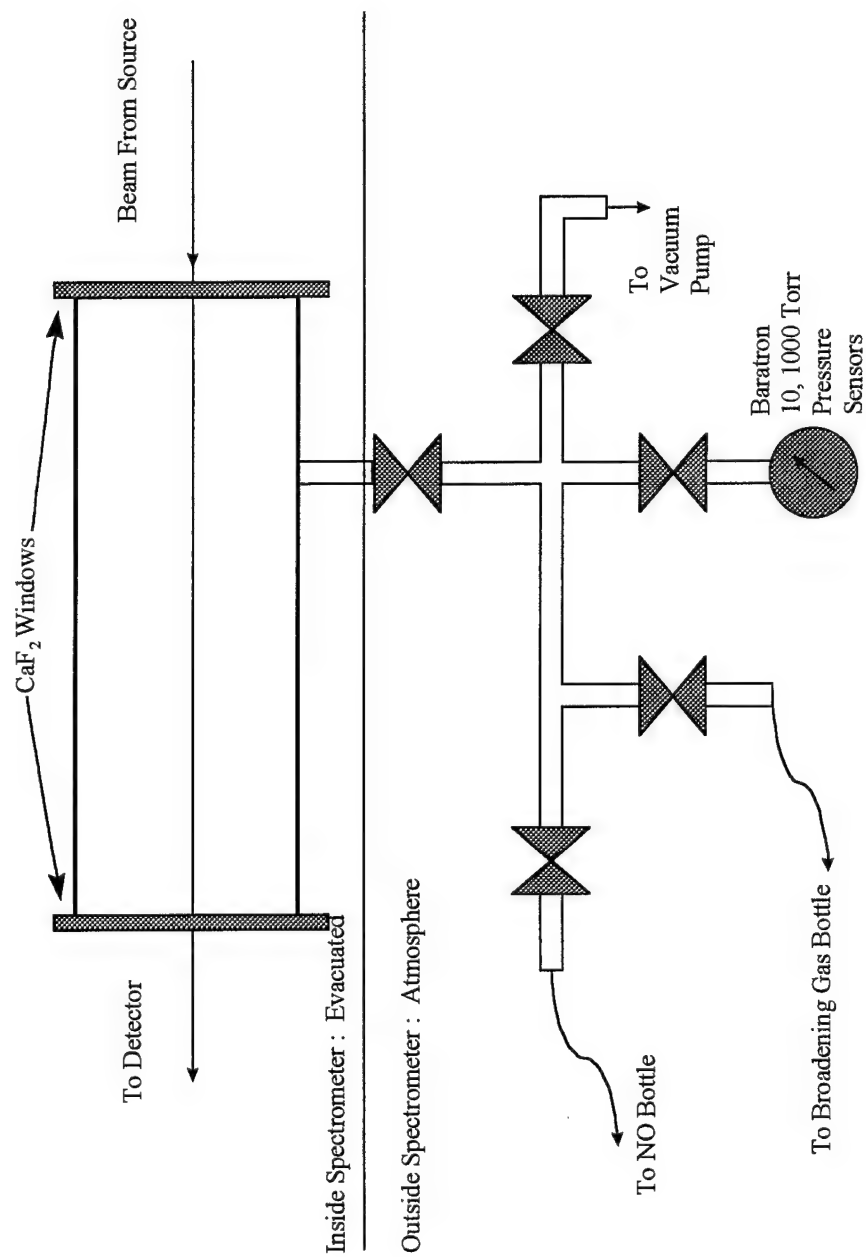
To NO Bottle

To Broadening Gas Bottle

Figure 2-9: NO cell and gas system.

43

Data Analysis

After collecting the data (spectra) we needed to measure the Lorentzian half width at half maximum (HWHM) of all of the lines, sorted by rotational quantum number, J". Then we had to plot HWHM against pressure for each line. By measuring the slope of this plot, we get the pressure broadening coefficients (PBC) for each line (Spencer, 1994). We then needed to plot PBC vs J" for each broadening gas and compare the pattern to other researchers' data in the case of O_2 (Spencer, 1994). For NO we just note the pattern and see if it makes sense with what we expect from quantum mechanics.

The raw spectra produced by the Bomem are actually transmission data, which we had to convert to absorption data using the Bomem software (Bomem system manual). This procedure is called "Absorption" and it subtracts out the background (filter) data and converts the data file to one which can be imported into our curve fitting program. We also need the data to be in terms of wave number (Peak Fit Manual), which is what the Bomem does anyway.

To measure Lorentzian HWHM, we used a curve fitting program called Peak Fit. The curve fitter uses the Voigt profile discussed in Chapter 1 (Jansson, 1984). We can rearrange Jansson's equation to match the equation used by Peak Fit if we assign parameters, a_1, a_2, a_3, and a_0 as follows:

$$a_1 = v_0 \qquad (2\text{-}13)$$

$$a_2 = \frac{\Delta v_D}{\sqrt{2 \ln 2}} \qquad (2\text{-}14)$$

$$a_3 = \Delta v_P \qquad (2\text{-}15)$$

44

$$a_0 = \frac{\alpha_0}{\pi\sqrt{2}} \frac{a_3}{a_2} \tag{2-16}$$

So we get, for the rearranged Jansson's equation:

$$y = \frac{a_0}{a_2\sqrt{2\pi}} \int_{-\infty}^{\infty} \frac{\exp(-t^2)dt}{\dfrac{a_3^2}{2a_2^2} + \left[\dfrac{x-a_1}{a_2\sqrt{2}} - t\right]^2} \tag{2-17}$$

where a_0 is the area under the curve, a_1 is the line center in cm^{-1}, a_2 is the Gaussian width (Doppler width half width standard deviation), and a_3 is the Lorentzian HWHM. Note that parameter a_0 includes parameters a_2 and a_3. "α_0" is the actual area under the Voigt curve. When we adjust Peak Fit's "area" parameter, we are actually adjusting an algebraic shortcut including the real area (Peak Fit Manual and Jansson, 1984). To make Peak Fit's equation more understandable, we removed this shortcut:

$$y = \frac{a_3\alpha_0}{a_2^2 2\pi\sqrt{\pi}} \int_{-\infty}^{\infty} \frac{\exp(-t^2)dt}{\dfrac{a_3^2}{2a_2^2} + \left[\dfrac{x-a_1}{a_2\sqrt{2}} - t\right]^2} \tag{2-18}$$

This matches Jansson's equation more closely, although Peak Fit uses the shortcut.

When fitting the curves, we first let the program fit the two hidden baseline parameters while holding the four above mentioned parameters constant. We then hold the Doppler HWSD constant and let the other parameters vary as the program iterates. We calculated Doppler FWHM for the band center of our O_2 spectra (13100 cm^{-1}), using the procedure mentioned in Chapter 1 to be .0281 cm^{-1}. This gives us a Doppler HWHM of 0.0140 cm^{-1}. We use the half width standard deviation in our analysis (Bevington, 1992):

45

$$\sigma = \frac{\Delta\omega_d}{2\sqrt{2\ln 2}}$$

<div align="right">(2-19)</div>

which gives us a value of 0.0119 cm^{-1}. This is consistent with the value Pope used for his self broadening study, and since we chose to use his self-broadening data point for our "zero pressure" point, we can be consistent in our analysis. Using the same procedure for NO at the band center 1880 cm^{-1}, we calculated a Doppler FWHM of 0.0042 cm^{-1}, a HWHM of 0.0021 cm^{-1}, and a HWSD of 0.0009 cm^{-1}. Examples of fitted peaks, residuals and numeric output for O_2 and NO are in Chapter 4. We were able to observe the quality of the fit using the numerical data output and residuals with each fit. We looked for patterns in the residuals which would have signaled a fitting algorithm problem. For example negative residuals in peak center, positive residuals in wings would mean the peak is more Lorentzian than a true Voigt curve. Positive in the center and negative in the wings tells us that our line is more Gaussian than Voigt (Pope, private conversations). A high r^2 value close to unity meant a good fit as well as a low standard error in the Lorentzian width (Wolf, private conversations). We were able to extract the Lorentzian width and the standard error from the data for our next step. We sorted the fitted peaks according to J" number and branch in preparation for the next step.

After we curve fit all the peaks the next step was to calculate the pressure broadening coefficients for each J" line. We used a program called Table Curve to plot Lorenzian HWHM vs. rotational quantum number. We then used a least squares fit to a straight line over our points (Bevington, 1992). First, we had to assign weights to the points using:

$$Weight = \frac{1}{error^2} \tag{2-20}$$

using the standard error in the peak width (Bevington, 1992). Usually, the sum of the weights are normalized to unity, but Table Curve allows us to avoid that last calculation with an internal normalization procedure. Examples of these plots, the residuals and numeric data can be found in Chapter 4 with the results discussion. Again, we were able to monitor the fit quality with the numerical output data. A high r^2 meant a good fit. Using the residuals, we were able to watch for points which were more than 2 standard deviations away from the fit line, which would signal bad data..

Using functions built into Table Curve, we were able to extract the slopes of the lines (parameter B) which gave us the pressure broadening coefficients for each J" and the standard error which we used for the error bars (Spencer, 1994). We then plotted the pressure broadening coefficients vs. J" and observed the pattern. We also converted γ_0 to cross section, σ, and plotted these vs. J" and observed the pattern. We also compared σ to polarizability and reduced mass of the collision pair for each line.

III. Results and Discussion

O₂ Study

Spectrum Production

We inspected the spectra to determine whether or not they were usable. The line centers were in the proper places (Burch, 1969), and the signal to noise ratio was acceptable in that the line peaks were more than an order of magnitude greater than the noise level. In the edges of the branches, $J''>17$ in the P- and R-branches, and less then $J''=2$ in the R-branch, the signal to noise ratio was too low for a usable fit. The peaks there were often asymmetrical due to low SNR and often were not resolvable from the noise. We didn't expect good fits to these peaks, but attempts were made, as shown in Figure 3-1. Data runs with 100 scans reduced this problem somewhat and allowed us to resolve peaks at $J''>15$ in both branches. In general, the signal to noise ratio was greater by a factor of 2 in the P-branch than in the R-branch due to the spectrum location with respect to the filter curve. Figure 3-2 shows this effect. Notice how the R-branch rides on the downswing of the curve where intensity from the source was decreased by the filter. We could not eliminate the filter without saturating the detector, and we were limited by time so we couldn't repeat the experiment with another filter centered in the R-branch. So we had to accept this problem in the R-branch. When we used the Bomem software's "Absorption" feature to convert the spectra from transmission to absorption data, we had no problems. We kept the baselines around zero by using the filter background file that matched the spectrum. See (Figure 3-3) for an example of a baseline curve.
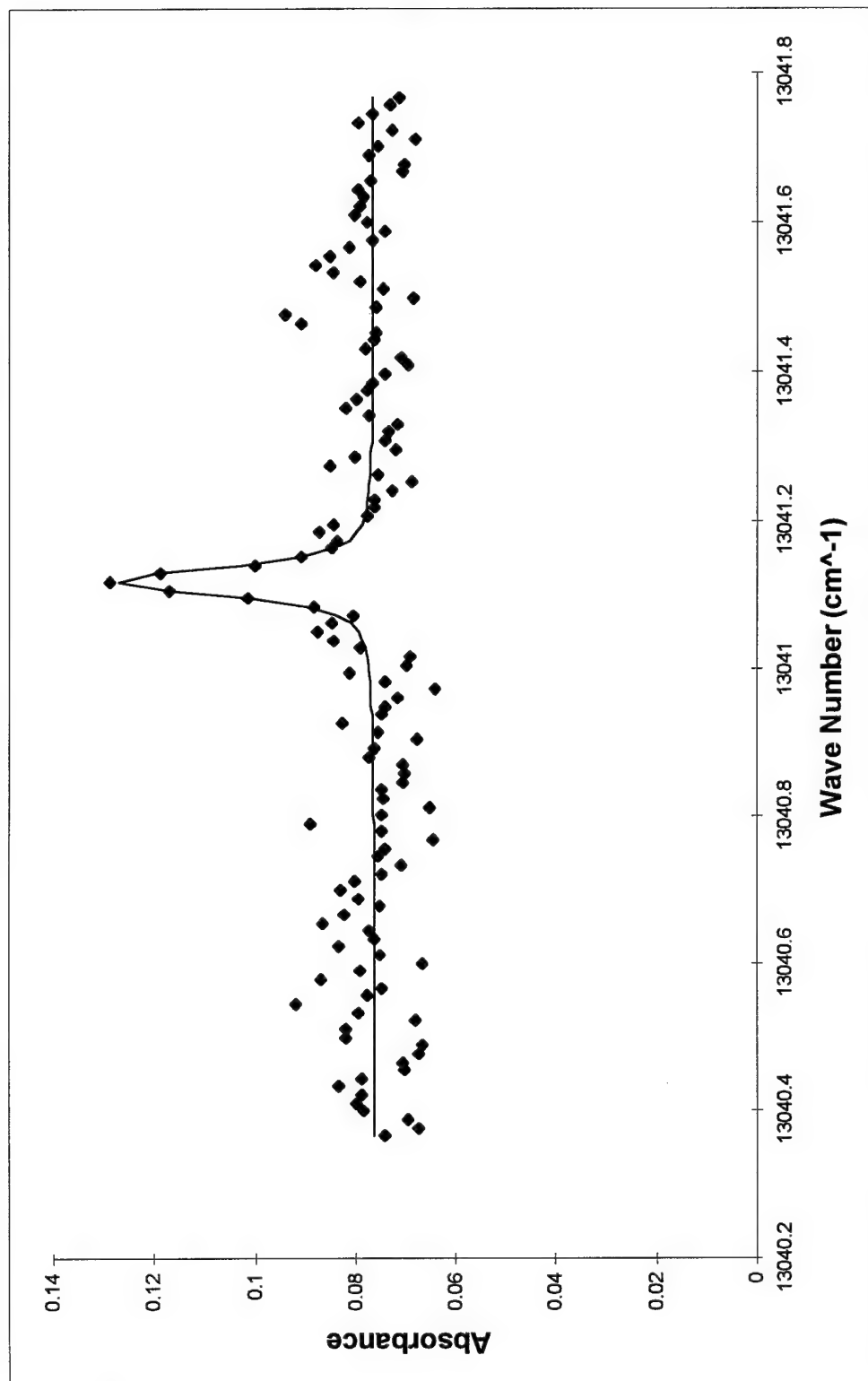
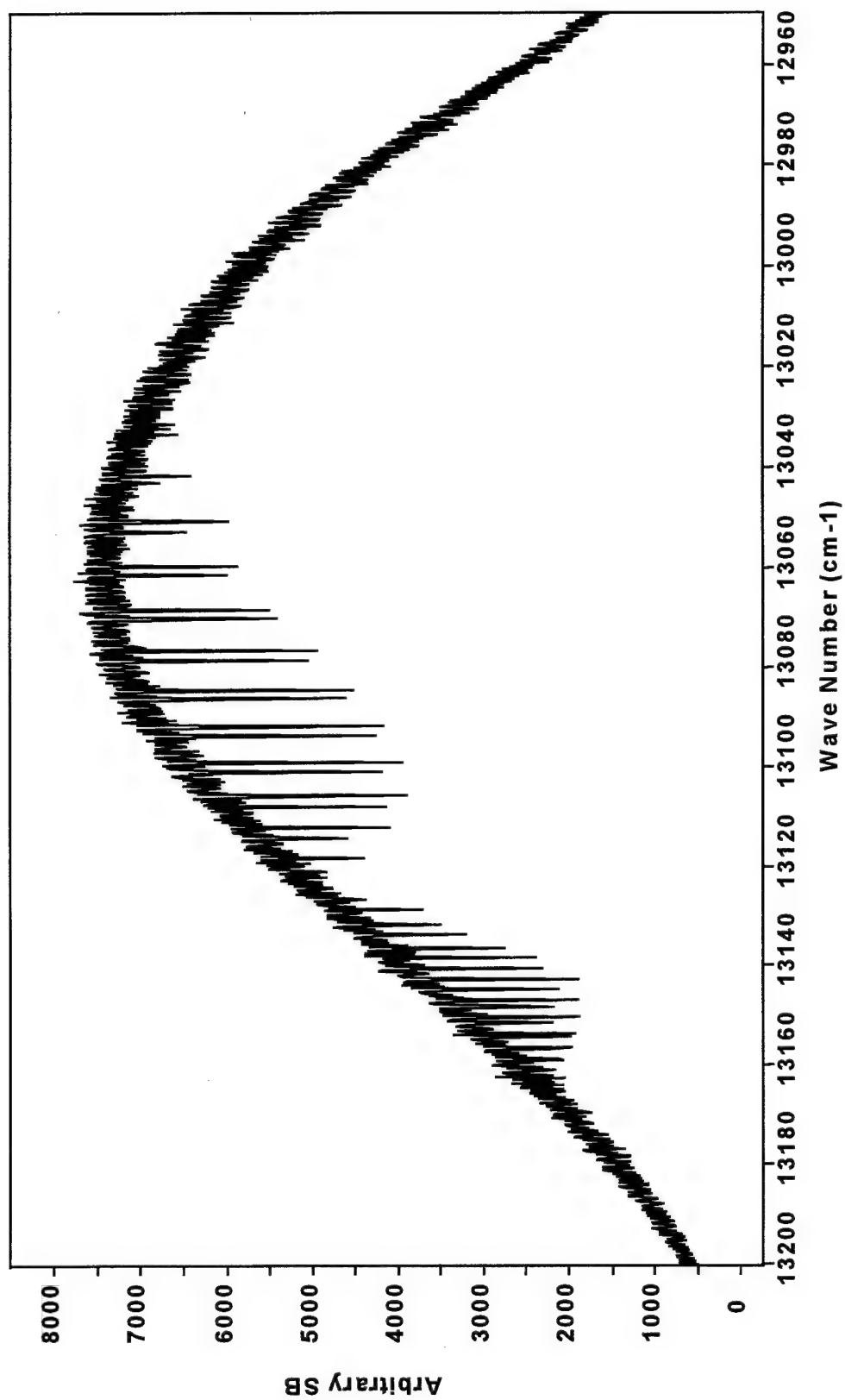**Figure 3-1:** O₂ line with low signal to noise ratio and Peak Fit attempt.

49

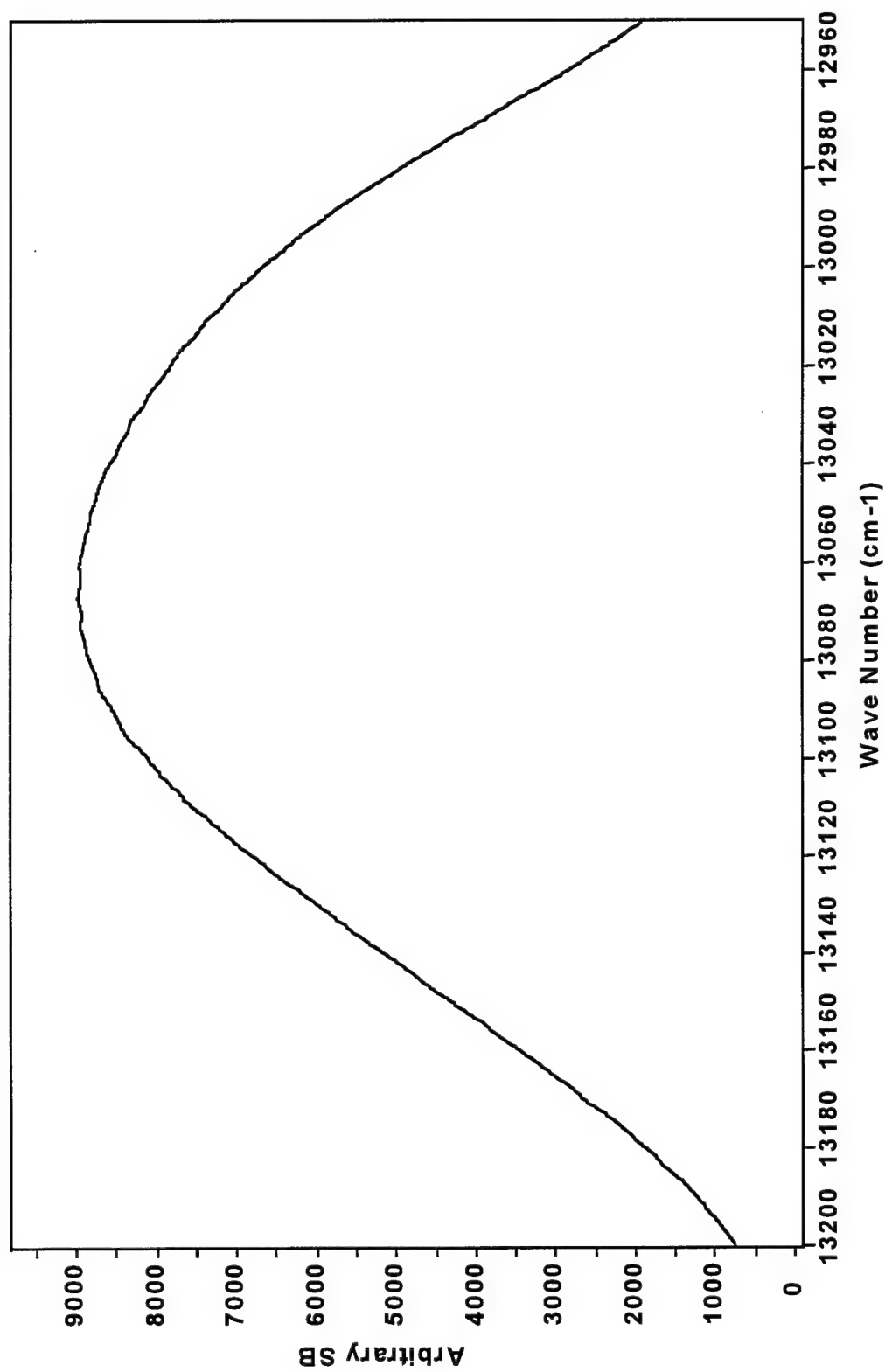Figure 3-2: Raw O₂ spectrum (output from spectrometer).

50

Figure 3-3: O$_2$ study filter background trace.

51

Peak Fitting

Using the method discussed in Chapter 2, we fit the data with Voigt curves. As it turned out, the curve fitting software corrects for non-zero baseline anyway using two baseline parameters. For the peaks where J"<17 in the P-branch and J"<15 in the R-branch, fits were generally good with r^2 greater than .960 in most cases. Where J"<13 and J"> 2 in both branches, r^2 were generally greater than .980 in both branches and in the center 7 lines of each branch, the r^2 were generally greater than .990. Deviations from this trend were greater with the heavier broadeners like xenon and nitrogen. We inspected the residuals during each fitting session for each peak and we did not notice any patterns which would signal a fitting function problem (Pope, private conversations). See Figure 3-4, 3-5, and Table 3-1 for an example of a fitted peak, residuals and numeric data output.

We did, however, notice a feature on either side of the peaks which we attributed to the slight misalignment of the spectrometer (Pope, private conversations and Eliades, private conversations). This feature was a small positive peak above and a small negative peak below in energy to the peaks themselves. See Figure 3-6 for an example. Time constraints prevented us from exploring this problem further, and this feature did not affect the fit. It did, however, increase the residuals on either side of the peak where the baseline should be zero and probably caused our r^2 values to be slightly higher. This probably led to slightly larger error bars on our data points, but as will be shown later, our data has not been affected.

We then extracted the Lorentzian half width at half maximum for each peak and plotted them vs. pressure of broadening gas to determine γ_0.
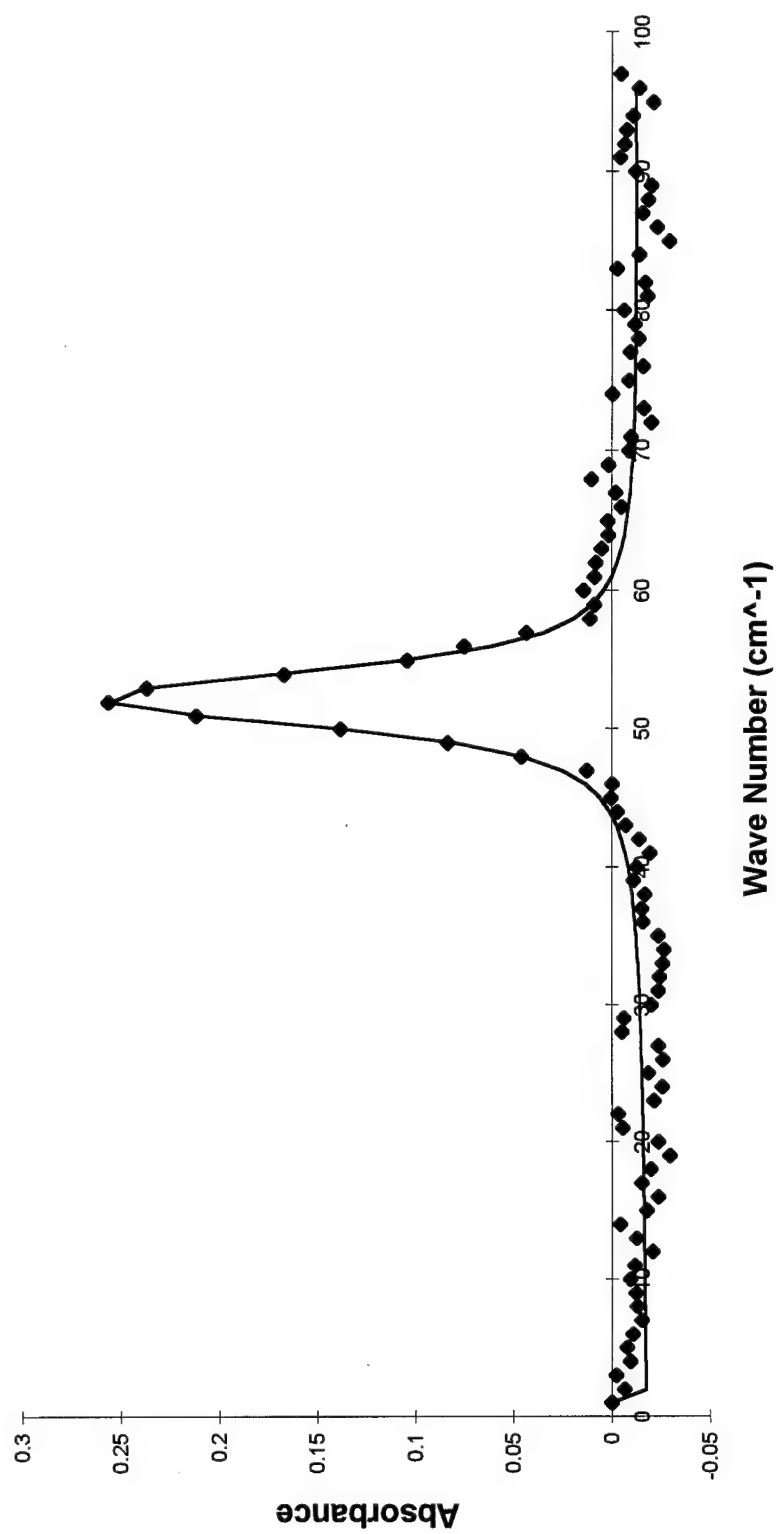
Figure 3-4: Example of a fitted O_2 peak at J''= 9 in the P-branch (200 Torr O_2, 200 Torr Kr).
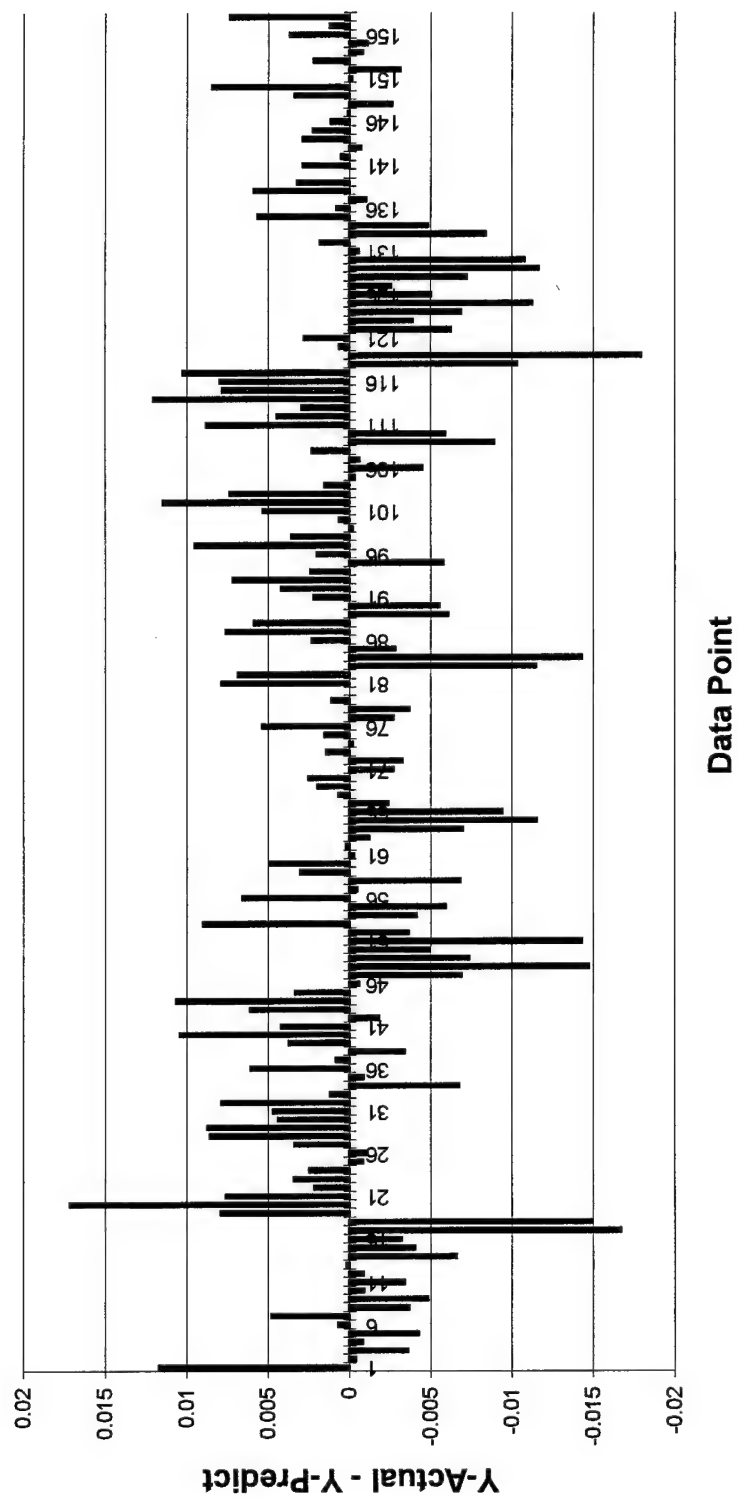
53

Figure 3-5: Residuals for Figure 3-4.

54

Table 3-1: Numeric output for curve fit of Figure 3-4

Fitted Parameters

r^2 Coef Det	DF Adj r^2	Fit Std Err	F-value	
0.97228002	0.97136818	0.00633341	1341.62128	

Peak	Type	a0	a1	a2	a3
1	Voigt Area G/L	0.02192464	13091.7031	0.01189051	0.02638213
B	Linear Bg	42.1652823	-0.0032245		

Measured Values

Peak	Type	Amplitude	Center	FWHM	Asym50	FW Base	Asym10
1	Voigt Area G/L	0.22852398	13091.7031	0.06545989	0.99831899	0.19511031	0.99937457

Peak	Type	Anlytc Area	% Area	Int Area	% Area	Centroid	Moment2
1	Voigt Area G/L	0.02192464	100.000000	0.02150610	100.000000	13091.7035	0.02533635
	Total	0.02192464	100.000000	0.02150610	100.000000		

Parameter Statistics

Peak 1 Voigt Area G/L

Parm	Value	Std Error	t-value	95% Confidence Limits	
Area	0.02192464	0.00018359	119.418725	0.02156193	0.02228734
Ctr	13091.7031	0.00022992	5.6941e+07	13091.7027	13091.7036
Wid	0.01189051				
Wid2	0.02638213	0.00035580	74.1490969	0.02567921	0.02708504

Baseline Linear Bg

Parm	Value	Std Error	t-value	95% Confidence Limits	
a0	42.1652823	5.10650157	8.25717602	32.0769272	52.2536373
a1	-0.0032245	0.00039006	-8.2667757	-0.0039951	-0.0024539
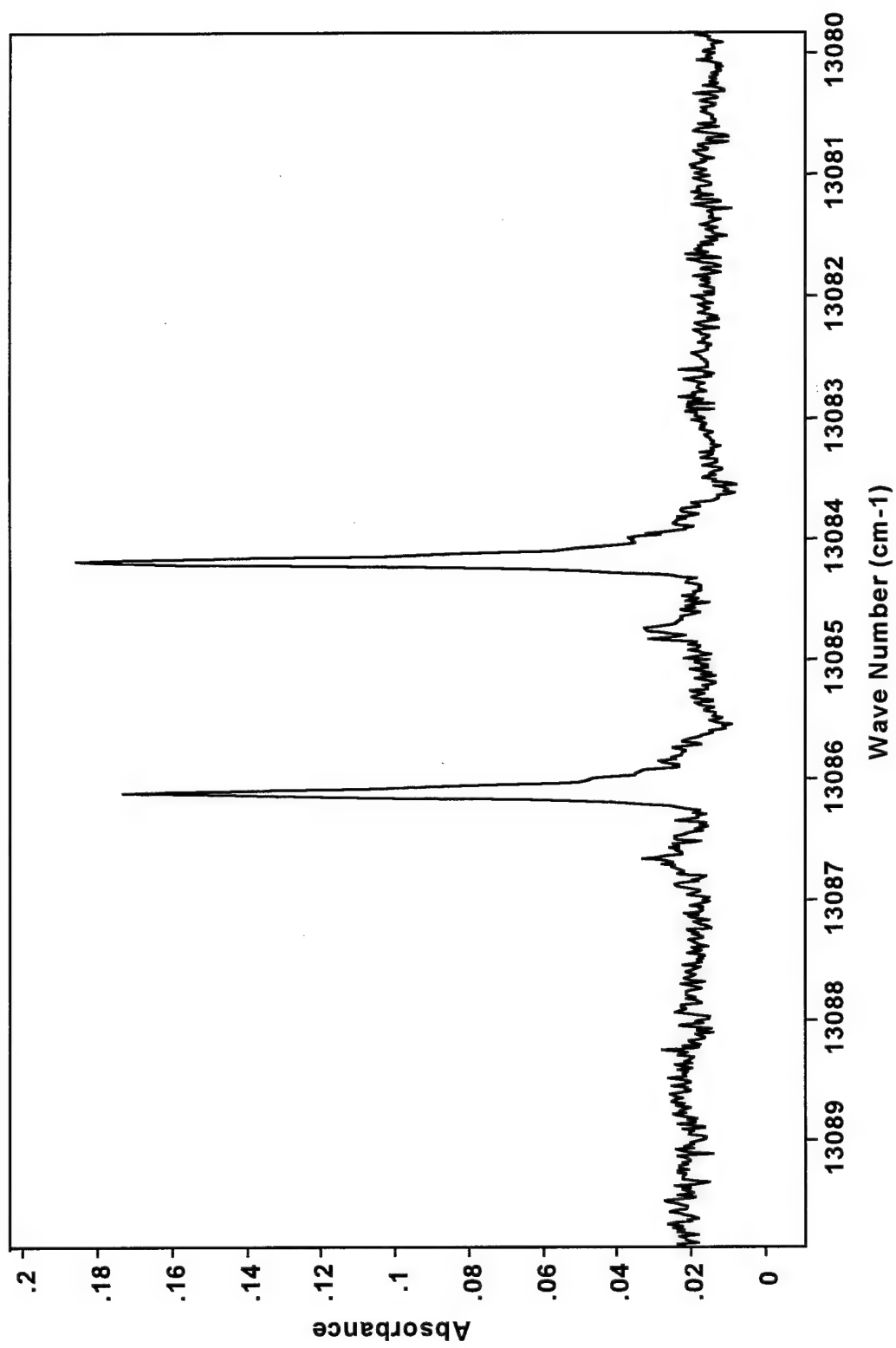
Figure 3-6: (Misalignment?) feature in O_2 spectrum lines J" = 10,11 in the P-branch (200 Torr O_2, 400 Torr N_2).

56

γ_0 Determination

γ_0 determination went well in that the peaks in the good range of each branch had linear least squares fits better than 0.960 in most cases. The edges of the branches were unreliable due to the original signal to noise problem at the branch ends. In the better parts of the branches, the deviations of the fits were most often less than one standard deviation from the data. An example of a γ_0 determination plot is in Figure 3-7. The software made it easy to extract and plot the slope of the linear fit, which gave us γ_0, since the slope is a parameter of the fit. We then plot γ_0 vs. J".

γ_0 vs. J" Pattern Study

We examined the pattern of γ_0 vs. J" and compared the pattern to other research. Theory states that γ_0 should increase with decreasing J" (Burch, 1969, and Ritter, 1987) and our data followed this pattern. The work of Ritter, et. al. (1987) was the only noble gas broadening data to compare to, and as discussed in Chapter 1, it was mostly theoretical and partially experimental. We then compared our pattern to Ritter's. His data fits well with ours but our data is much more precise. Our data neatly overlays his and we got increasing γ_0 with increasing reduced mass of broadener, except for helium. We do not know why helium does not fit this trend. We did notice a smoother adherence to the pattern in the P-branch, in that the data were not as scattered above and below the theoretical γ_0 line. All of the γ_0 vs. J' plots are in Appendix B.
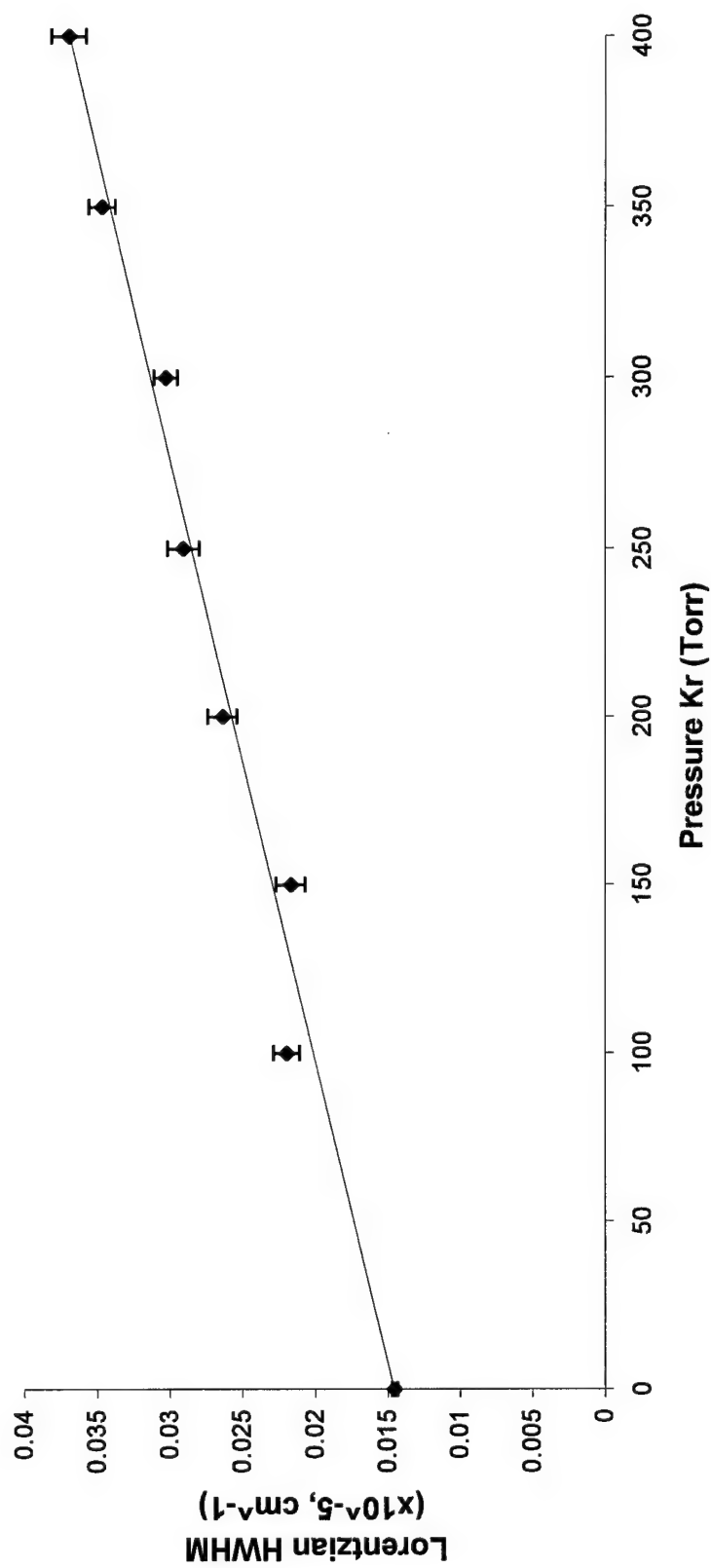
Figure 3-7: Example of Pressure Broadening Coefficient determination for the J''=9 line of O_2 in the P-branch (200 Torr O_2, 200 Torr Kr).

58

Table 3-2: Numerical output accompanying O₂ Pressure Broadening Coefficient determination plot.

Description: Oxygen Broadened With Krypton J = -9 (P-Branch)
Rank 1 Eqn 8160 [Line Robust None, Gaussian Errors] y=a+bx

r^2 Coef Det   DF Adj r^2   Fit Std Err   F-value
0.9935770575   0.9910078805   0.0005940455   928.15128717

Parm	Value	Std Error	t-value	95% Confidence Limits		P>|t|
a	0.014542606	0.000234882	61.91448221	0.01396787	0.015117341	0.00000
b	5.61088e-05	1.84171e-06	30.46557544	5.16023e-05	6.06154e-05	0.00000

Area Xmin-Xmax Area Precision
10.305749984   0

Function min	X-Value	Function max	X-Value
0.0145426056	1.073612e-10	0.0369861444	400
1st Deriv min	X-Value	1st Deriv max	X-Value
5.610885e-05	97.882266076	5.610885e-05	24.960226003
2nd Deriv min	X-Value	2nd Deriv max	X-Value
-5.42101e-12	38.569973566	5.421011e-12	58.043112471

Procedure   Minimization   Iterations
LevMarqdt   Least Squares 6
r^2 Coef Det   DF Adj r^2   Fit Std Err
0.9935770575   0.9910078805   0.0005940455

Source	Sum of Squares	DF	Mean Square	F Statistic	P>F
Regr	0.00032753535	1	0.00032753535	928.151	0.00000
Error	2.1173403e-06	6	3.5289004e-07		
Total	0.00032965269	7			

Date   Time   File Source
Sep 16, 1997   9:34:58 AM   c:\cornice\analysis\o2kr\p branch\o2kr jn9b.prn

NO Study

Spectrum Production

Now, let's consider the NO experiment. As with O_2 we inspected the spectra for usability. The centers were in the correct places (Spencer, 1984) and the signal to noise ratio was good. For both the 1/2 and 3/2 state, the peak intensities were more than an order of magnitude greater than the noise except where J">18.5 in the P-branch and J">14.5 in the R-branch (See Figure 3-8). The Q-branch lines were of usable signal to noise ratio for J"<6.5 for the 3/2 state. All of the 1/2 state lines in the Q-branch were not resolvable over the noise (see Figure 3-9). The reduced intensity problem we had with the O_2 R-branch was not evident with NO as the spectrum was centered well on the filter curve. See Figure 3-10 for an example of this raw NO spectrum.

Peak Fitting

Here is where our experiment with NO begins to produce substandard results. We knew from the fact that all of our lines were Λ-doubled, and that we would have to fit two very closely spaced lines for the 1/2 state. The individual e and f lines of the 3/2 state were not resolvable. So we attempted to fit the 1/2 state lines with two Voigt curves, and fit the 3/2 state lines with one Voigt as an unresolved doublet. The 3/2 state lines were not able to be fitted this way and r^2 values were rarely better than 0.800 (See Figure 3-11, 3-12 and Table 3-2). We concluded that we would concentrate solely on the 1/2 state. See Figure 3-13, 3-14 and Table 3-3 for an example of a fitted NO doublet of the 1/2 state. Fits here were better, although not to the same quality as with O_2. Our r^2 values were on the orders of 0.920 for the best part of the spectra and 0.880 for the edges of the

P- and R-branches. The Q-branch was not resolvable for the 1/2 state. We concluded that we were probably not fitting the curves with the proper function for the 1/2 state as well. When we examined the 3/2 state fits themselves we noticed a difference between the e and f Λ-double line widths inconsistent with Spencer's N_2 data. We concluded that the curve fitting of the double peaks was not proper in that the Λ-doublets' Lorentzian widths were being allowed to vary. We did not think we should lock them at the time since this would prevent the fit from accurately representing the actual data. Time constraints prevented us from examining other functions or curve fitting algorithms, so we pressed on to see what kind of γ_0 values we would get.

γ_0 Determination

γ_0 determination went better than expected in that the peaks in the good range of each branch had linear least squares fits better than .960 in the very center of the branches. Outside the branch centers, the r^2 dropped into the .900 -.950 range and in the edges of the branches the fits were unreliable due to the original signal to noise problem at the branch ends. In the best parts of the branches, the deviations of the fits were most often less than one standard deviation from the data. An example of a γ_0 determination plot is in Figure 3-15. We then plot γ_0 vs. J" and studied the pattern. We also converted γ_0 to a cross section, σ, plotted it vs. J" and studied the pattern. We proceeded by comparing cross section to polarizability for each line and cross section to reduced mass of the collision pair for each line.
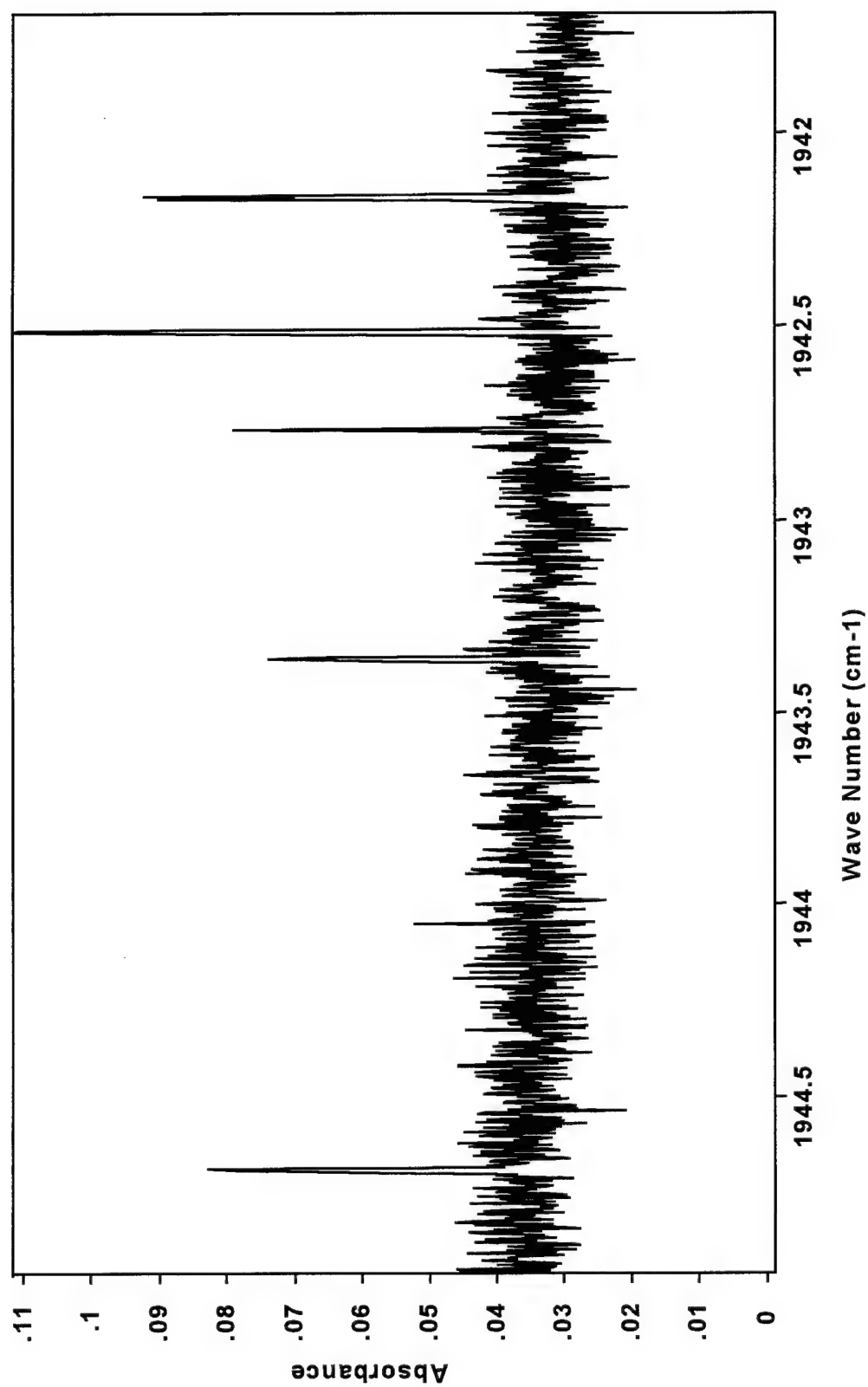
61

Figure 3-8: Unresolvable NO lines at J″ = 21.5 in the P-branch (500mTorr NO, 10 Torr Xe).
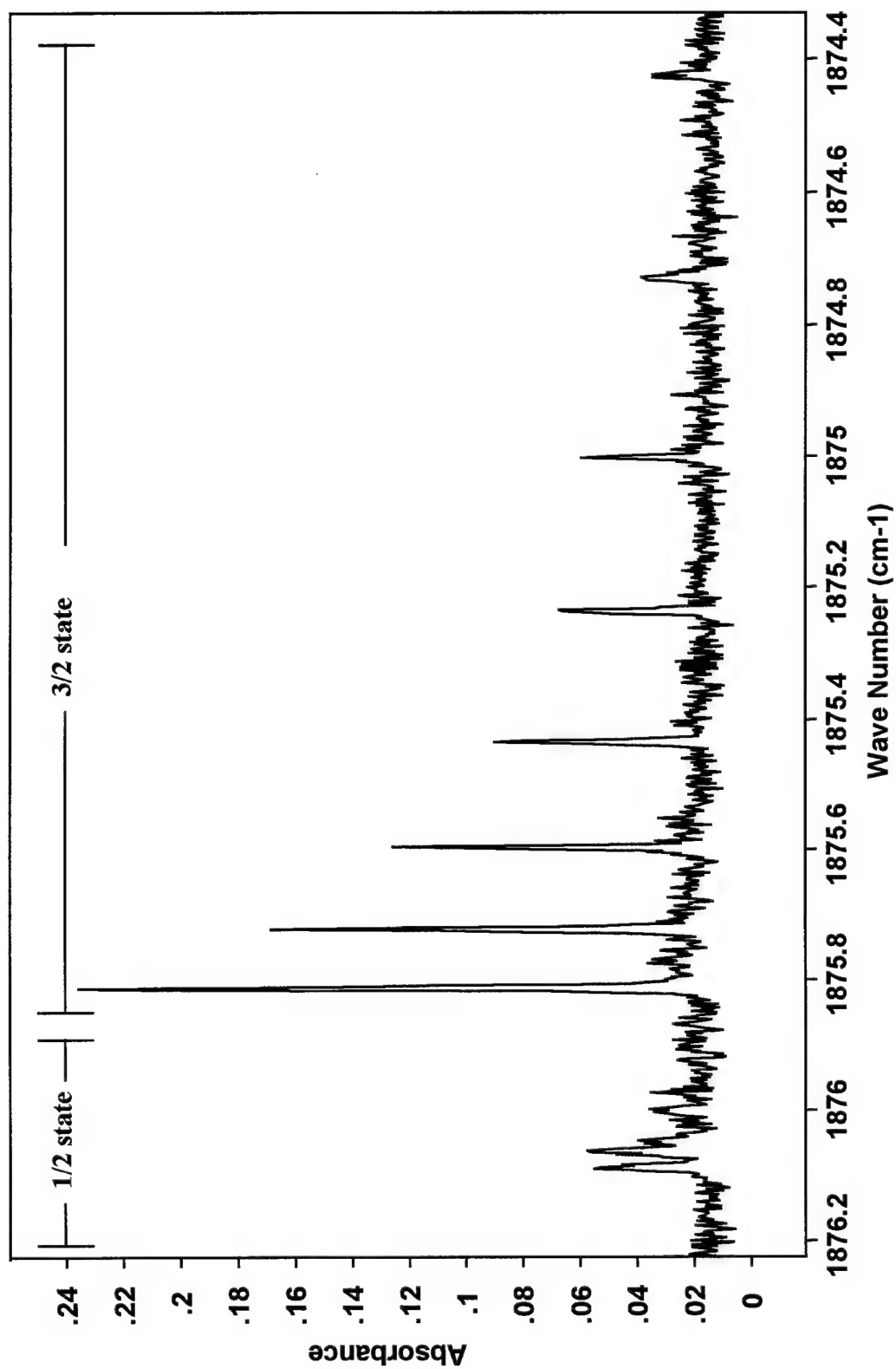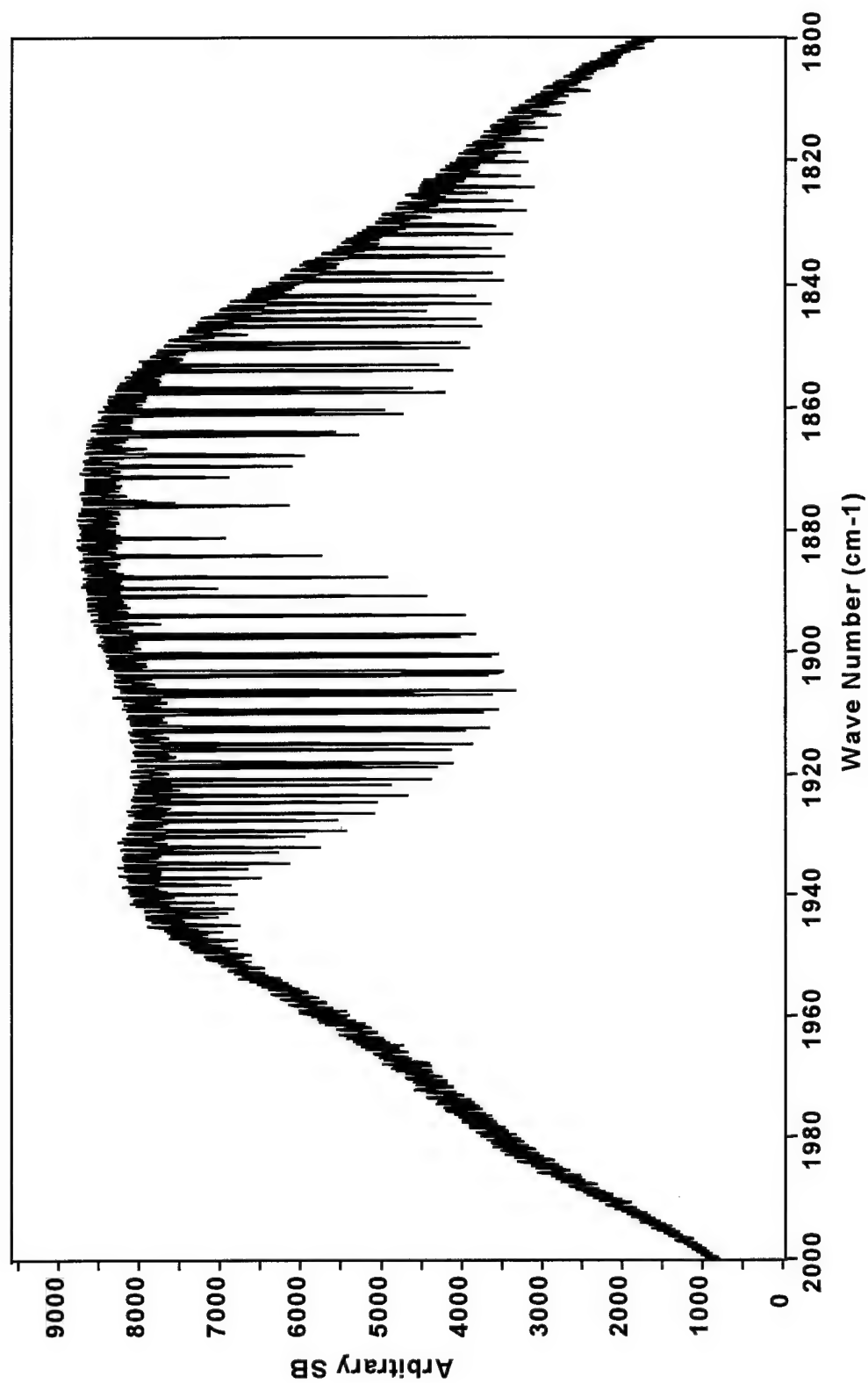
Figure 3-9: NO Q-branch (500 mTorr NO, 10 Torr Xe)

63

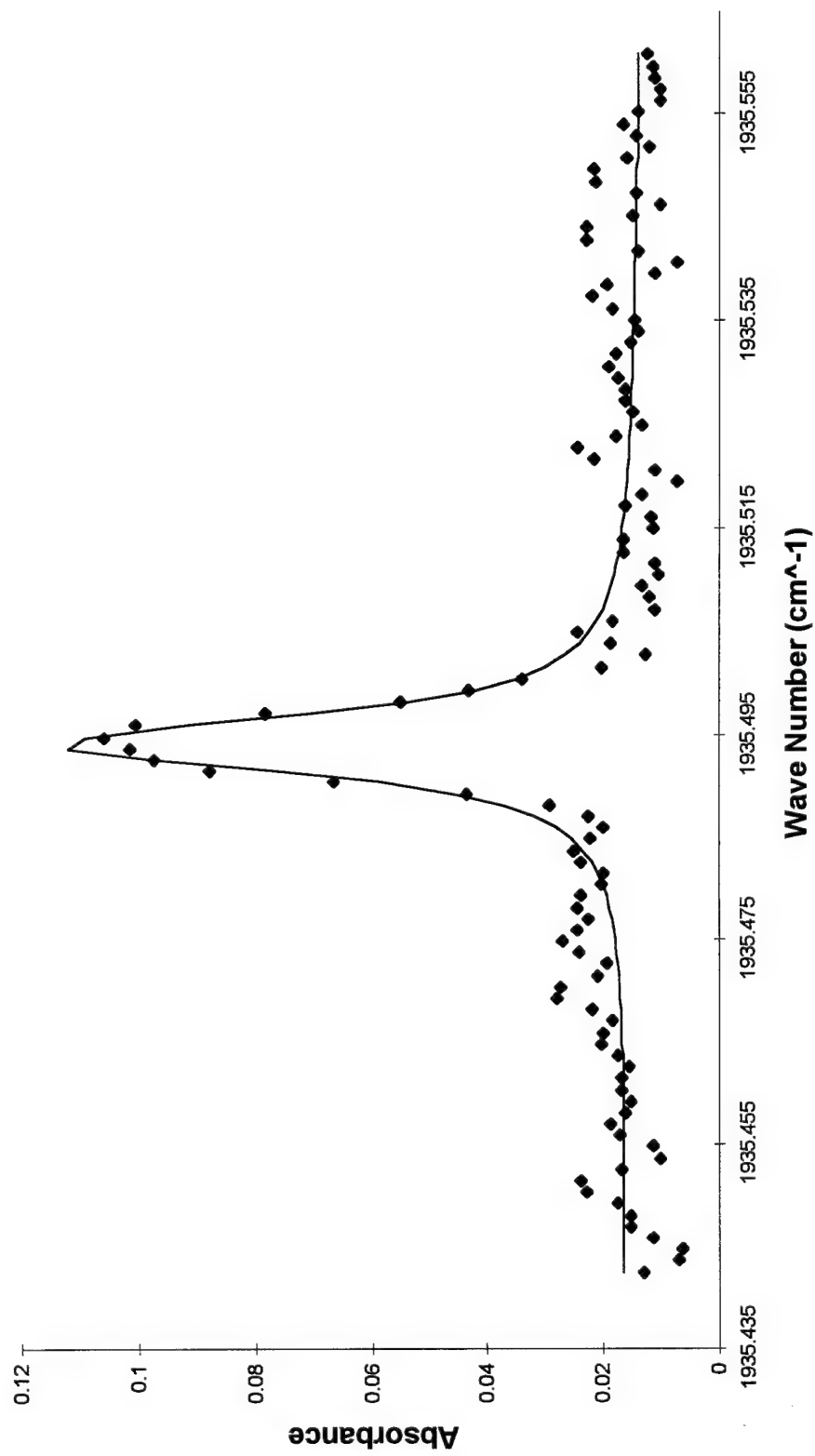Figure 3-10: Raw NO spectrum (500 mTorr NO, 40 Torr Ar).

64

Figure 3-11: Curve fit of an unresolved 3/2 state Λ-doublet of NO at J'' = 18.5 in the R-branch (500 mTorr NO, 55 Torr Kr).

Figure 3-12: Residuals for Figure 3-11: Note high values in peak region.
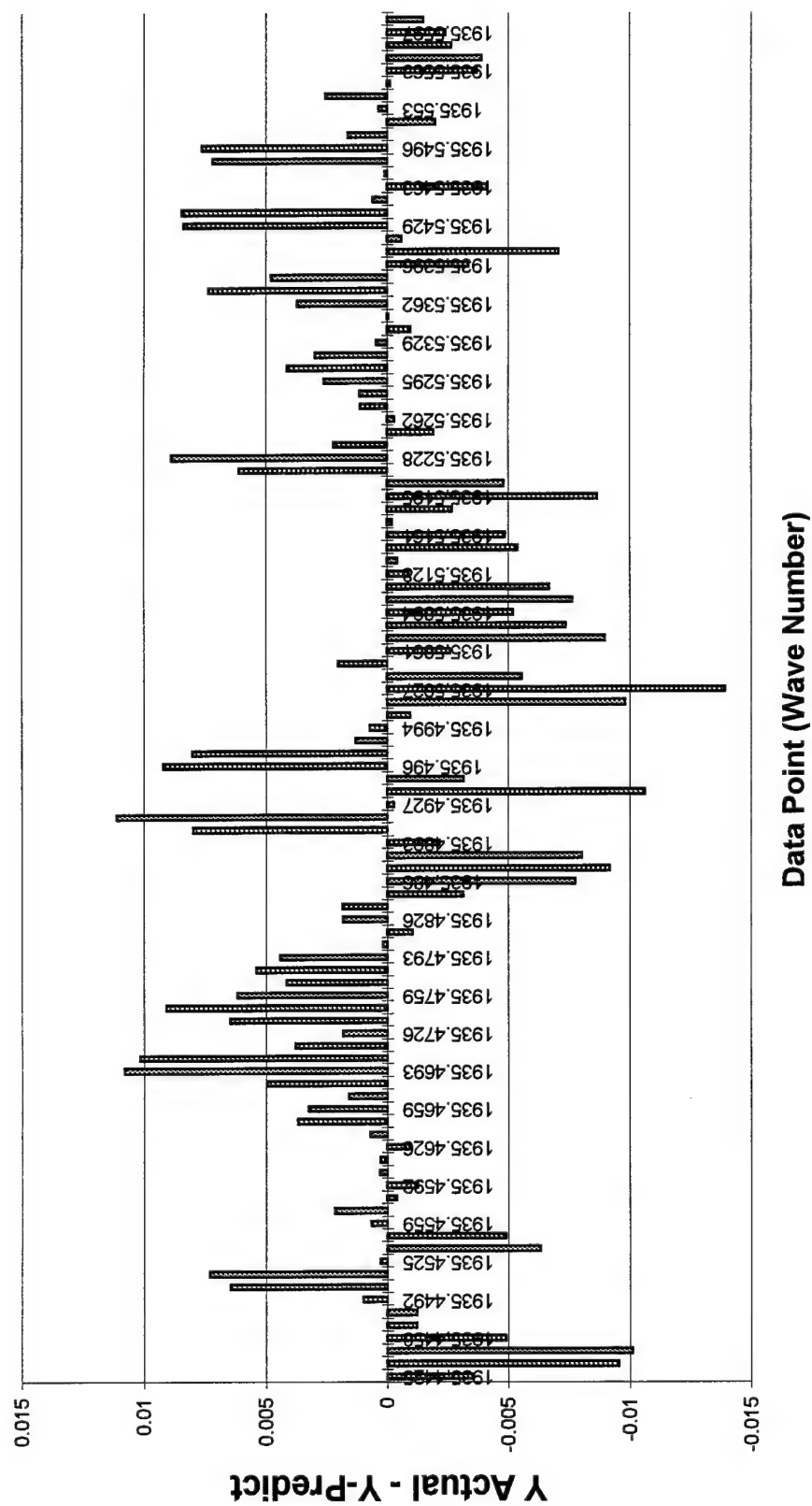
99

Table 3-3: Numeric output for curve fit of 3/2 state NO line at J" = 18.5 in the R-branch (500 mTorr NO, 55 Torr Kr).

Description: C:\Cornice\Nokr004a.prn
File Source: c:\cornice\nokr004a.prn

Fitted Parameters

r^2 Coef Det	DF Adj r^2	Fit Std Err	F-value
0.92792494	0.92435687	0.00542198	328.297840

Peak	Type	a0	a1	a2	a3
1	Voigt Area G/L	0.00099319	1935.49422	0.00089596	0.00298624
B	Linear Bg	40.6595230	-0.0209995		

Measured Values

Peak	Type	Amplitude	Center	FWHM
1	Voigt Area G/L	0.09817163	1935.49422	0.00668381

Peak	Type	Anlytc Area	% Area	Int Area	% Area	Centroid
1	Voigt Area G/L	0.00099319	100.000000	0.00096078	100.000000	1935.49447
	Total	0.00099319	100.000000	0.00096078	100.000000	

Parameter Statistics

Peak 1 Voigt Area G/L

Parm	Value	Std Error	t-value	95% Confidence Limits	
Area	0.00099319	1.7311e-05	57.3732070	0.00095885	0.00102752
Ctr	1935.49422	4.6875e-05	4.1291e+07	1935.49413	1935.49431
Wid	0.00089596				
Wid2	0.00298624	7.4152e-05	40.2720367	0.00283916	0.00313332

Baseline Linear Bg

Parm	Value	Std Error	t-value	95% Confidence Limits	
a0	40.6595230	11.7582276	3.45796360	17.3371343	63.9819117
a1	-0.0209995	0.00607502	-3.4567025	-0.0330493	-0.0089498
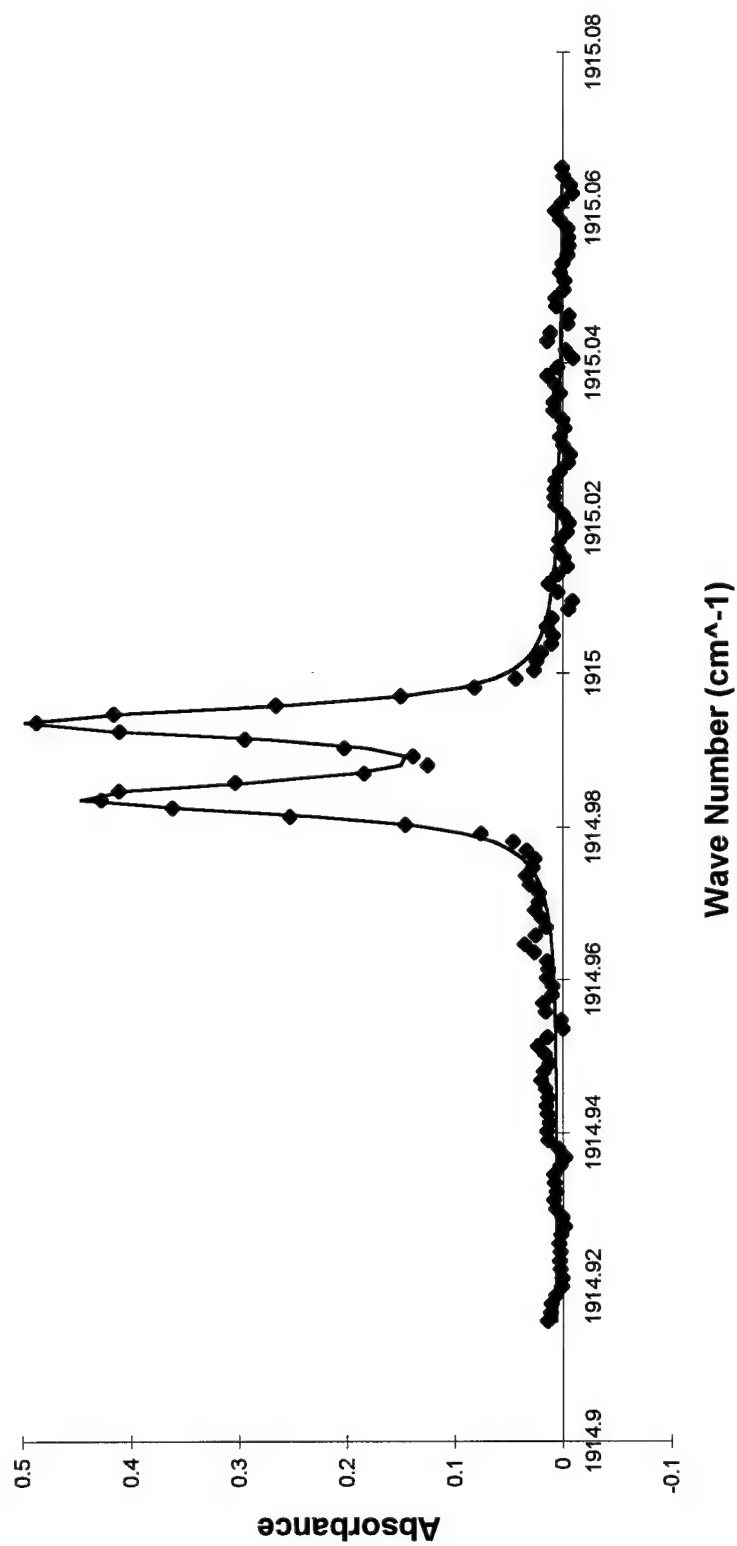
Figure 3-13: Curve fit of 1/2 state Λ-doublet of NO at J" = 11.5 in the R-branch (500 mTorr NO, 40 Torr Xe).

68

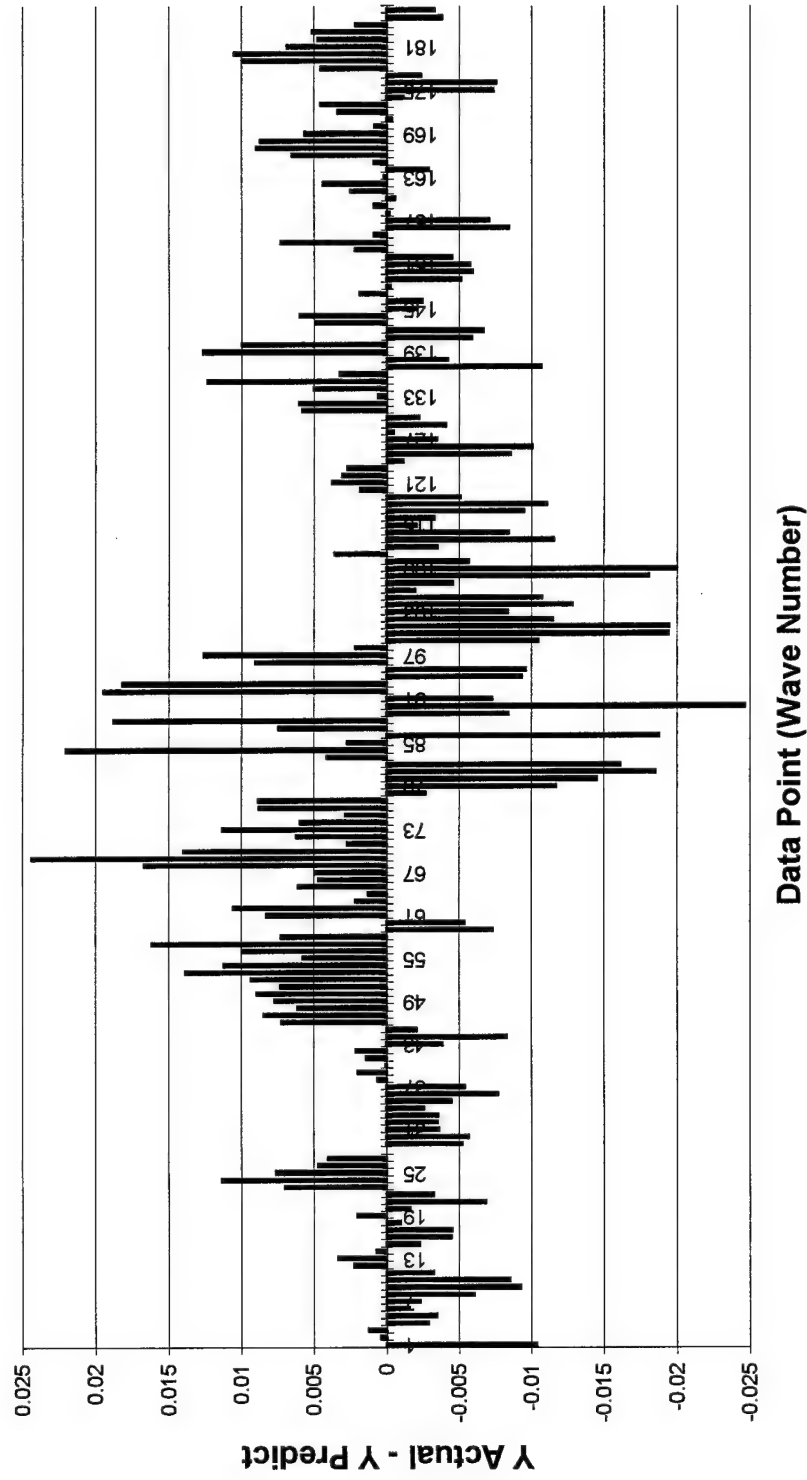**Data Point (Wave Number)**

Y Actual - Y Predict

Figure 3-14: Residuals for Figure 3-13.

69

Table 3-4: Numeric output for curve fit of 1/2 state NO line at J" = 11.5 in the R-branch (500 mTorr NO, 40 Torr Xe).

<u>Fitted Parameters</u>

r^2 Coef Det	DF Adj r^2	Fit Std Err	F-value	
0.99069350	0.99027286	0.00849623	2706.91583	

Peak Type	a0	a1	a2	a3
1 Voigt Area G/L	0.00305848	1914.98390	0.00089596	0.00195231
2 Voigt Area G/L	0.00309749	1914.99375	0.00089596	0.00173255
B Linear Bg	85.7730886	-0.0447891		

<u>Measured Values</u>

Peak Type	Amplitude	Center	FWHM	Asym50	FW Base Asym10
1 Voigt Area G/L	0.42902518	1914.98390	0.00487265	1.00630255	0.01448215 1.00234583
2 Voigt Area G/L	0.47542920	1914.99375	0.00450853	1.00218328	0.01313590 1.00082939

Peak Type	Anlytc Area	% Area	Int Area	% Area	Centroid Moment2
1 Voigt Area G/L	0.00305848	49.6831294	0.00302143	49.6470078	1914.98400 0.00012771
2 Voigt Area G/L	0.00309749	50.3168706	0.00306439	50.3529922	1914.99374 0.00011288
Total	0.00615598	100.000000	0.00608582	100.000000	

<u>Parameter Statistics</u>

Peak 1 Voigt Area G/L

Parm	Value	Std Error	t-value	95% Confidence Limits	
Area	0.00305848	2.3062e-05	132.618776	0.00301297	0.00310399
Ctr	1914.98390	1.4457e-05	1.3246e+08	1914.98388	1914.98393
Wid	0.00089596				
Wid2	0.00195231	2.3527e-05	82.9813428	0.00190588	0.00199874

Peak 2 Voigt Area G/L

Parm	Value	Std Error	t-value	95% Confidence Limits	
Area	0.00309749	2.1937e-05	141.197793	0.00305420	0.00314079
Ctr	1914.99375	1.2457e-05	1.5373e+08	1914.99373	1914.99378
Wid	0.00089596				
Wid2	0.00173255	2.0314e-05	85.2881380	0.00169246	0.00177264

<u>Baseline Linear Bg</u>

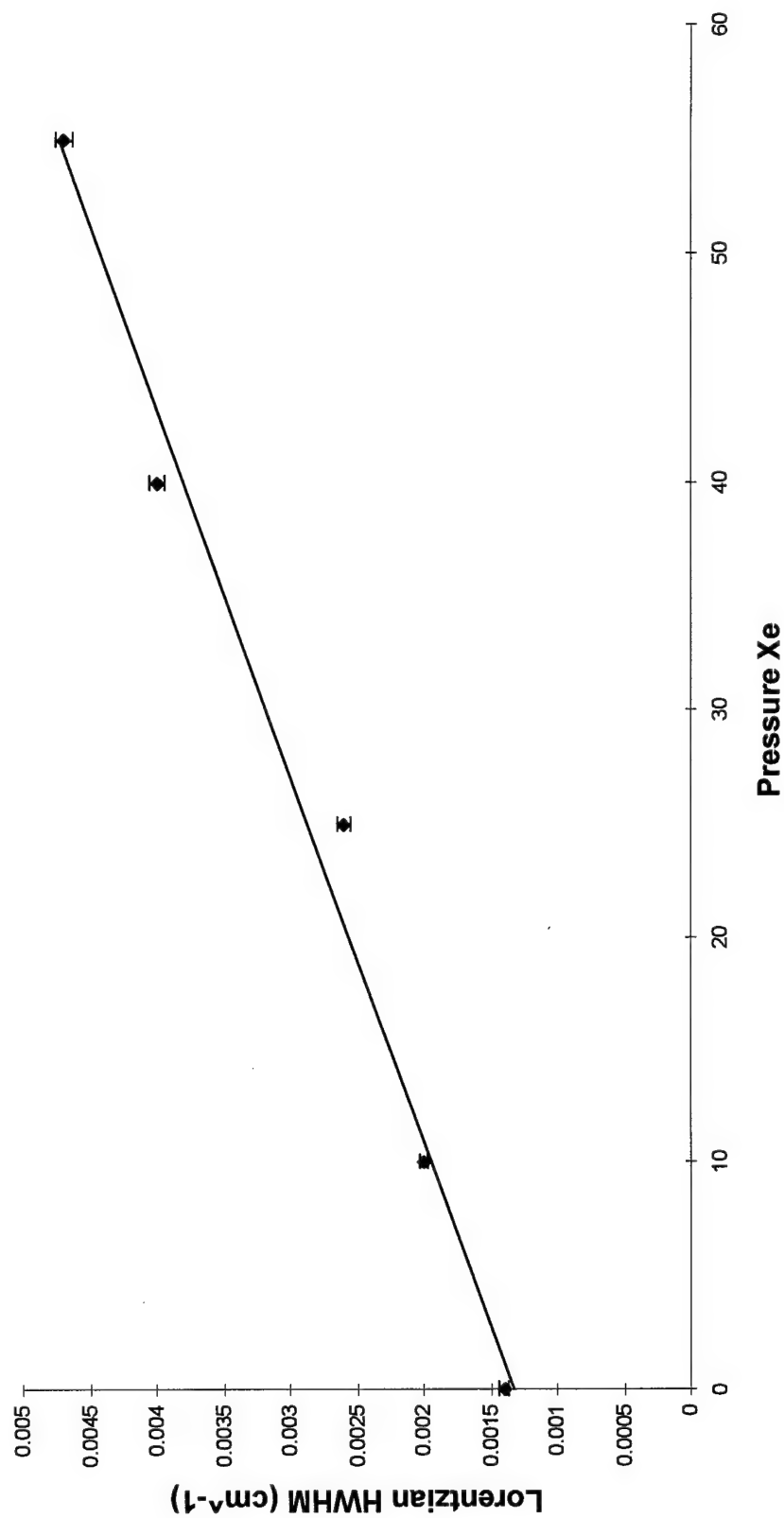| Parm	Value	Std Error	t-value	95% Confidence Limits

Figure 3-15: Example of Pressure Broadening Coefficient determination for the J''=6.5 e line of NO in the P-branch (500 mTorr NO, 40 Torr Xe).

71

Table 3-5: **Numerical output accompanying NO Presure Broadening Coefficient determination.**

Description: NO Broadened with Xenon J6.5e (P-Branch)
Rank 1 Eqn 8160 [Line Robust None, Gaussian Errors] y=a+bx

XY *	X Value	Y Value	Y Predict	Residual	Residual%	Weights
1	0	0.0014	0.0014753	-7.53e-05	-5.376212	3.2e-05
2	10	0.0018	0.0019425	-0.000142	-7.916277	2.9e-05
3	25	0.0029	0.0026433	0.0002567	8.8506194	4.6e-05
4	40	0.0033	0.0033442	-4.42e-05	-1.338518	5.4e-05
5	55	0.004	0.004045	-4.5e-05	-1.125253	6.4e-05

r^2 Coef Det	DF Adj r^2	Fit Std Err	F-value
0.9790382962	0.9580765923	0.0001728954	140.1181369

Parm	Value	Std Error	t-value	95% Confidence Limits		P>|t|
a	0.001475267	0.0001469	10.04265301	0.001007765	0.001942769	0.00210
b	4.67226e-05	3.94712e-06	11.83715071	3.41611e-05	5.92841e-05	0.00130

Area Xmin-Xmax	Area Precision
0.15180762	1.828339e-16

Function min	X-Value	Function max	X-Value
0.001475267	1.954254e-10	0.0040450101	55

1st Deriv min	X-Value	1st Deriv max	X-Value
4.67226e-05	30.259750649	4.67226e-05	33.975567574

2nd Deriv min	X-Value	2nd Deriv max	X-Value
-3.58414e-11	27.499946953	3.584144e-11	38.385123631

Procedure	Minimization	Iterations
LevMarqdt	Least Squares	6

r^2 Coef Det	DF Adj r^2	Fit Std Err
0.9790382962	0.9580765923	0.0001728954

Source	Sum of Squares	DF	Mean Square	F Statistic	P>F
Regr	4.1885279e-06	1	4.1885279e-06	140.118	0.00130
Error	8.9678496e-08	3	2.9892832e-08		
Total	4.2782064e-06	4			

Date	Time	File Source
Sep 16, 1997	9:33:04 AM	c:\cornice\analysis\noxe\p-branch\noxep6.5e.prn

γ_0 vs. J" Pattern Study

Here is where we were able to see direct evidence of our problem with NO. We had no actual experimental data to compare our noble gas broadening to and no researcher has calculated theoretical values like Ritter's with O_2. When we plotted γ_0 vs. J", we compared our data to Spencer's 1994 N_2 experimental broadening data for an idea of how our pattern should look. We expected NO to follow a similar pattern as with O_2 and Spencer's N_2 broadening data in that γ_0 should increase with decreasing J". We expected a trend of increasing γ_0 with increasing mass of broadener just like with our O_2 experiment and we expected helium to buck the trend. Since Spencer's N_2 data showed similar values for the e and f Λ-double lines, we expected the same trend with our noble gas broadening.

Our γ_0 data did not have similar values for the e and f Λ-doubles in the P-branch, which was our first deviation from what was expected, but the values were close in the R-branch. In the R-branch, the e and f lines were separated by more than the separation of the P-branch lines and this helped the fitting algorithm treat them separately in most cases. The P-branch f lines always had a greater value of γ_0 than the e lines, and the difference decreased to almost zero, but never quite consistently zero, in the lower 5 or 6 J" doublets. In the R-branch, the doublets were nearly equal, although not as close as Spencer's, with no pattern of either the e or f lines having consistently higher g_0 than the other. This gave us an idea of where the actual γ_0 is, although our errors were high. In the R-branch we saw a similar pattern as with O_2 where the higher mass broadeners produced higher γ_0. Since our experimental error was low, we conclude that this trend is

73

reliable. We were concerned that our experimental error was not consistent with the separation of values in the P-branch. This is understood to be caused by the fitting algorithm itself. It is fitting the peaks as it sees them, as two Voigts which are close together, with no restraints on their amplitudes or widths. So the fits are good, although nor physically representative, since we know the widths and amplitudes should be similar (Spencer, 1994),

In general, our data is not more than an order of magnitude further from where we expected them to be. A hint of where we expect them to be is shown in Appendix B, where we averaged the e and f values. Although this gives us a ballpark figure to shoot for in further research, this averaging is not valid for determining actual values. We considered this theory, but when we examined the Voigt function, we discovered that the relationship of intensity to Lorentzian width is not quite linear.

We did not convert γ_0 to σ for the NO study, nor did we compare σ to polarizability and reduced mass as with O_2.

IV. Conclusion and Recommendation

O_2 Study

We were satisfied with our γ_0 data and its correlation with Ritter's data. We were satisfied with the performance of both the curve fitting method and the method for determining γ_0. Here is how we would improve the data if given the time: First, we would ensure the spectrometer was better aligned to eliminate the spectral feature discussed in Chapter 3. This requires contractor intervention to determine if in fact it is aligned or not, and if not, what the problem is. Next, we would repeat the experiment with a filter centered over the R-branch to reduce signal to noise ratio there. We could also increase signal-to-noise ratio by coadding many 100 scan runs. This increases the time required for each data point, but as can be seen by comparing Figures 4-1 and 4-2, the signal to noise ratio seems to increases by about factor of the square root of the number of additional coads of 100 scan runs.

When we examined our plots of σ vs. J" (Figure 4-3) we found that the pattern of increasing σ with decreasing J" followed the same trend as with γ_0. It is not known quantitatively why this pattern should be so, but it is nonetheless understandable that there should be a variation. Using a classical analogy, imagine a collision between a spinning molecule and a hard sphere. The collision will act differently if the molecule is spinning rapidly than if it is spinning slowly with respect to the speed of collision. In the collision between the slow spinning molecule and the sphere, the sphere has more of a chance to

enter deeply into the potential of the molecule and approach the internuclear axis. During the collision process, the sphere will "see" different potentials depending on the direction of approach to the molecule. A collision between a fast-spinning molecule and a hard sphere will approach being a collision between two hard spheres. See Figure 4-3 for an example of a σ vs. J" plot.

When we analyzed our plots of σ vs. polarizability,, we found a linear relationship. This is understandable, since collisions are not hard sphere interactions. The collision partners' electron clouds interact during the collision, and depending on the size of the collision partner, there can be large or small changes to the cloud. Polarizability is a representation of the ability to change the cloud significantly enough to induce a dipole moment, and the moment will affect the collision potential. Understandably, the larger collision partners like Xenon had larger polarizabilities and hence, larger cross section, σ. Notice that N_2 did not fit with the linear relationship, it being a diatomic molecule whose polarizability is more complex than the spherical noble gases. See Figure 4-4 for an example of a σ vs. polarizability plot. This kind of relationship will help us understand the collision potentials.

Next we compared σ to reduced mass of the collision pair. Using a classical approach, the linear dependence makes sense. Heavier collision partners will have larger crosss sections. Figure 4-5 is an example of such a plot. Notice how N_2 falls more into line with its mass. This, too will move us towards an understanding of the collision potentials.

Further research in this area can be done using H_2O as a broadener with the same pressures of O_2. A method of measuring the partial pressure of water vapor in the cell would be needed as well as a method of efficiently removing the water from the cell between measurements.

Another interesting experiment would be to do a study of temperature variation on collisional broadening of O_2 using the noble gases as collision partners. Using materials available at present, we can cool the cell to temperatures of liquid nitrogen (77K), liquid helium (23K), the freezing point of water (273K), and room temperature (295K) (Wolf, private conversations). We would use these four temperature points and keep the pressure constant. We could then determine the temperature dependence of the collisional broadening of the O_2 lines. Other methods of cooling the cell exist, including immersion in a liquid nitrogen bath and regulating the temperature with heating elements (Spencer, 1997). Heating the cell above room temperature is possible using either a heating element installed in the cell or by exciting the vibrational states of H_2O using microwave radiation. What is useful to the Air Force here is that the temperature range we would use spans the atmospheric temperature range, leading us to a method of temperature sounding the atmosphere remotely from space or ground.

NO Study

Here, we have not sufficiently satisfied our goal of the determination pressure broadening coefficients for the two states of NO. If we had time here's what we planned to do to improve our results: First, we would eliminate the spectrometer feature discussed in Chapter 3. Again, this requires contractor intervention. We think our method of producing the spectra is sound, and can only be improved with higher resolution, which requires a spectrometer with a longer path length for the movable mirror (See Appendix A). We can improve signal to noise ratio next time by doing longer runs (greater than 100 scans per run) for each measurement, or by using the method of coadding many 100 scan runs discussed in the O_2 section. Since this requires much more time, this would require improving the gas handling system to eliminate leaks over the long term. The best idea is to pre-fill a glass cell with a rubber-seal-on-glass valve and place it in the spectrometer by itself each time with _no_ gas handling system. We tried this once using CO as a broadening gas and got our highest signal to noise ratio so far and better resolution on the far lines in each branch. See Figures 4-1 and 4-2 for a comparison of our CO spectra. Note how the signal to noise ratio increases by a factor of the square root of the number of additional coads in both the wing of the R-branch (Figure 4-6) and in the Q-branch (Figure 4-7).

Clearly, we are not fitting the peaks well. We need to modify the curve fitting algorithm to better handle the split peaks of the 1/2 state and the unresolved doublets of the 3/2 state The Voigt profile should work, but we must reduce the number of free parameters in the fitting algorithm. With a single peak, we have three. But with a double

peak, we have six. If we lock the distance between the peak centers (Spencer, 1994) we will reduce the parameters by one. Our Peak Fit software does not have this feature. Next would be to try to hold the Lorentzian widths and/or the amplitudes of the two peaks constant (Liou and Torbert, 1987). This is physically acceptable, given that the populations in the two states should be equal at a given temperature (Burggraf, private conversations). This would further reduce the number of free parameters to four.

If that does not work, we could try fitting the peaks with a Galatry profile or a speed-dependent Voigt profile (Ritter, 1987). These were compared by Ritter, et. al. for their oxygen spectroscopy experiment in 1987, and they had the lowest residuals using the Galatry profile.

We are satisfied with the table Curve software for determining γ_0 from the Lorentzian widths, since it works well with what it's fed. Future researchers are welcome to use our data and it has been archived in the Physics Department for this reason. Since, in general, NO collisional broadening is new research, the next step would be to explore molecular gas broadening of NO.
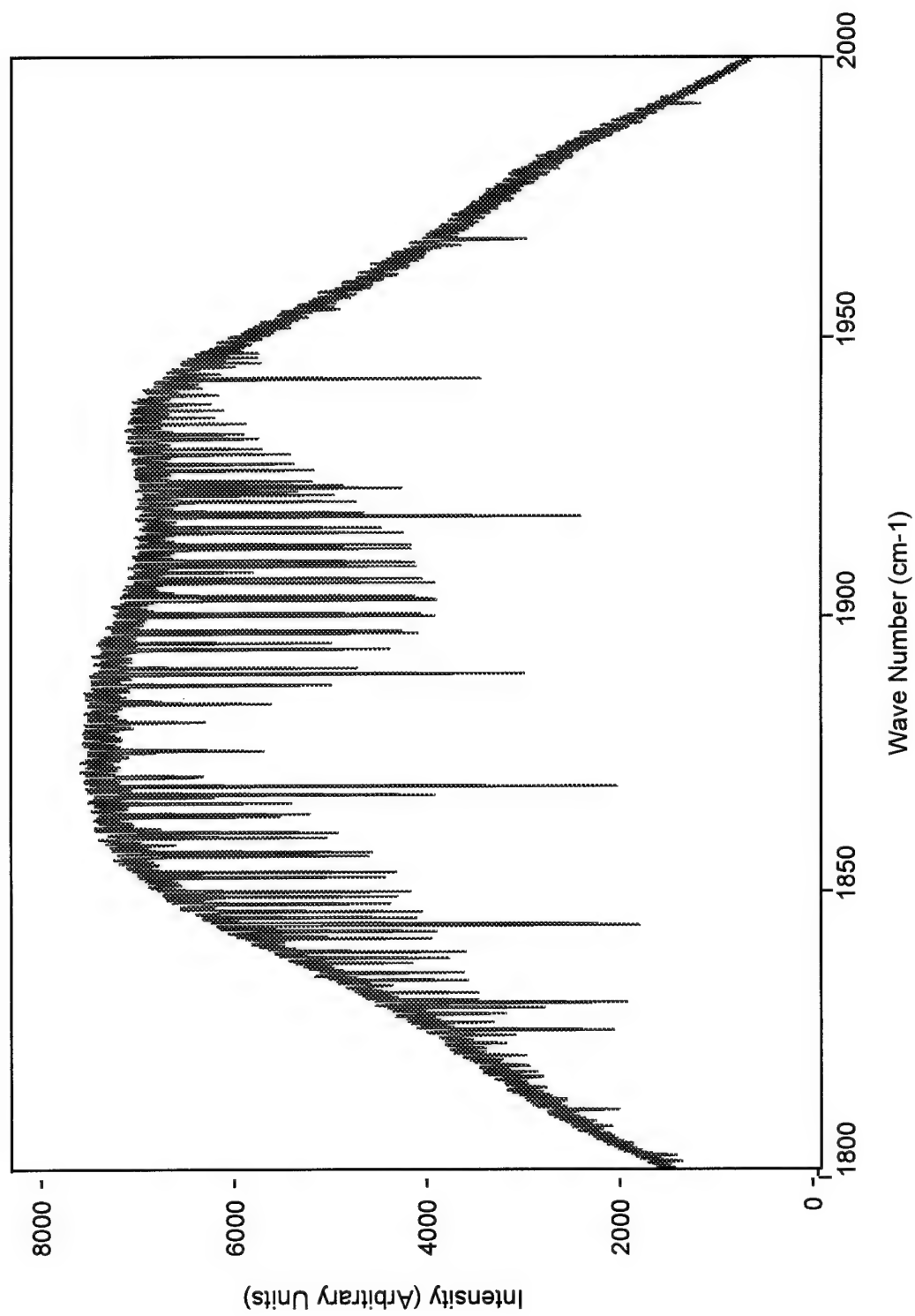
Figure 4-1: NO broadened by CO spectrum, 20Torr CO, 500m Torr NO, 100scans (coads).

80
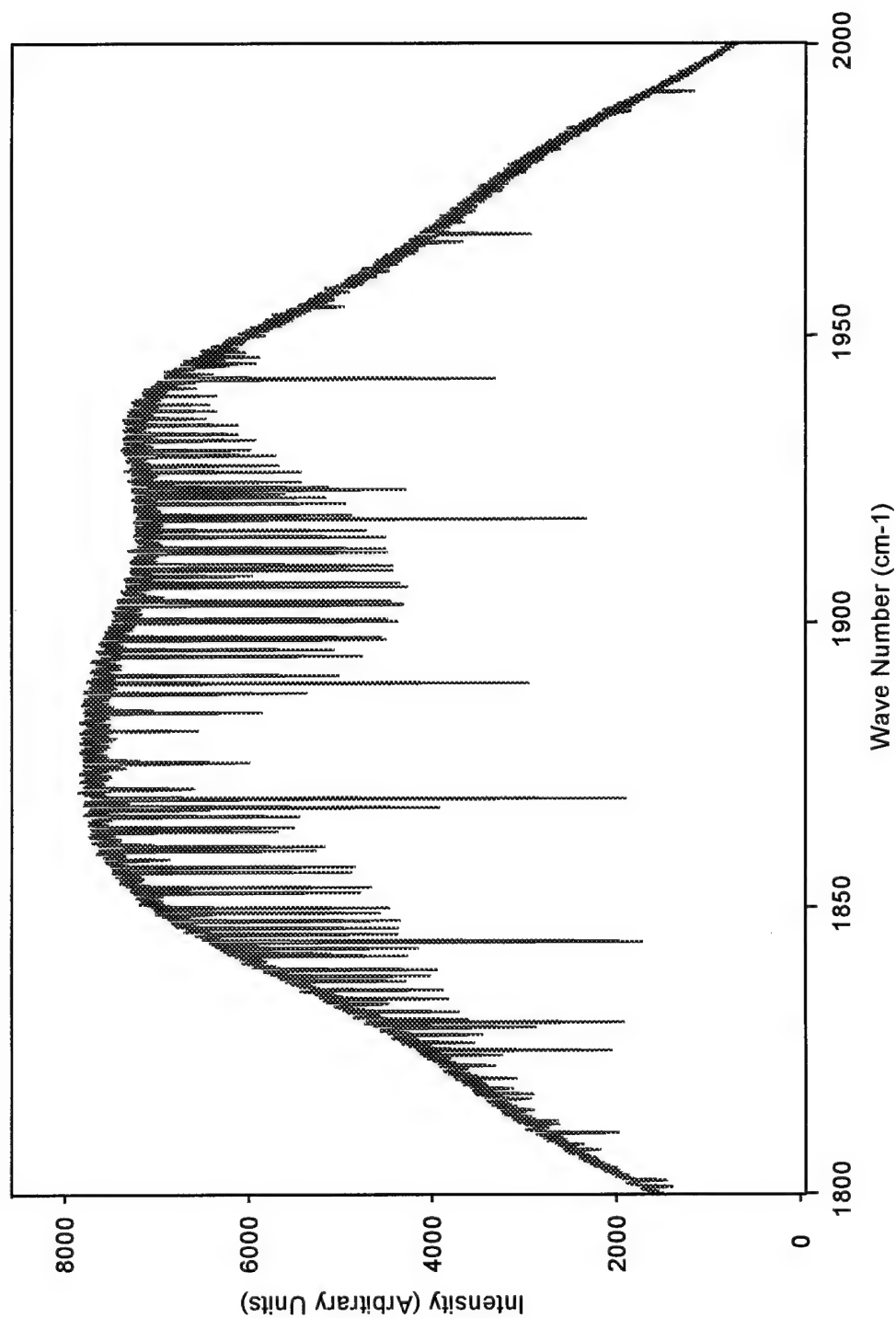
Figure 4-2: NO broadened by CO spectrum, 20Torr CO, 500m Torr NO, 3 coadded spectra of 100 coads each.

81
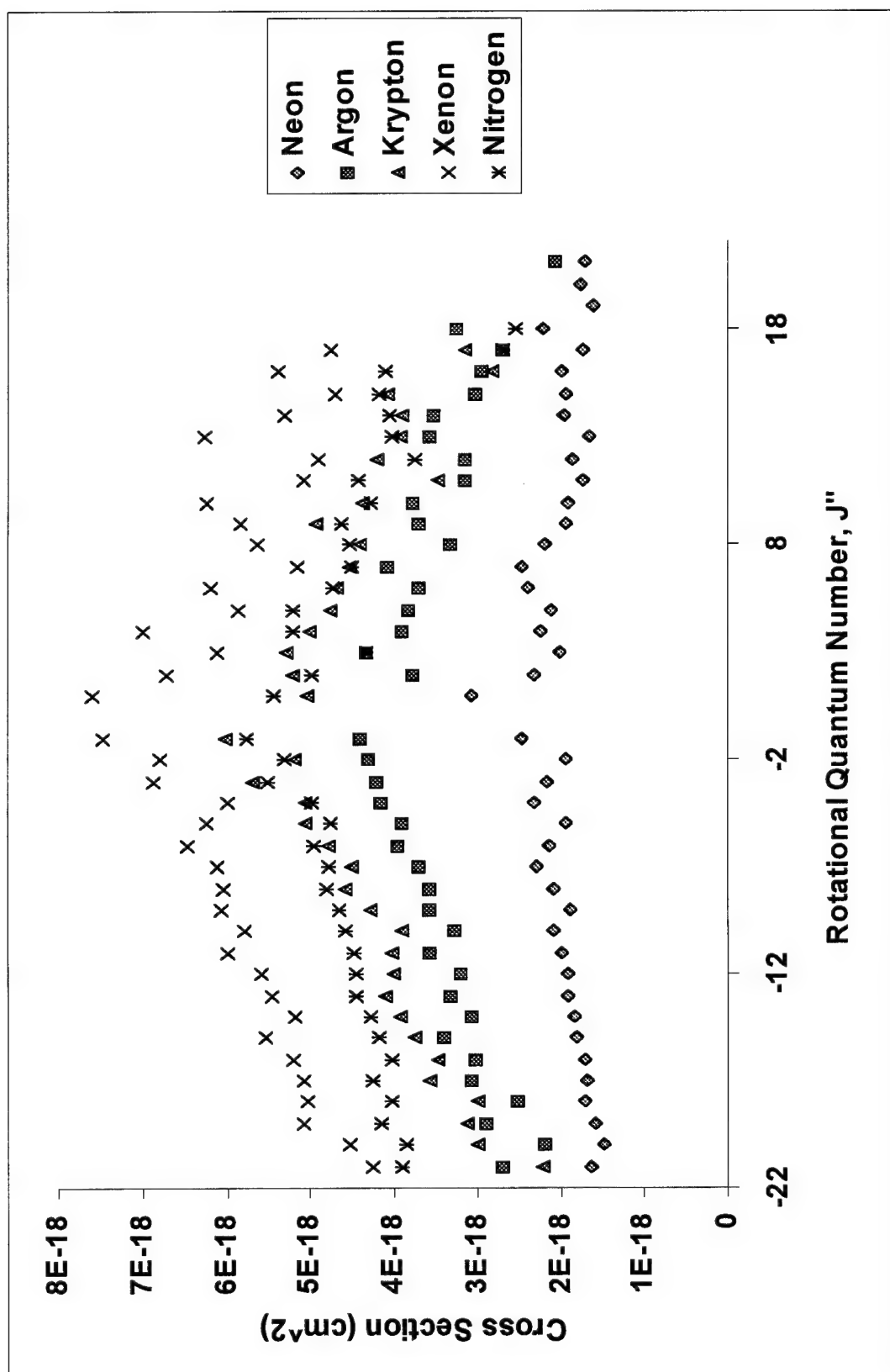
Figure 4-3: σ vs. J" plot for O₂ noble gas broadening.

82
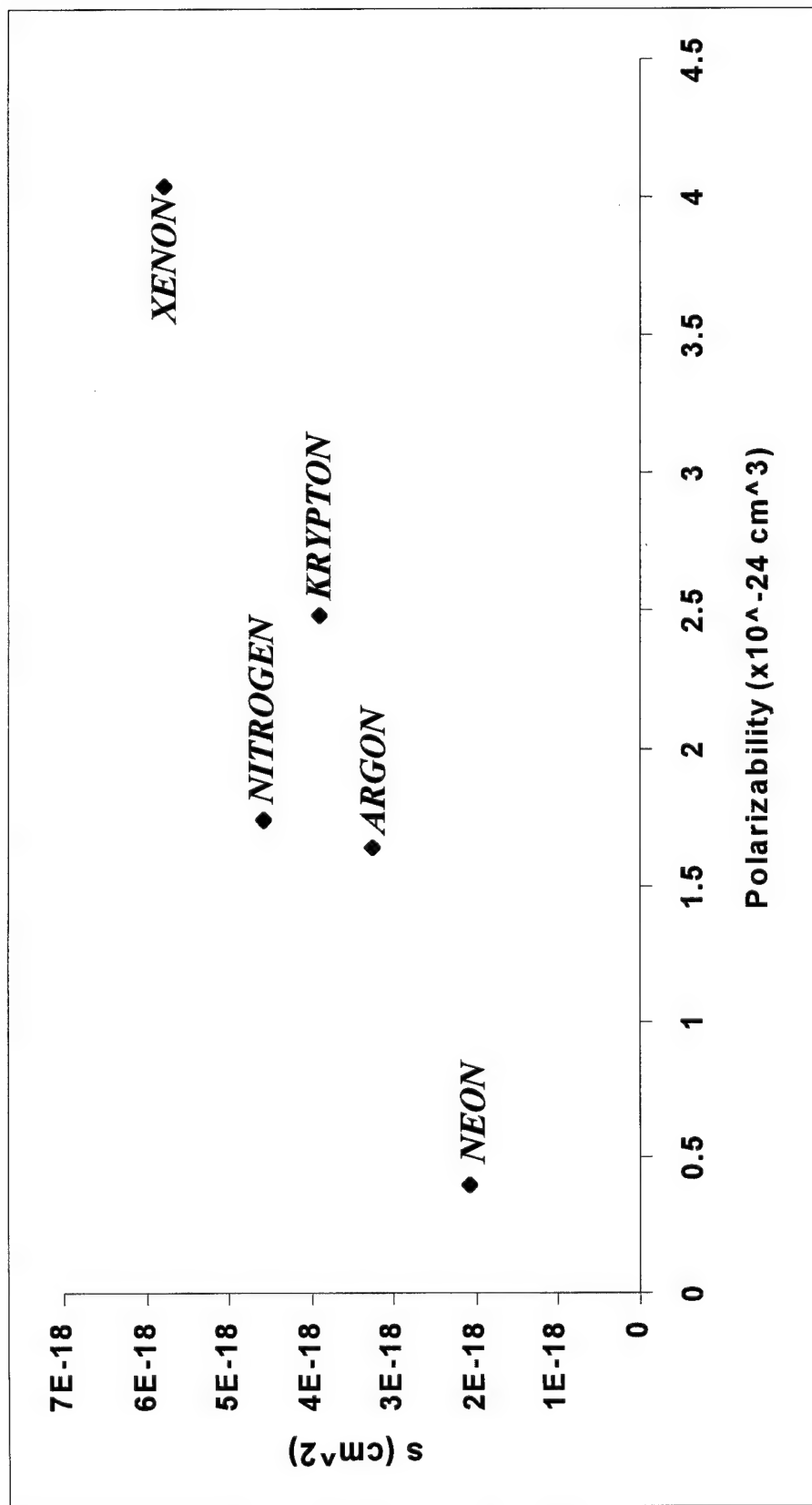
Figure 4-4: σ vs. polarizability for the $J''=9$ line of O_2 broadening.

83
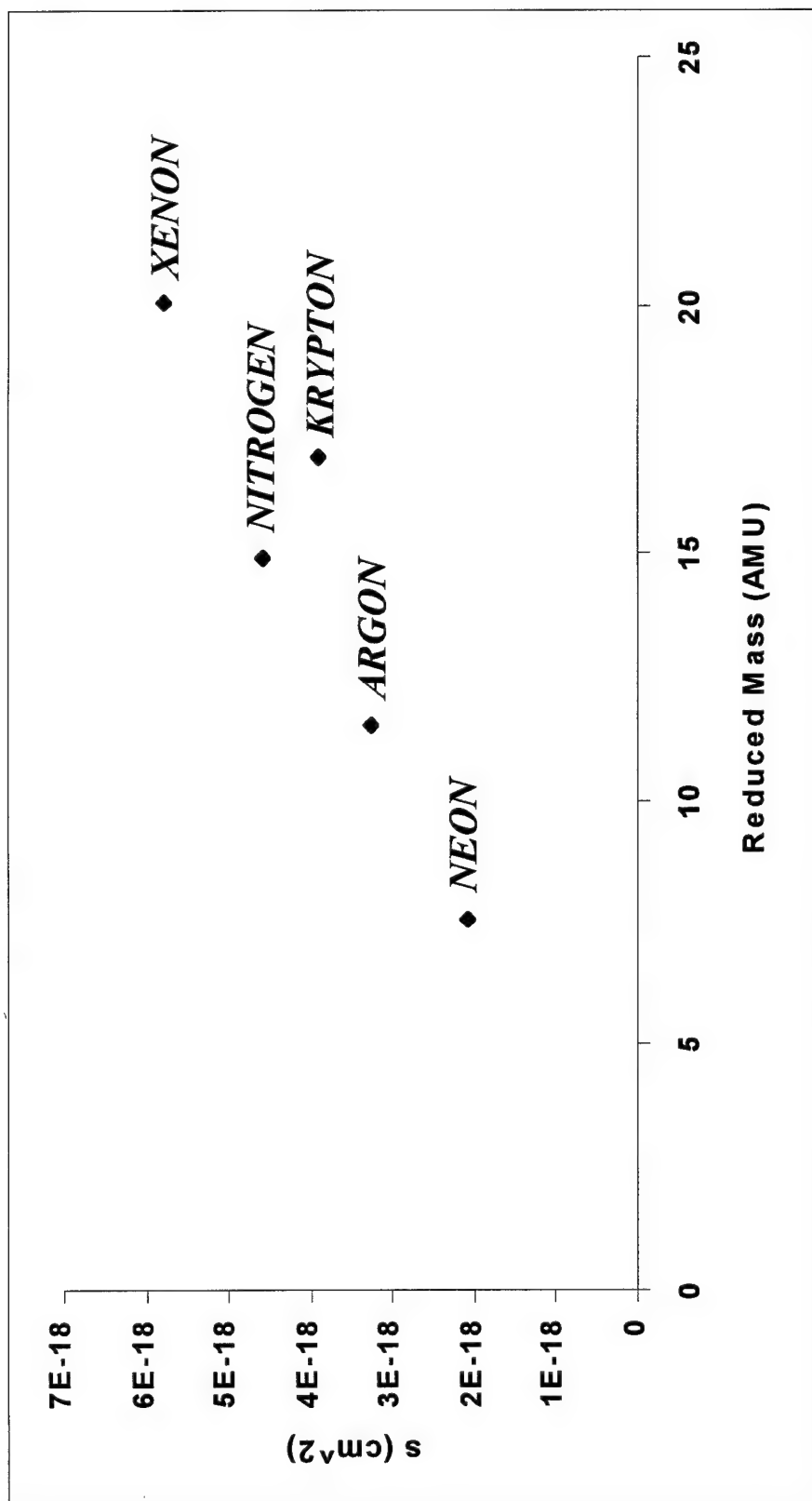
Figure 4-5: σ vs. reduced mass of collision pair, O_2 broadening $J''=9$ line.

84
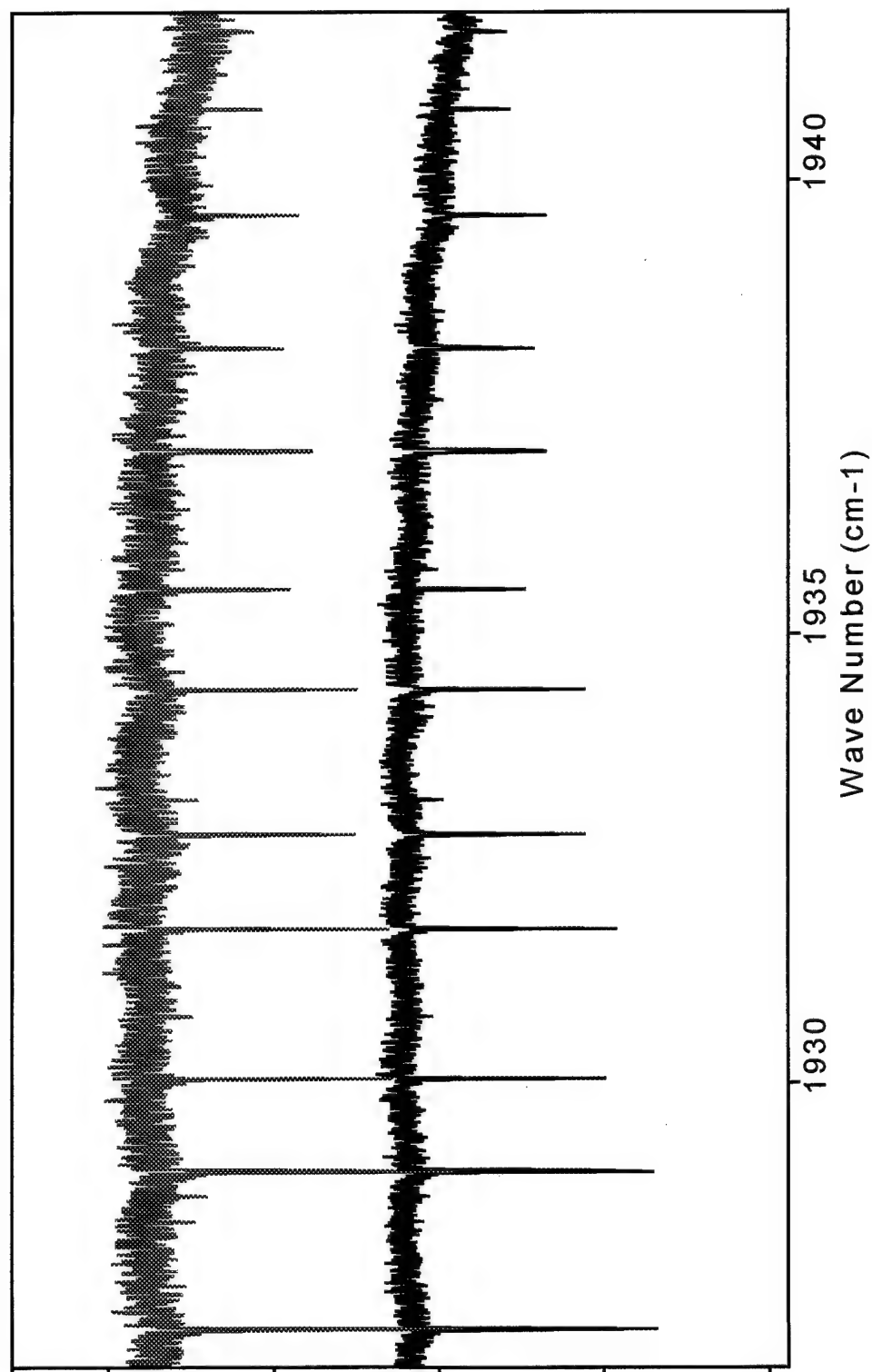
Figure 4-6: Comparison of single 100 scan spectrum and 3 coadded spectra, all at 20 Torr CO and 500mTorr NO. Top trace is single spectrum, bottom is 3 coadded spectra, both are the region around J" = 18.5 in the R-branch.

85
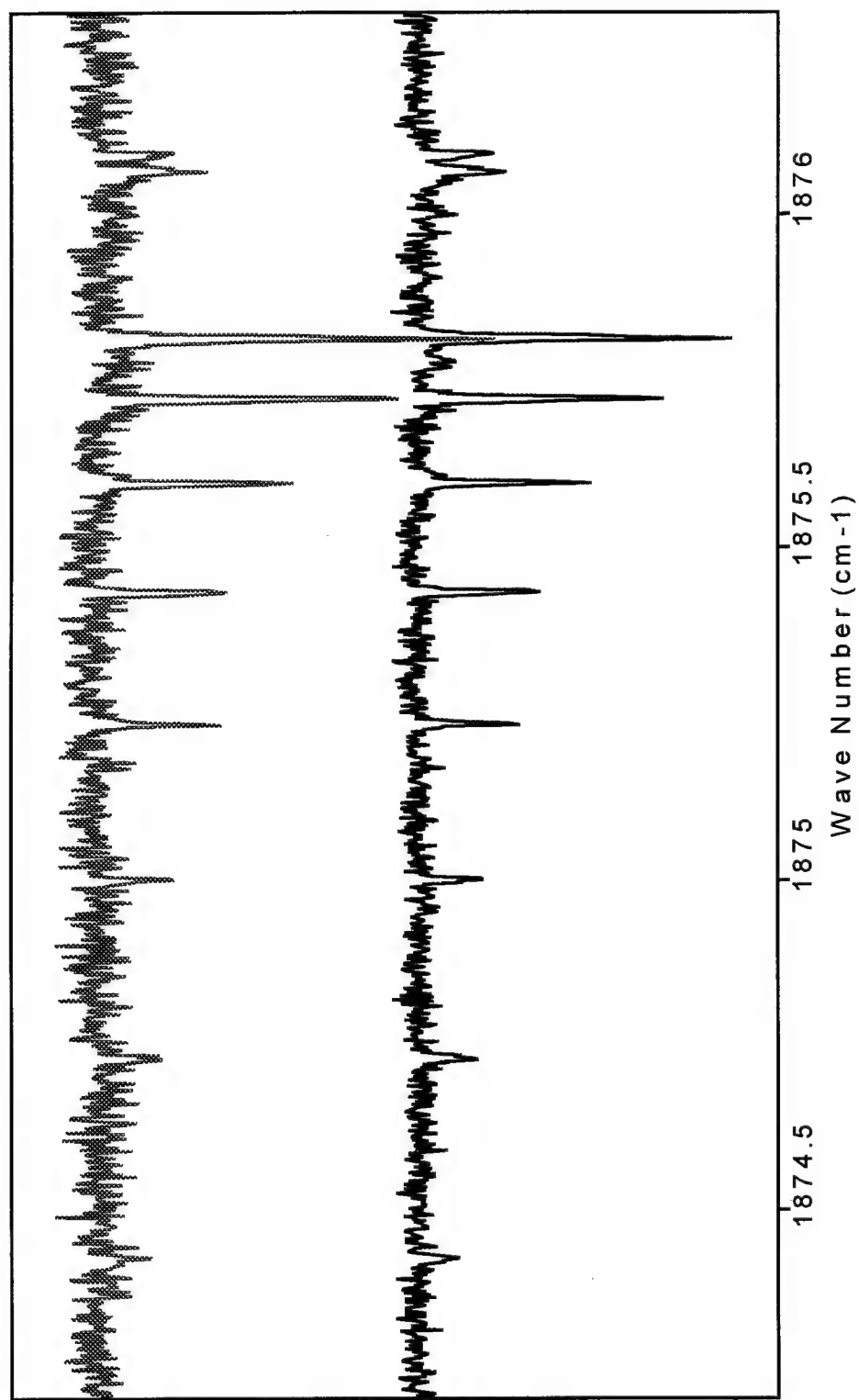
Figure 4-7: Comparison of single 100 scan spectrum and 3 coadded spectra, all at 20 Torr CO and 500mTorr NO. Top trace is single spectrum, bottom is 3 coadded spectra, both are the Q-branch.

86

Appendix A: Fourier Transform Spectroscopy Theory

The Bomem DA-8 200 Fourier transform spectrometer is basically a Michelson interferometer where one mirror arm is mounted on a movable track. (Bomem spectrometer manual). See Figure 2-1 for a diagram of the apparatus. Imagine an interferometer with a monochromatic source. If the mirrors are exactly the same distance from the beam splitter the beams recombine at the detector and interfere constructively (add) to give a detector output at maximum. Likewise with an integral number of wavelengths ifference. If the mirrors are off by exactly ½ wavelength distance, destructive interference occurs and the detector senses a minimum. In between ½ integral and integral wavelength differences, the detector output will be in between minimum and maximum output (Sears, 1984). Now if we smoothly move the mirror from its zero point out, we will see alternating intensity with a sinusoidal variation. If we record the intensity vs. time, this is our "interferogram" which is shown for three different frequencies in Figure A-1 (Goodman, 1989). Different monochromatic sources will produce sinusoidal interferograms with different frequencies. A Fourier transform of a perfect sine wave is a delta function in frequency space (Kreyszig, 1996). This frequency space representation *IS* our spectrum. So looking at Figure A-1, the spectra of the three monochromatic sources are to the right and display *one* frequency at *one* intensity. This is the basis of the FT spectrometer's operation (Goodman, 1989). Now, demonstrate with the use of three frequencies as if we had three monochromatic sources. See Figure A-2. The interferograms show constructive and destructive addition of the three frequencies (here we are have equal intensities of frequencies in the source). The Fourier transform of this

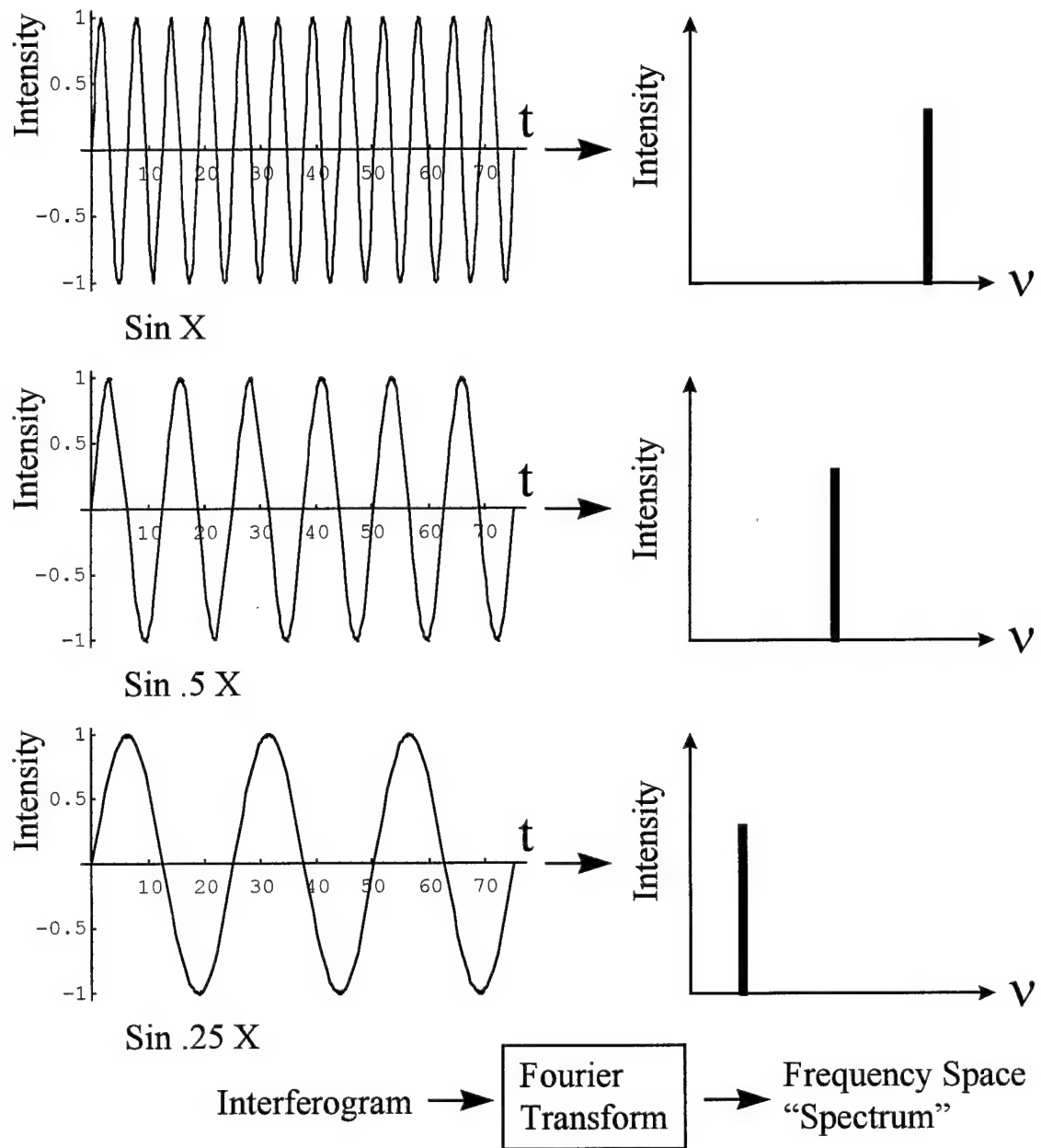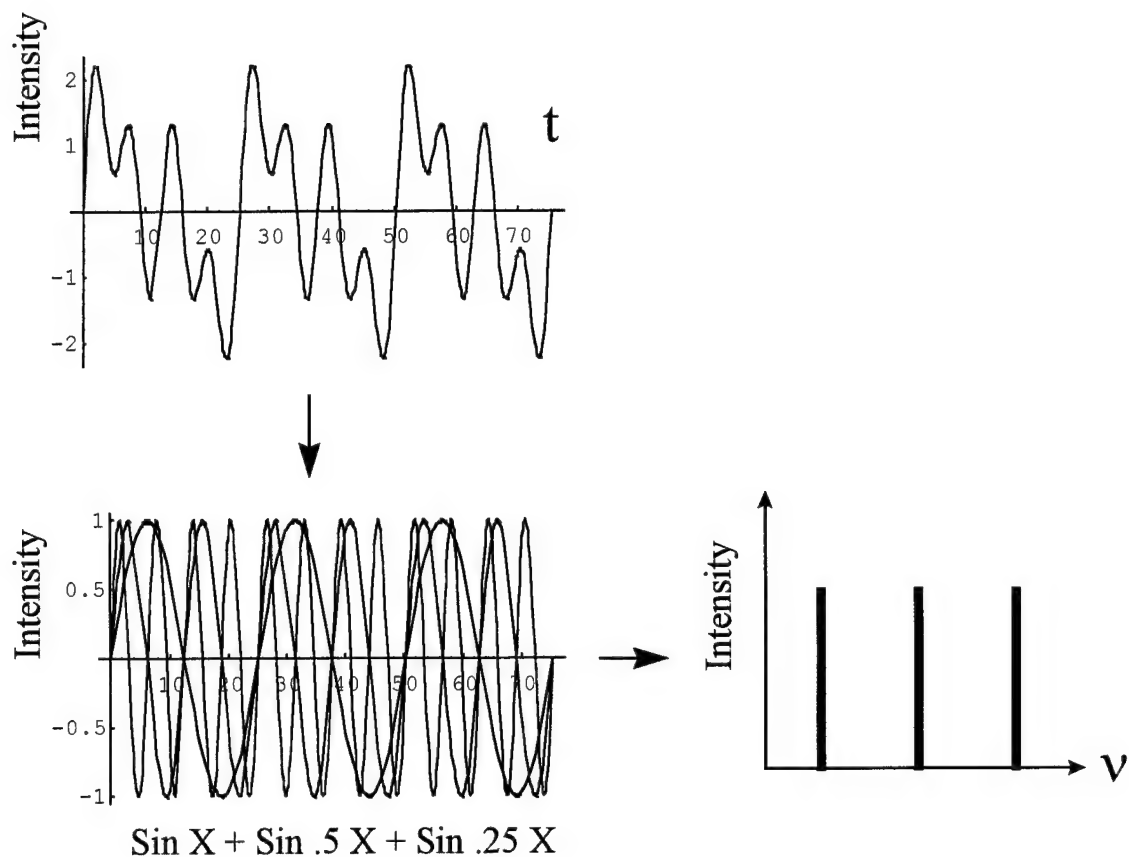gives us a spectrum with three delta functions at the locations of each frequency of the source.

Figure A-1: Fourier transform spectrum production process using individual monochromatic sources.

Figure A-2: Fourier transform spectrum production process using three monochromatic sources at once.

Remember, we use a continuum source in our spectrometer, in the visible range for the O_2 experiment and infrared for NO. The interferogram will contain many added sine waves of many frequencies. What you would see then, after the Fouier transform, is a spectrum with an infinite number of delta functions with intensities proportional to the intensity of the individual source frequency "parts" (Goodman, 1989). This will look like our background trace, which is exactly what it is. The background trace is the spectrum

of the SOURCE (Goodman, 1989). Figure A-3 shows the interferogram and spectrum for the source (Banwell, 1972).

Now, add a cell of absorbing gas which completely *removes* certain frequencies from the source (or a filter!). This will be represented in the interferogram as missing sine waves at the frequencies where the sample absorbs. That is how we get our spectrum. The Fourier transform will not see those frequencies and will not place "delta functions" where the absorption takes place. It will display zero intensity there. If only partial absorption takes place at a certain frequency, the interferogram will display a sine wave at that frequency, but at decreased intensity (amplitude). The Fourier transform will show partial absorption in the spectrum. Figure A-3 shows an interferogram and spectrum with absorbing gas in the beam path (Banwell, 1972).

Interferogram → Fourier Transform → Frequency Space "Spectrum"
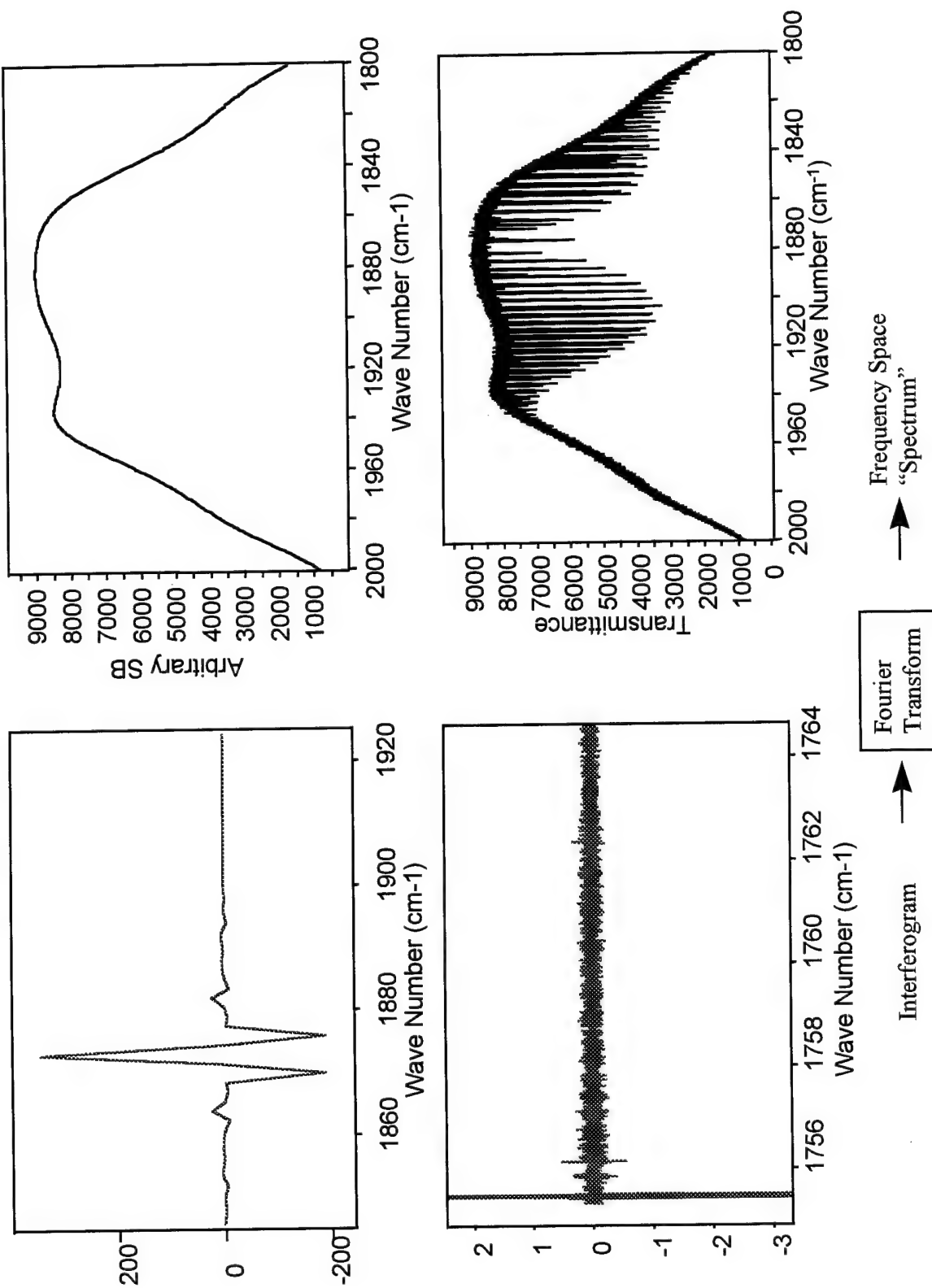
Appendix B: Results Graphs

Pressure broadening coefficient vs. rotational quantum number, m for O_2 study

Pressure broadening coefficient vs. rotational quantum number, m for NO study

Noble Gas Broadening of Oxygen
Cornicelli '97

Legend:
- ◇ Neon
- ▣ Argon
- ◢ Krypton
- × Xenon
- ✳ Nitrogen

X-axis: Rotational Quantum Number, m

Y-axis: Pressure Broadening Coefficient (x10^-5, cm-1, Torr-1)

O2 Broadened With N2

Pressure Broadening Coefficient
$(x10^{-5}\ cm^{-1}\ Torr^{-1})$

Rotational Quantum Number, m

95

O2 Broadened With Neon

Pressure Broadening Coefficient (x10^-5 cm^-1 Torr^-1)

Rotational Quantum Number, m

◆ Cornicelli '97
▨ Ritter '87

Oxygen Broadened With Argon

Legend:
- ♦ Comicelli '97
- ▦ Ritter '87

X-axis: Rotational Quantum Number, m

Y-axis: Pressure Broadening Coefficient ($\times 10^{-5}$, cm^{-1}, Torr^{-1})

Oxygen Broadened With Krypton

- Comicelli '97
- Ritter '87

Pressure Broadening Coefficient (x10^-5, cm^-1, Torr^-1)

Rotational Quantum Number, m

98

Oxygen Broadened With Xenon

NO - He, Cornicelli 1997
vs NO - N2, Spencer 1994

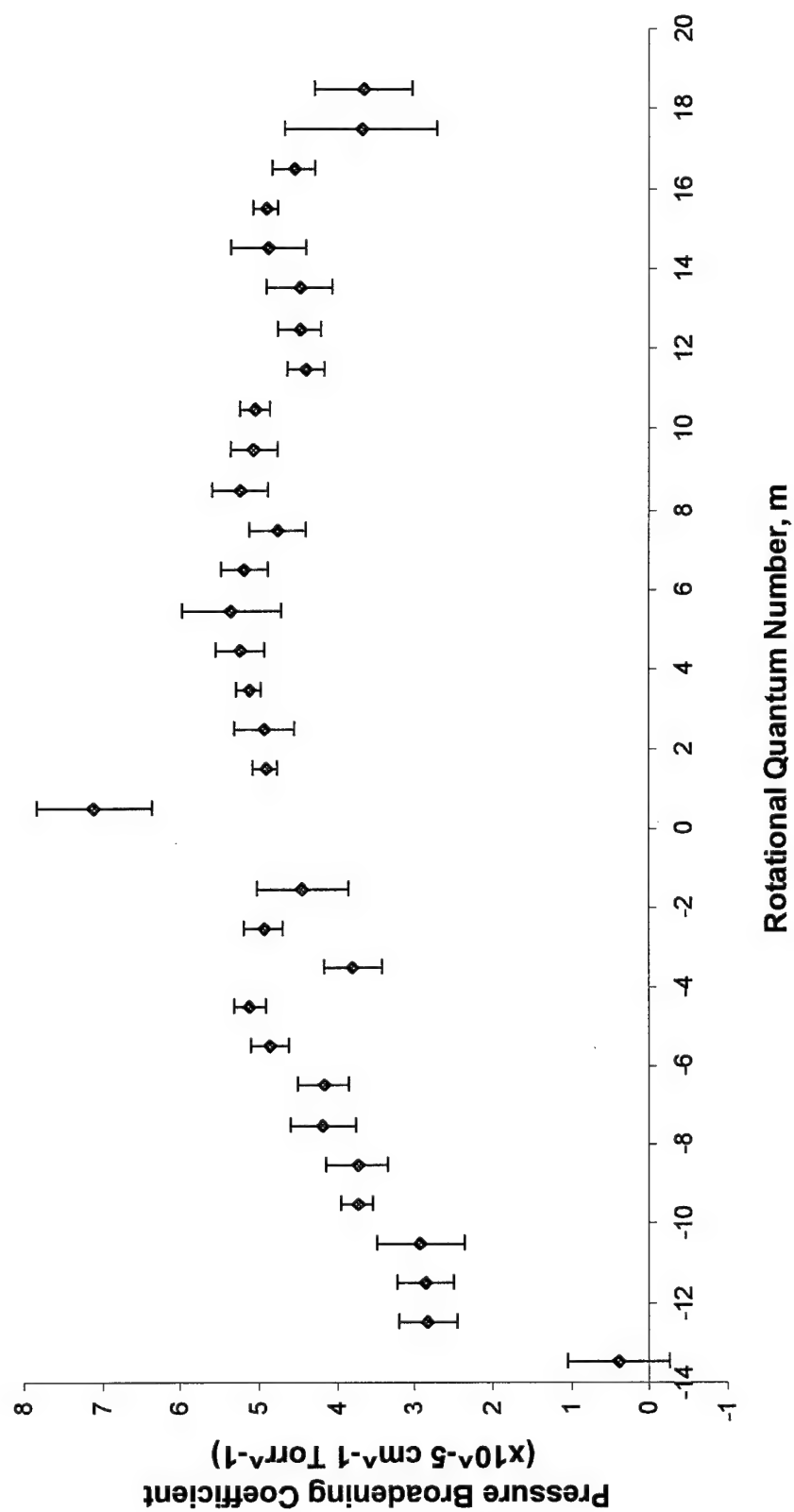Rotational Quantum Number, m

Pressure Broadening Coefficient
(x10^-5 cm^-1 Torr^-1)

- ◆ NO-He f
- ⊛ NO-He e
- ○ NO-N2 f
- ✕ NO-N2 e
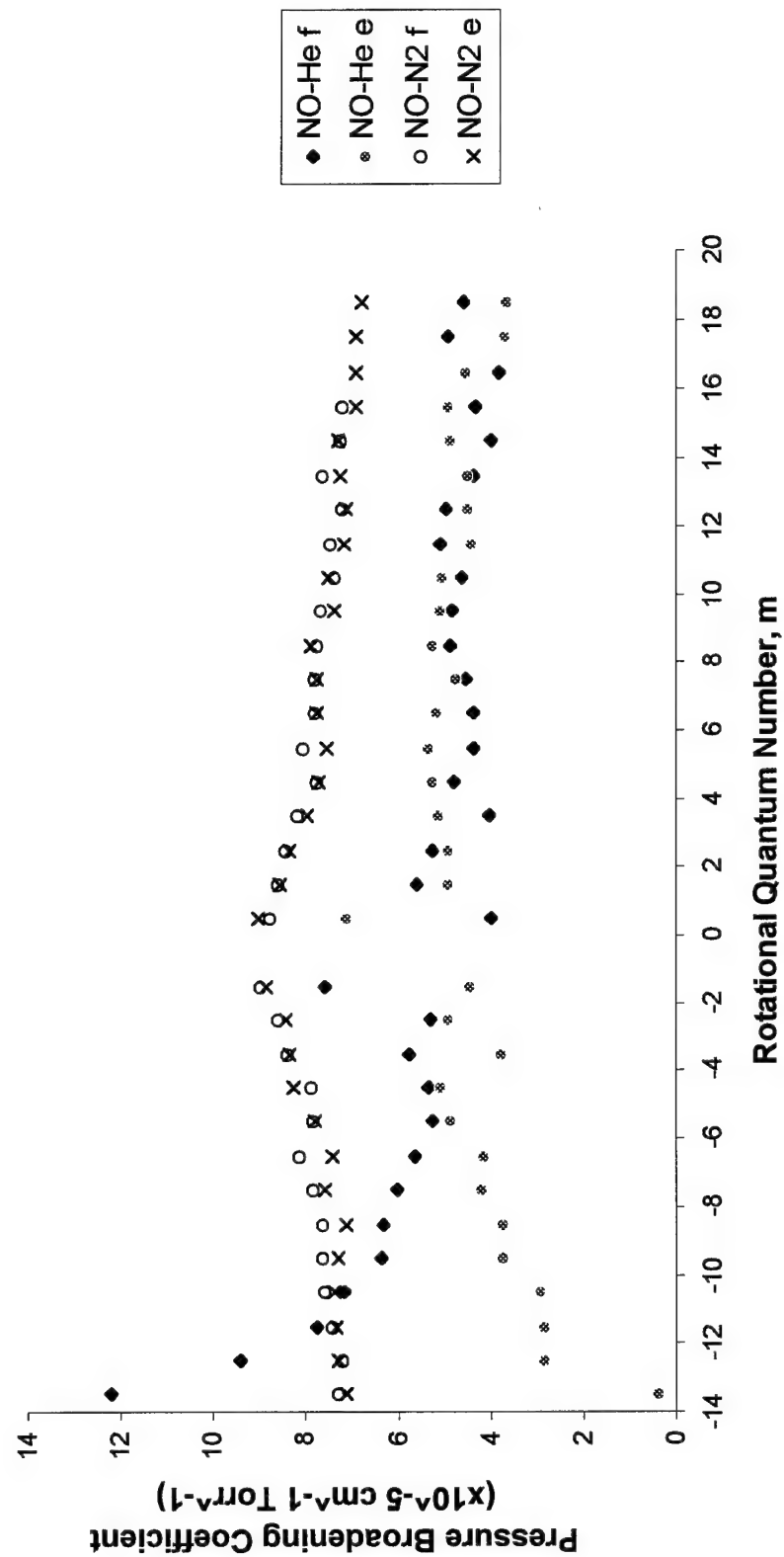
NO Broadened With He (e-state)

NO Broadened With He (f-state)

Pressure Broadening Coefficient (x10^-5 cm^-1 Torr^-1)

Rotational Quantum Number, m

NO - Ne, Cornicelli 1997
vs. NO - N2, Spencer 1994

Legend:
- ◆ NO-Ne f
- ▨ NO-Ne e
- ○ NO-N2 f
- ✕ NO-N2 e

X-axis: Rotational Quantum Number, m

Y-axis: Pressure Broadening Coefficient (x10^-5 cm^-1 Torr^-1)
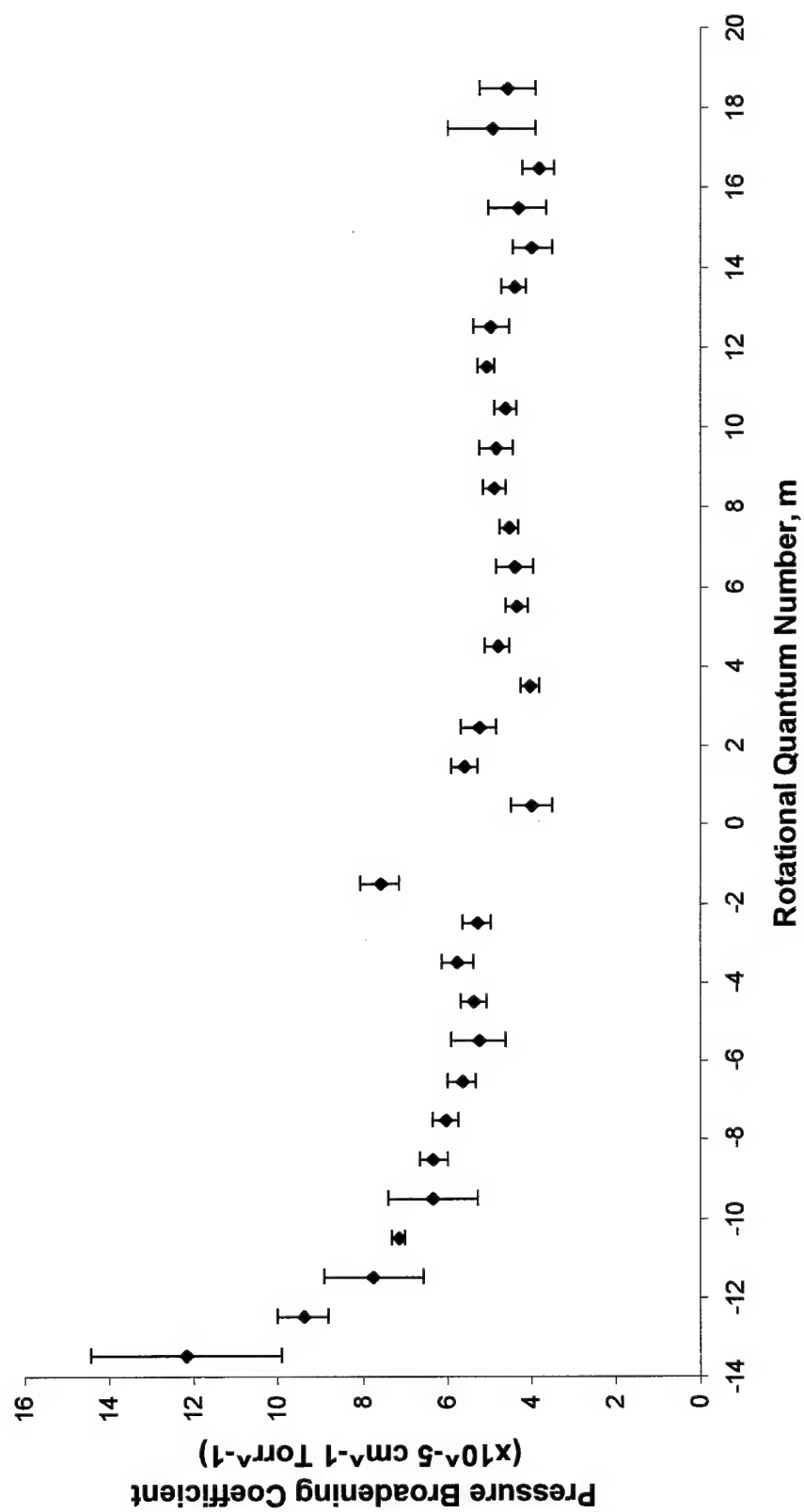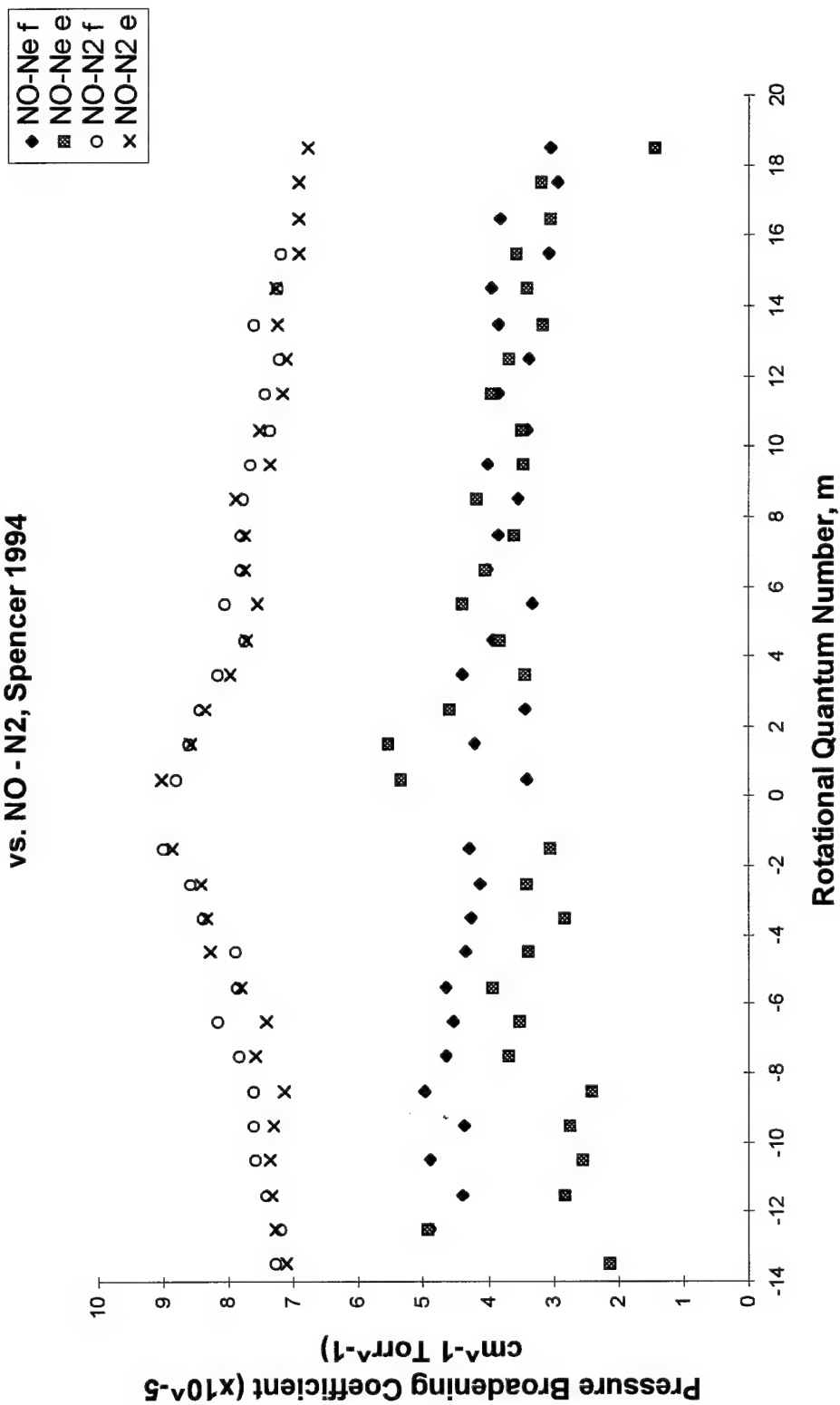
NO Broadened With Ne (e-state)

Rotational Quantum Number, m

Pressure Broadening Coefficient
($\times 10^{-5}$ cm^{-1} Torr^{-1})

104
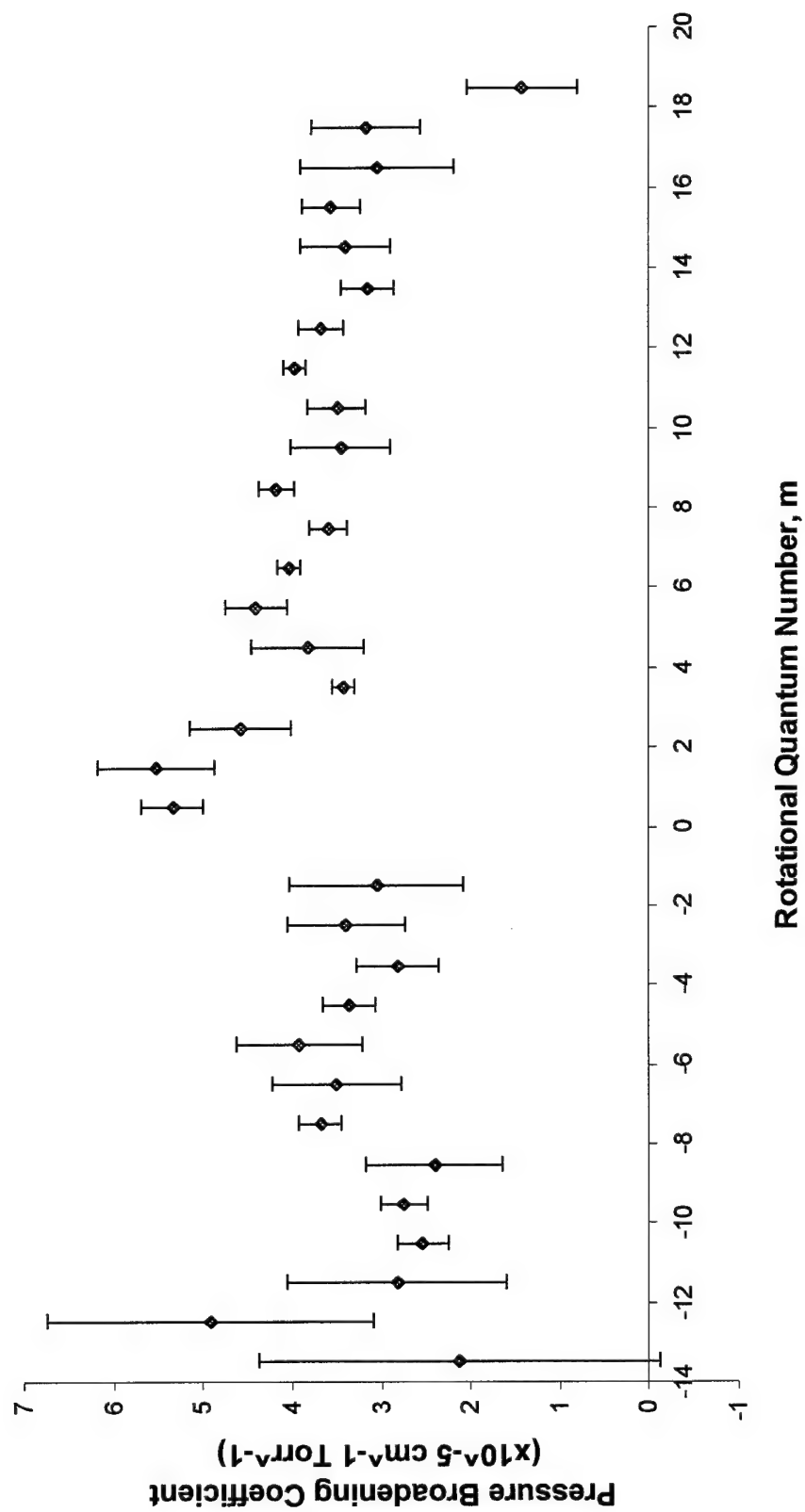
NO Broadened With Ne (f-state)

Pressure Broadening Coefficient (x10^-5 cm^-1 Torr^-1)

Rotational Quantum Number, m

NO - Ar, Cornicelli 1997
vs NO - N2, Spencer 1994

Pressure Broadening Coefficient
(x10^-5 cm^-1 Torr^-1)

Rotational Quantum Number, m

Legend	
●	NO-Ar f
✳	NO-Ar e
○	NO-N2 f
×	No-N2 e
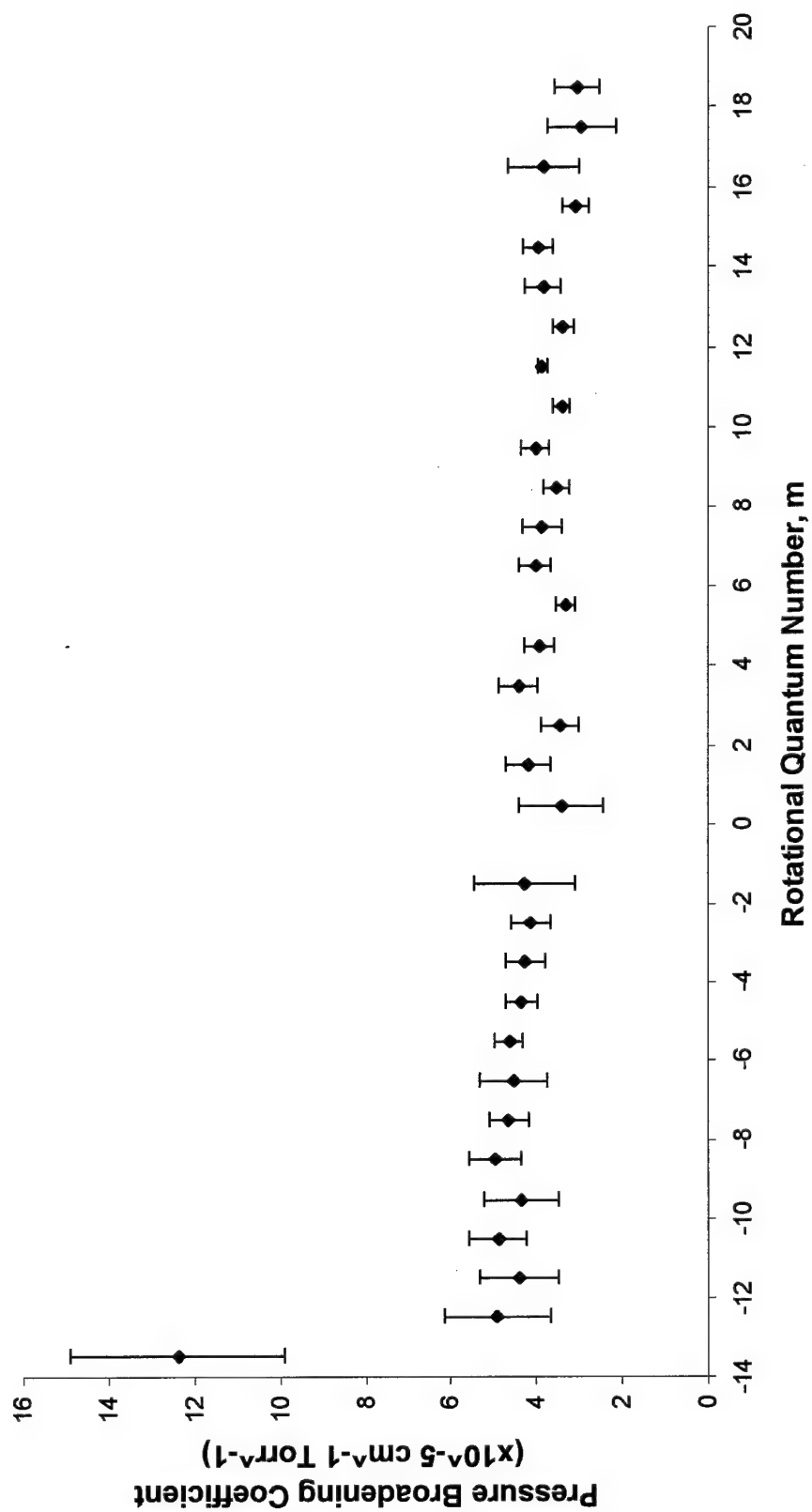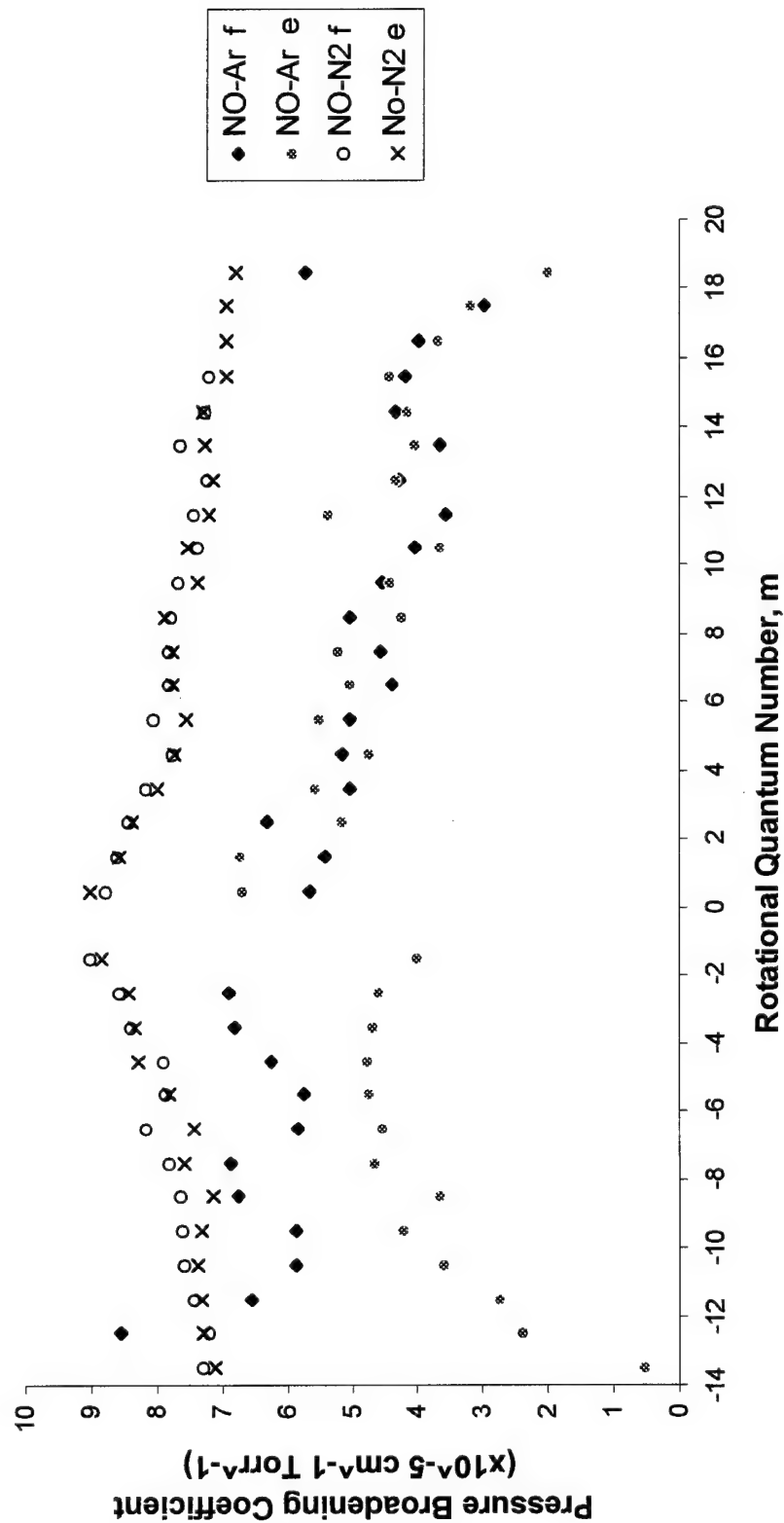
NO Broadened With Ar (e-state)

Pressure Broadening Coefficient ($\times 10^{-5}$ cm^{-1} Torr^{-1})

Rotational Quantum Number, m

107
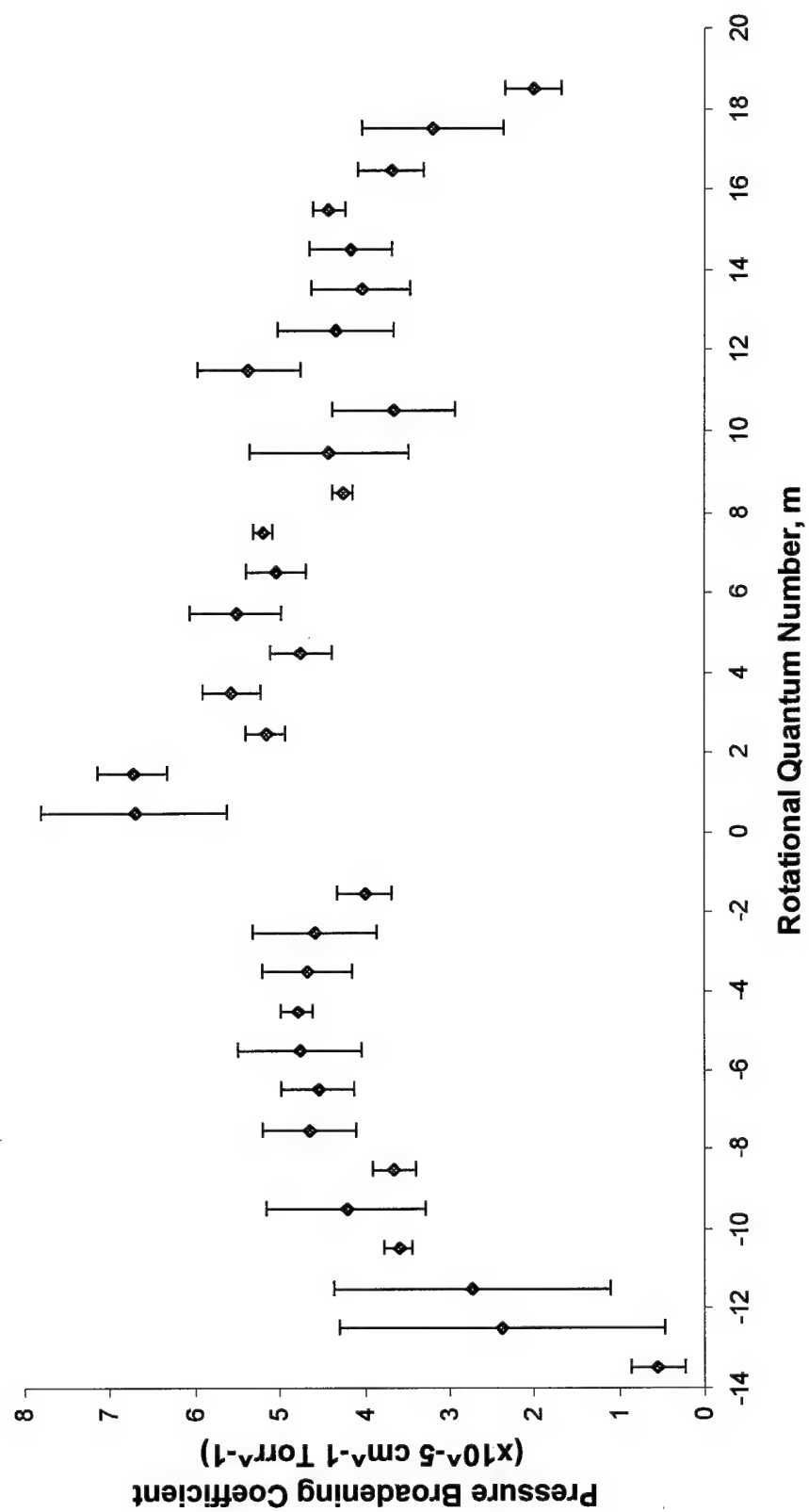
NO Broadened With Ar (f-state)

Pressure Broadening Coefficient (x10^-5 cm^-1 Torr^-1)

Rotational Quantum Number, m

108

NO - Kr, Cornicelli 1997
vs NO - N2, Spencer 1994

Rotational Quantum Number, m

Pressure Broadening Coefficient (x10^-5 cm^-1 Torr^-1)

Legend:
- ◆ NO-Kr f
- ✳ NO-Kr e
- ○ NO-N2 f
- ✕ NO-N2 e
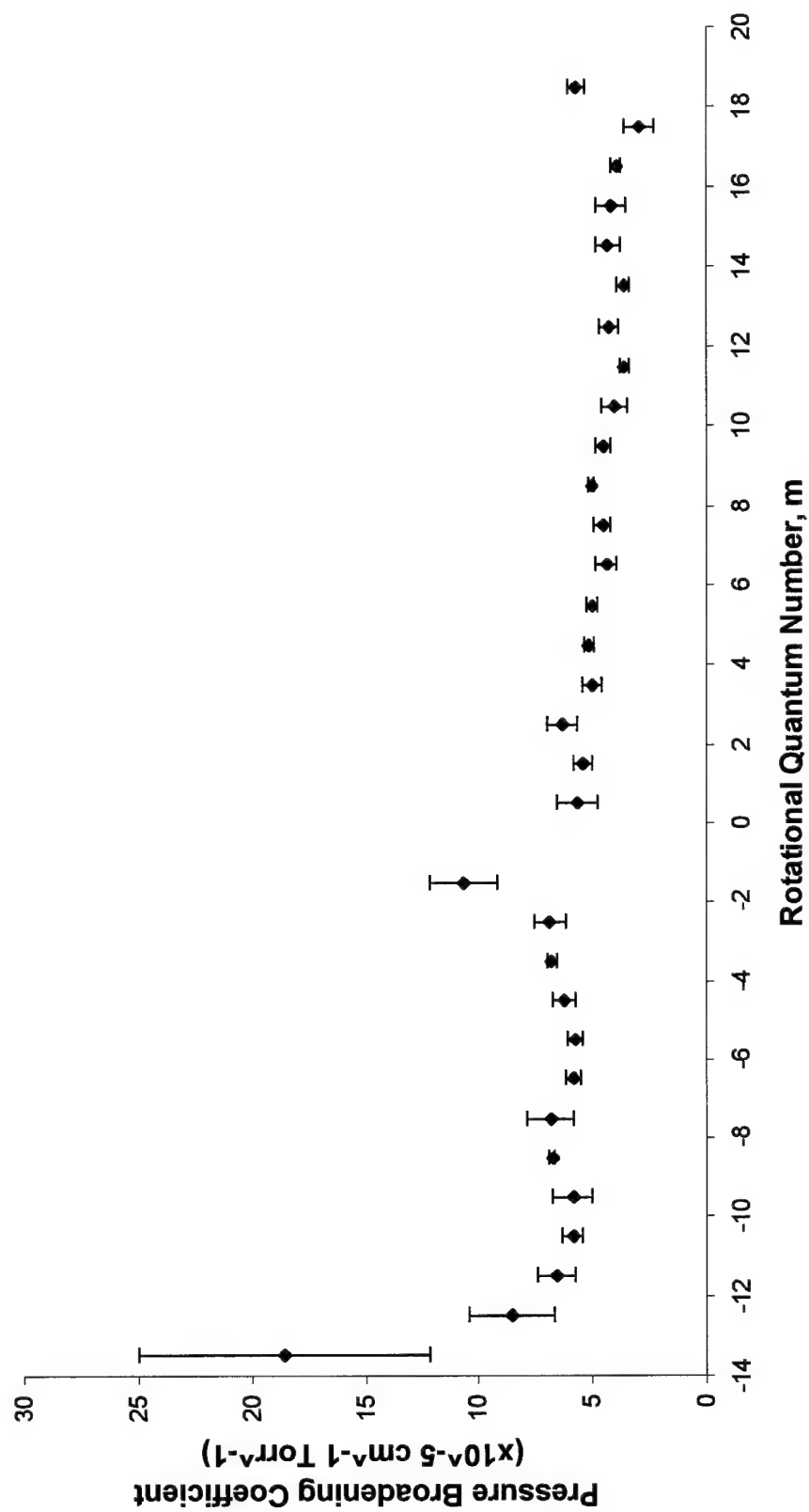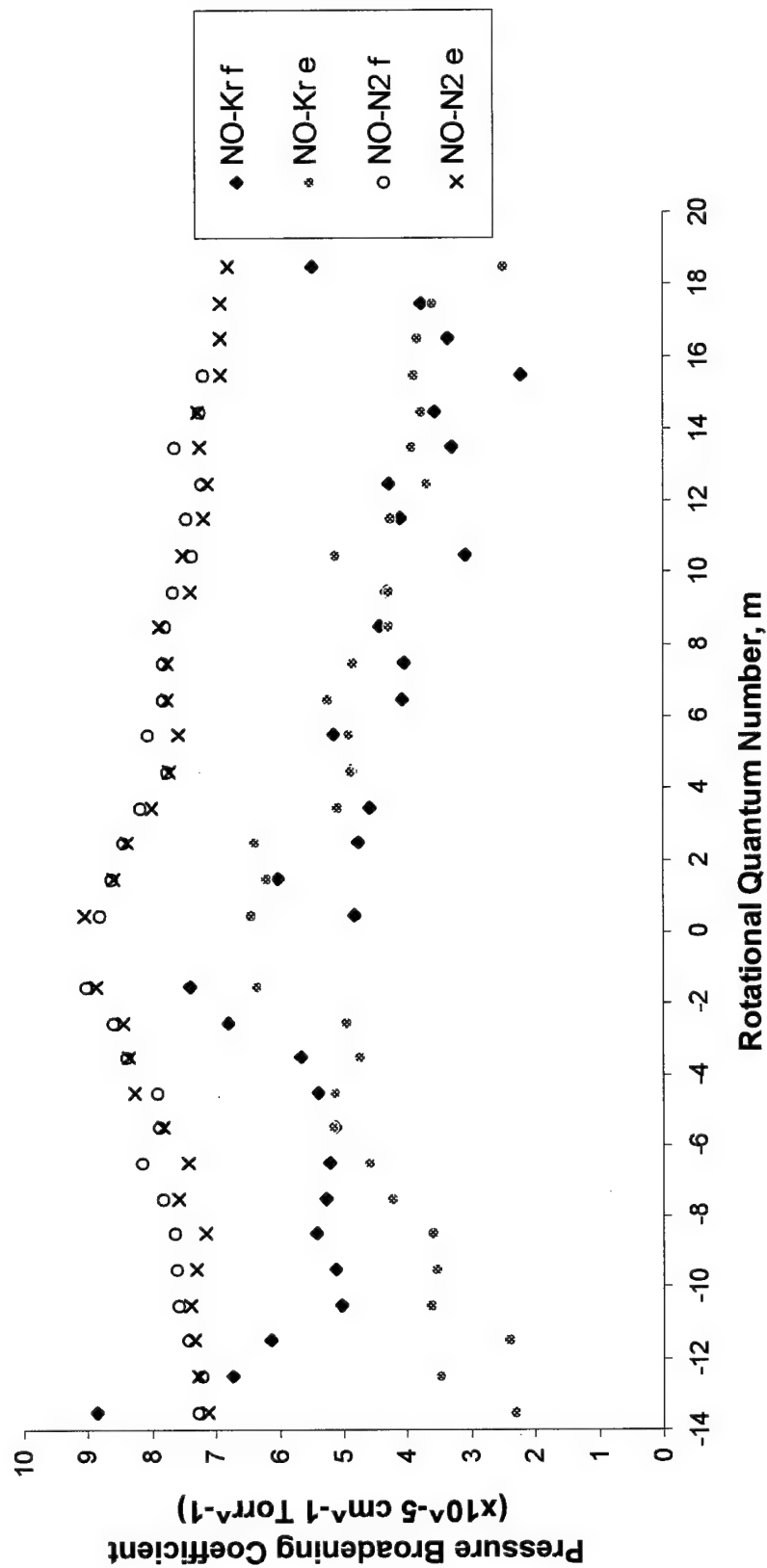
NO Broadened With Kr (e-state)

Pressure Broadening Coefficient (x10^-5 cm^-1 Torr^-1)

Rotational Quantum Number, m
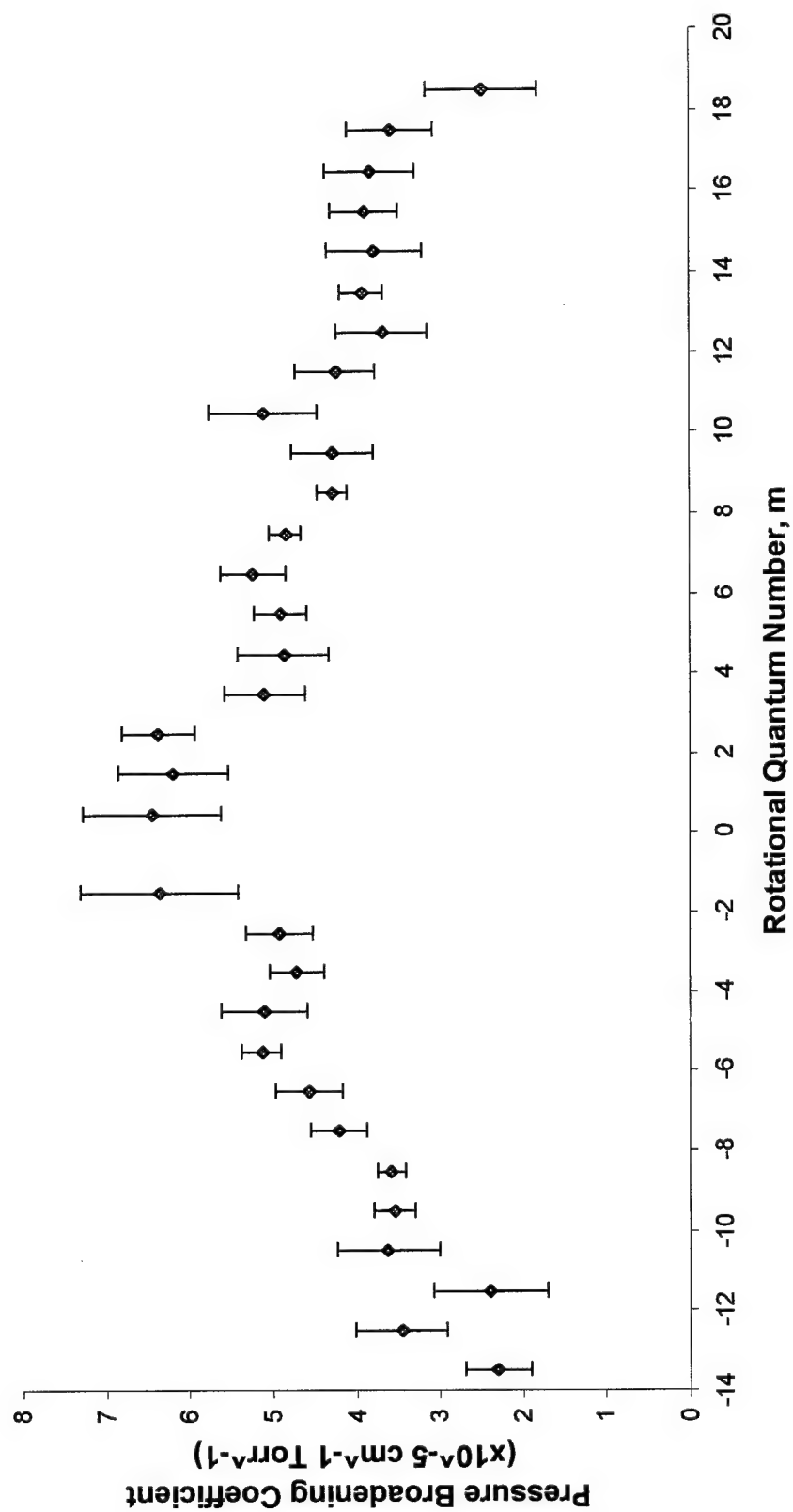
NO Broadened With Kr (f-state)

Pressure Broadening Coefficient (x10^-5 cm^-1 Torr^-1)

Rotational Quantum Number, m

111

NO - Xe, Cornicelli 1997
vs NO - N2, Spencer 1994

Pressure Broadening Coefficient (x10^-5 cm^-1 Torr^-1)

Rotational Quantum Number, m

- NO-Xe f
- NO-Xe e
- NO-N2 f
- NO-N2 e
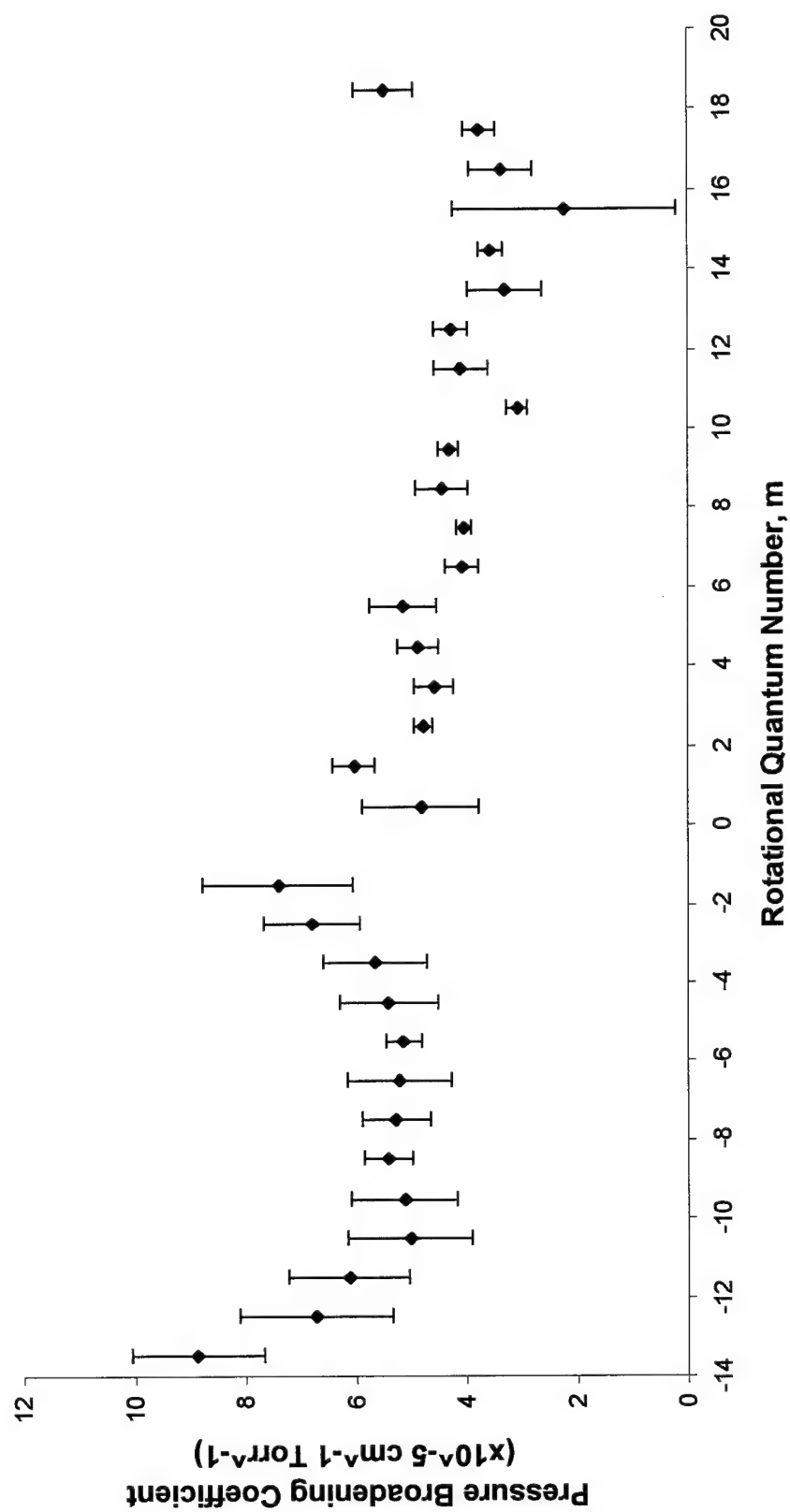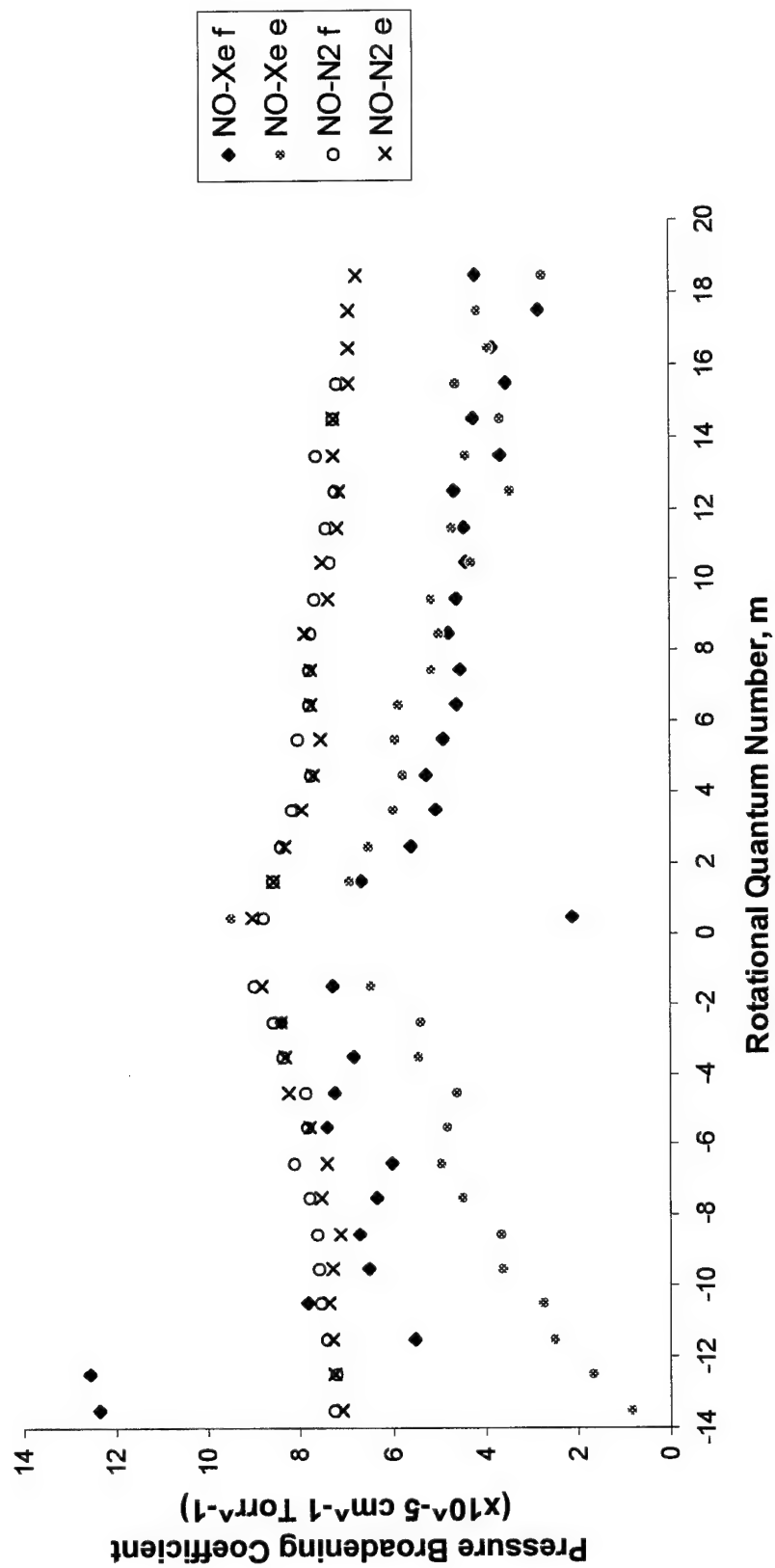
NO Broadened With Xe (e-state)

Rotational Quantum Number, m

Pressure Broadening Coefficient
($\times 10^{-5}$ cm^{-1} Torr^{-1})

113
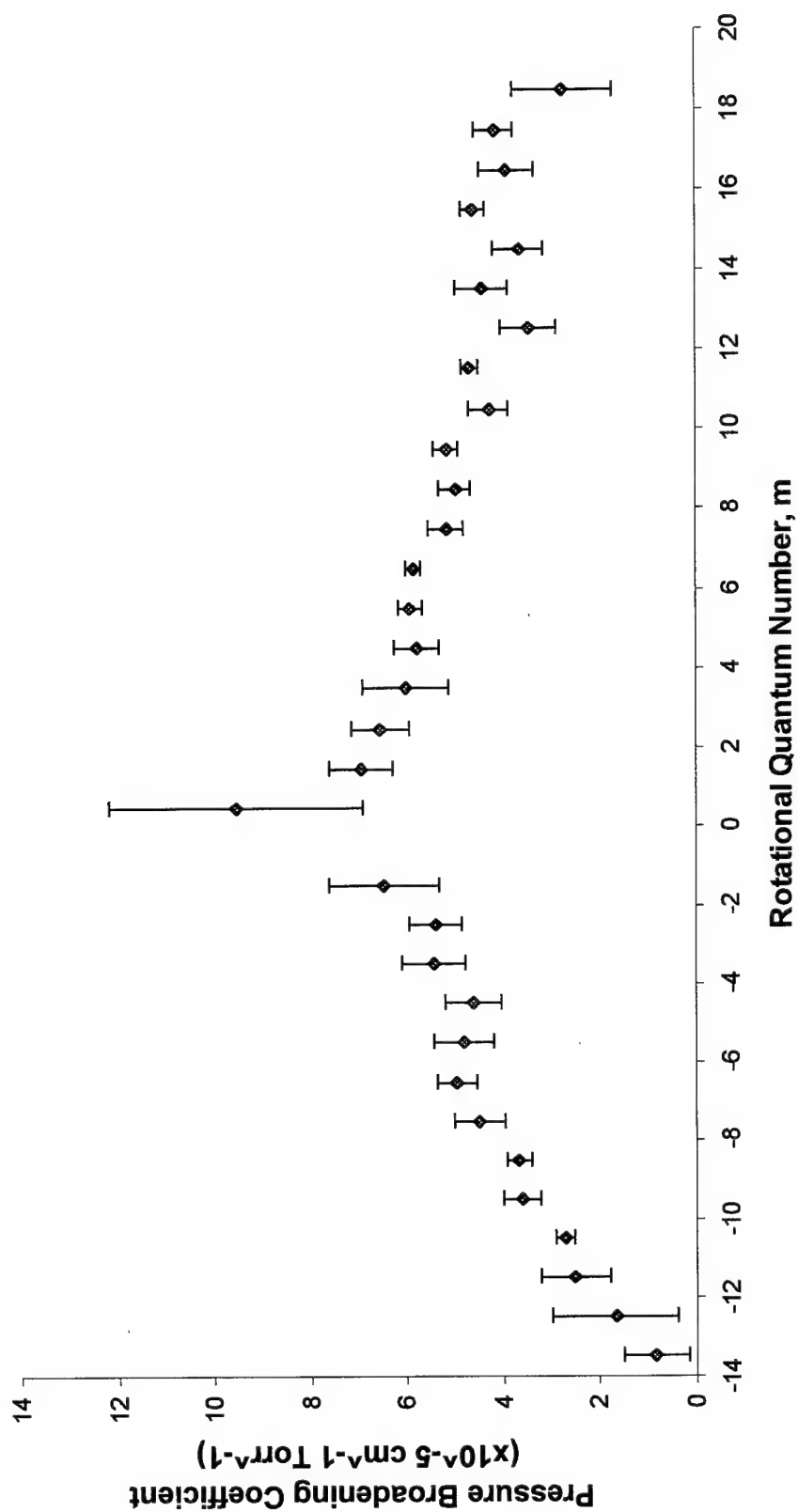
NO Broadened With Xe (f-state)

Pressure Broadening Coefficient (x10^-5 cm^-1 Torr^-1)

Rotational Quantum Number, m

114

γ (x10^-5 cm^-1 Torr^-1)

m

Helium
Neon
Argon
Krypton
Xenon

115
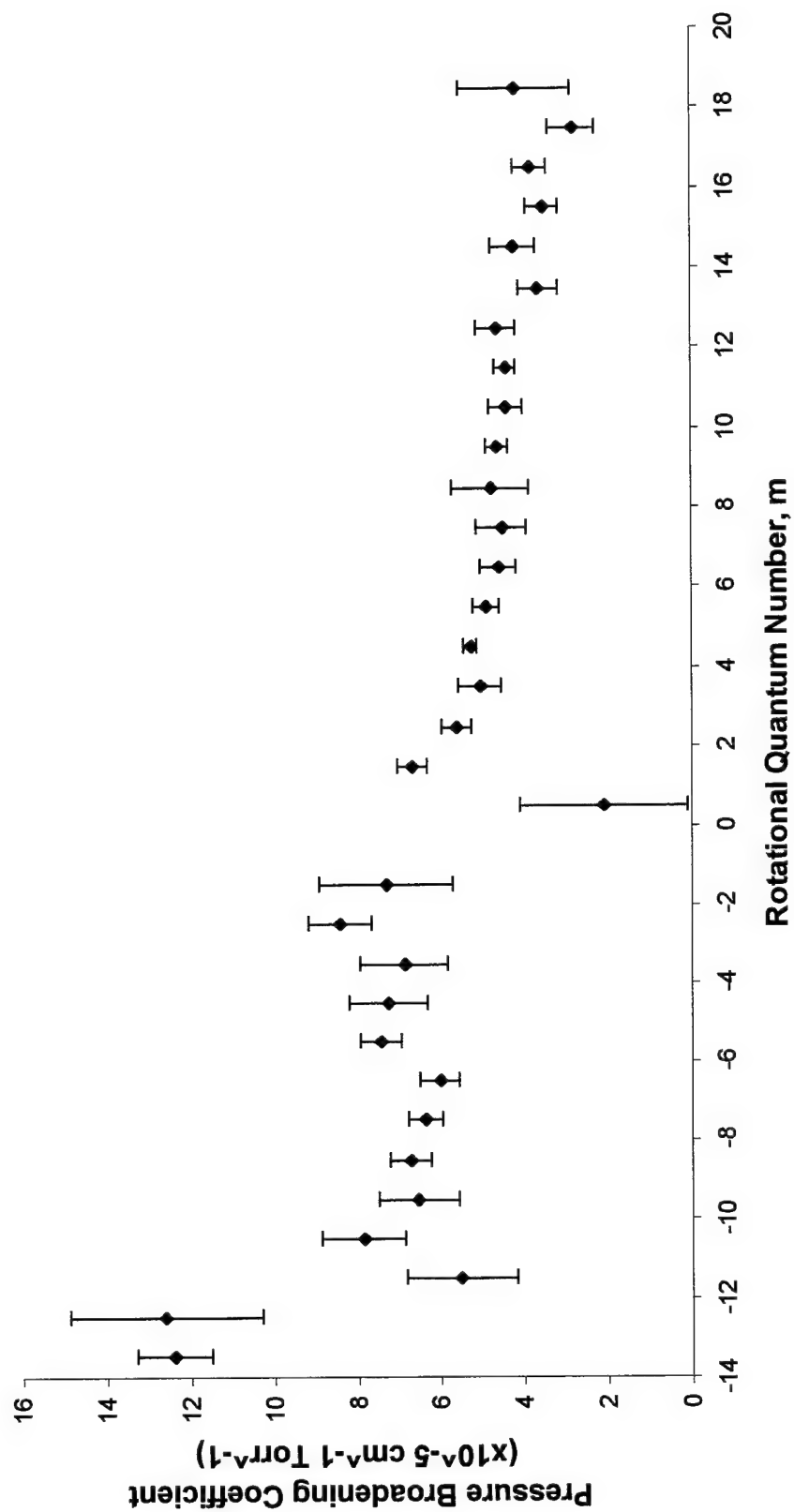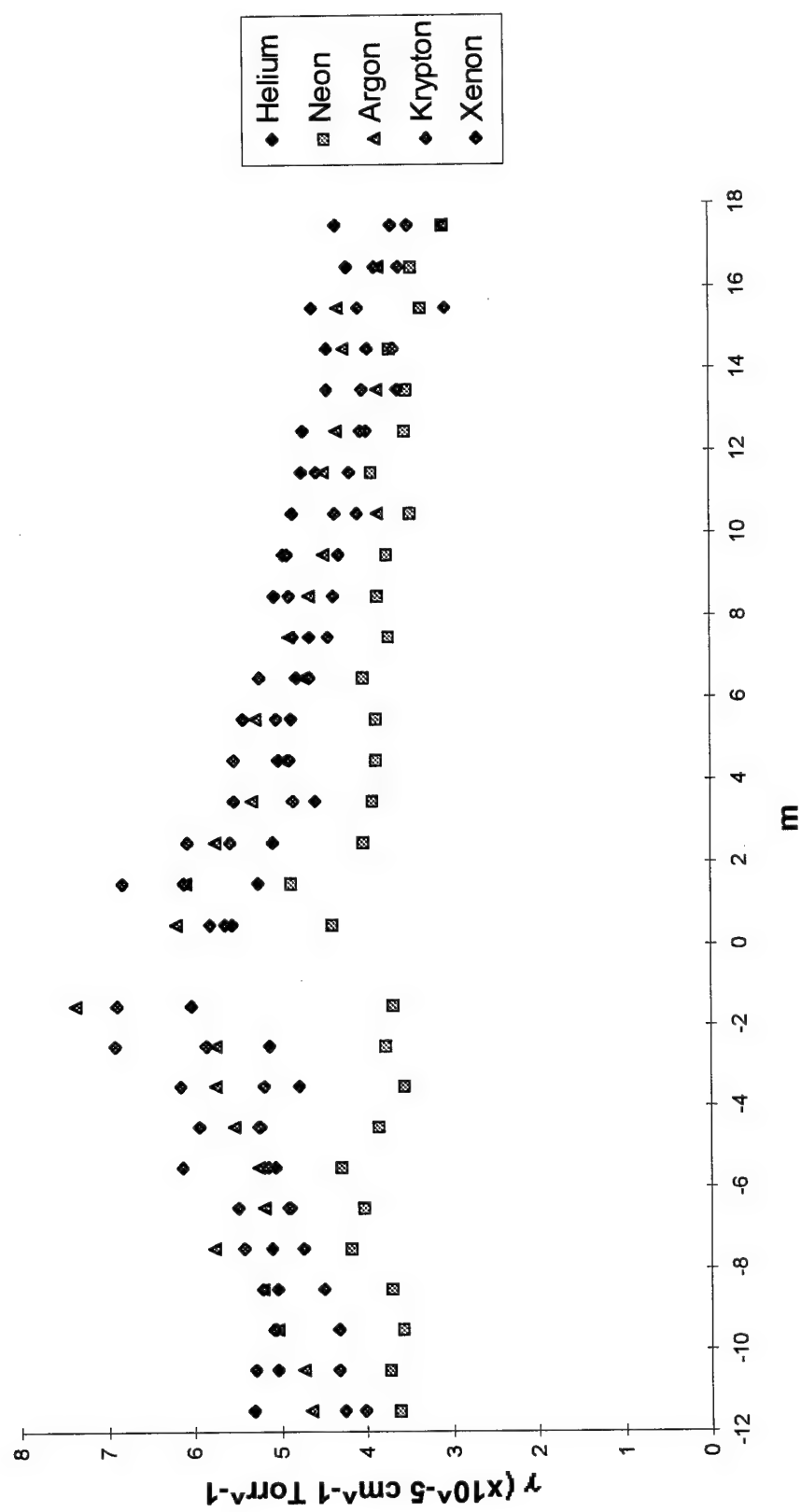
Bibliography

Abels, L. L., and Shaw, J. H., "Widths and Strengths of Vibrational-Rotational Lines in the Fundamental Band of Nitric Oxide," Journal of Molecular Spectroscopy, Vol 20, 11-28, 1966.

Amiot, C., Bacis, R. and Guelachvili, G., "Infrared Study of the $X^2\Pi$ v=0, 1, 2 levels of $^{14}N^{16}O$, Preliminary Results on the v=0,1 levels of $^{14}N^{17}O$, $^{14}N^{18}O$ and $^{15}N^{16}O$," Canadian Journal of Physics, Vol 56, 1978.

Ballard, J. and W. B. Johnston, "Experimental Spectral Line parameters in the 1-0 Band of Nitric Oxide," Journal of Molecular Spectroscopy, Vol 127, 83-96, May 1988.

Banwell, C. N., Fundamentals of Molecular Spectroscopy. New York: McGraw-Hill, Inc., 1972.

Bevington, Philip, R., Data Reduction and Error Analysis for the Physical Sciences. New York: McGraw-Hill, Inc., 1992.

Billingsley, F. P., "Calculated Vibration - Rotation Intensities for NO $(X^2\Pi)$," Journal of Molecular Specroscopy, Vol. 61, 53-70, 1976.

Burch, D. E. and. Gryvnak, D. A "Strengths, Widths and Shapes of the Oxygen Lines Near 13100 cm^{-1} (7620 A)," Applied Optics: Vol. 8 No. 7, 1493-1499, July 1969.

De Angelis, Gianfrani M. L., Pavone F., Sasso, A and. Tino G. M, "Temperature Dependence of Self Broadening in Molecular Oxygen Spectrum," Il Nuovo Cimento, Vol. 18 D, No. 5, May 1996.

Di Rosa, M. D. and Hanson R. K., " Collision Broadening and Shift of NO Absorption Lines by H_2O, O_2, and NO at 295K," Journal of Molecular Spectroscopy, Vol. 164, 97-117, 1994.

Galkin, V. D. "Line Shifts in the Oxygen A-Band as a Function of the Pressure," Optical Spectroscopy: Vol. 35 No. 4, 367-369, October 1973.

Gillette, R. H., and Eyster, E. H., "The Fundamental Rotation-Vibration Band of NO," Physical Review, Vol 56, December, 1939.

Goodman, Joseph W., Statistical Optics. New York: John Wiley and Sons, 1989.

Hastings, N.A.J., Statistical Distributions. London: Butterworth and Co., 1975.

Herzberg, G. <u>Molecular Spectra and Molecular Structure, Vol. III, Electronic Spectra and Electronic Structure of Polyatomic Molecules</u>. Princeton, New Jersey: D. Van Nostrand Company, 1966.

Jansson, Peter A. <u>Deconvolution and Applications in Spectroscopy.</u> Orlando: Academic Press, Inc., 1984.

Kearns, D, R., "Physical and Chemical Properties of Singlet Molecular Oxygen," <u>Chemical Reviews</u>: Vol. 71, No. 4, December 1971

Kreyszig, E., <u>Advanced Engineering Mathematics</u>. New York: John Wiley and Sons, 1993.

Miller, J. H., Boese, R. W., and Giver, L. P., "Intensity Measurement and Rotational Intensity Distribution for the Oxygen A-Band," <u>Journal of Quantitative Spectroscopy and Radiative Transfer</u>: Vol 9, pp. 1507-1517, 1974.

Sears, F. W., Zemansky M. W. and Young, H. D., <u>University Physics</u>. London: Addison Wesley Publishing, 1984.

Rees, M. H. <u>Physics and Chemistry of the Upper Atmosphere</u>. Great Britain: Cambridge University Press, 1989.

Ritter, K. J., and Wilkerson, T. D., "High Resolution of the Oxygen A-Band," <u>Journal of Molecular Spectroscopy</u>: Vol 121, pp. 1-19, 1987.

Ritter, K. J., Ph. D. Dissertation, University of Maryland., 1986.

Perram, G. A., Private conversations with advisory committee member.

Pine, A. S. and Maki, A. G., "Pressure Broadening, Lineshapes and Intensity Measurements in the 2-0 Band of NO," <u>Journal of Molecular Spectroscopy</u>, Vol 114, pp. 132-147, 1985.

Pope, R. S. et. al., "Collision Broadening of Spectral Lines in the X to b System of O2," Conference Paper: International Conference on Fourier Transform Spectroscopy.

Pope, R. S., Private conversations.

Spencer, M. N., C. Chackerian, L. P. Giver, and L. R. Brown, "The Nitric Oxide Fundamental Band: Frequency and Shape Parameters for Rovibrational Lines," <u>Journal of Molecular Spectroscopy</u>, Vol. 165, 506-524, 1994.

Spencer, M. N., C. Chackerian, L. P. Giver, and L. R. Brown, "Temperature Dependence of Nitrogen Broadening of the NO Fundamental Vibrational Band," Journal of Molecular Spectroscopy, Vol. 181, 307-315, 1997.

Steinfeld, J. I., Introduction to Modern Molecular Spectroscopy. Great Britain: Cambridge University press, 1993
Verdeyen,

Vyrodov, A. O., J. Heinze, and U. E. Meier, "Collisional Broadening of Spectral Lines in the A-X (0-0) System of NO by N_2, Ar, and He at Elevated Pressures Measured by Laser Induced Flourescence," Journal of Quantitative Spectroscopy and Radiative Transfer, Vol. 53, 277-287, 1995.

Wolf, P. J., Private conversations with advisory committee chairman.

Vita

John Joseph Cornicelli was born on 31 December 1966 in Amityville, New York to Salvatore Joseph and Marie Vivian Cornicelli. He graduated from high school in Bethpage, New York in 1984 and attended Duquesne University, Pittsburgh, Pennsylvania, from which he earned the degree of Bachelor of Science in Physics in 1988. Upon graduation, he was employed as a laboratory chemist for Pittsburgh Criminalistics, Pittsburgh, Pennsylvania. He received his commission from the Reserve Officer Training Corps in May 1988 and entered Air Force active duty in December 1988. Through the Air Force Institute of Technology, he attended Texas A & M University, College Station, Texas, from which he earned the degree of Bachelor of Science in Meteorology in 1989. He served as Wing Weather Officer with the 380th Bombardment Wing at Plattsburgh AFB, New York, and then as Flight Commander at Shemya AFB, Alaska. He then served as Officer-in-Charge, Weather Department, with the 66th Military Intelligence Brigade in Augsburg, Germany, and then on the staff of the Director of Operations, Weather, with Air Force Special Operations Command at Hurlburt Field, Florida. He entered the School of Engineering, Air Force Institute of Technology, in June 1996 and is a member of the American Nuclear Society. He is married to the former Nathalie Murielle Veillette of Repentigny, Quebec and has one daughter, Marianne Lise.

Permanent Address: 5 Laurel Place
Bethpage, New York 11714

21 Rue Champlain
Repentigny, Quebec J6A-5L5

REPORT DOCUMENTATION PAGE

Public reporting burden for this collection of information is estimated to average 1 hour per response, including the time for reviewing instructions, searching existing data sources, gathering and maintaining the data needed, and completing and reviewing the collection of information. Send comments regarding this burden estimate or any other aspect of this collection of information, including suggestions for reducing this burden, to Washington Headquarters Services, Directorate for Information Operations and Reports, 1215 Jefferson Davis Highway, Suite 1204, Arlington, VA 22202-4302, and to the Office of Management and Budget, Paperwork Reduction Project (0704-0188), Washington, DC 20503.

1. AGENCY USE ONLY *(Leave blank)*	2. REPORT DATE	3. REPORT TYPE AND DATES COVERED
		Maters Thesis May 96-Dec 97

4. TITLE AND SUBTITLE
Collisional Broadening of Spectral Lines in the X to b System of O2 and the First Vibrational Band of NO by the Noble Gases

5. FUNDING NUMBERS

6. AUTHOR(S)
John J. Cornicelli, Captain, USAF

7. PERFORMING ORGANIZATION NAME(S) AND ADDRESS(ES)

8. PERFORMING ORGANIZATION REPORT NUMBER

AFIT/ENP/GAP/97D-01

9. SPONSORING/MONITORING AGENCY NAME(S) AND ADDRESS(ES)
Air Force Research Laboratory AFRL/DELC
Kirtland AFB, NM
Attn: Matthew Rotondaro
DSN: 246-0718

10. SPONSORING/MONITORING AGENCY REPORT NUMBER

11. SUPPLEMENTARY NOTES
Approved for Public Release, Distribution Unlimited

12a. DISTRIBUTION AVAILABILITY STATEMENT

12b. DISTRIBUTION CODE

13. ABSTRACT *(Maximum 200 words)*

Collisional broadening of the rotational spectral lines of the X to b system of O2 and the first vibrational band of NO by the noble gases is examined by Fourier transform spectroscopy. Peaks of the individual rotational lines are modeled with a Voigt function, from which Lorentzian half widths are extracted. Lorentzian widths are plotted vs. pressure of foreign gas, from which the pressure broadening coefficients and pressure broadening cross sections are calculated. The pressure broadening coefficients are compared to theoretical values determined by past research for O2. NO coefficients are compared to similar research using N2 as collision partner. O2 broadening coefficients/cross sections were found to increase with decreasing rotational quantum number. Also, a linear dependence is found between cross section and both polarizability of the collision partner and reduced mass of the collision pair

14. SUBJECT TERMS
Collisional broadening, line broadening, rotational spectrum, vibrational transition, electronic transitiona, Fourier transform spectroscopy, Voigt function, pressure broadening coefficients

15. NUMBER OF PAGES

16. PRICE CODE

17. SECURITY CLASSIFICATION OF REPORT	18. SECURITY CLASSIFICATION OF THIS PAGE	19. SECURITY CLASSIFICATION OF ABSTRACT	20. LIMITATION OF ABSTRACT
Unclassified	Unclassified	Unclassified	UL